UNIVERSIDADE FEDERAL DE MINAS GERAIS

SCHOOL OF ENGINEERING

GRADUATE PROGRAM IN CHEMICAL ENGINEERING

DOCTORAL THESIS

Author: Dalila Chaves Sicupira

Advisor (UFMG): Profª Drª Vanessa De Freitas Cunha Lins

Co-advisor (OSU): Prof. Dr. Gerald Frankel

Evaluation of corrosion resistance of thick UNS S32304 lean duplex stainless steel plates welded by SMAW, GMAW and FCAW in corrosive environment of biodiesel industry

Belo Horizonte

Dec/2015

UNIVERSIDADE FEDERAL DE MINAS GERAIS

ESCOLA DE ENGENHARIA

PROGRAMA DE PÓS-GRADUAÇÃO EM ENGENHARIA QUÍMICA

Dalila Chaves Sicupira

Avaliação da resistência à corrosão de chapas espessas de aço inoxidável lean duplex UNS S32304 soldadas pelos processos SMAW, GMAW e FCAW em meio corrosivo da indústria de biodiesel

Tese de doutorado apresentada ao Programa de Pós-Graduação em Engenharia Química da Universidade Federal de Minas Gerais

Linha de pesquisa: Corrosão e Engenharia de Superfície

Orientadora (UFMG): Profª Drª Vanessa De Freitas Cunha Lins

Co-orientador (OSU): Prof. Dr. Gerald S. Frankel

Belo Horizonte

Dec/2015

ACKNOWLEDGEMENTS

First I'm very grateful to GOD because without his graces and blessings, this study would not have been possible.

I also offer my sincerest gratitude to my advisors, Prof. Vanessa Lins at UFMG and Prof. Gerald Frankel at OSU. Both have supported me throughout my thesis with their patience and knowledge. I attribute the level of my PhD degree to their encouragement and effort and without them this thesis would not have been completed or written. I couldn't wish for better or friendlier advisors.

Thanks are expressed to Prof. Alexandre Bracarense and Ronaldo Junior from ESAB Indústria e Comércio LTDA, who have contributed with samples and technical discussions.

I have been aided in the various laboratories for over the years. I would like to thanks all from LABCOR (Bruna, Cíntia, Fernanda, Gabriela, Layane, Luiza, Renata and Thalys) that have helped, exchanging knowledge and expectations. Thank to Prof. Dagoberto Brandão and the entire group from the LABMET (Felipe, Sara e Zé Alberto in special), for all the friendship and sample preparation support. Also, I couldn't forget Prof. Vicente Buono and the group of Thermical Analysis Lab (Bárbara, Bebel, Diego, Guilherme, Laís, Leandro, Naty and Pedro) that was also my lab. Thanks for the reception and the good daily laughter. And also all colleagues and professors of UFMG.

In my period at Fontana Corrosion Center (OSU) I was blessed with a friendly and cheerful group. I could not forget all that you made for me (Angie, Huang, Jermain, Jinwook, Jichao, Juheo, Mark, Santiago, Sara, Xi, Yuehlien and Zhicao). And also I would like to say thank to all my Brazilian friends that I met in USA (Camilo, Cláudia, João, Juliana, Raphael, Ricardo and Roberto). You made me feel at home even though I was so far.

The Department of Chemical Engineering, Metallurgical Engineering Department (UFMG), Fontana Corrosion Center (OSU) and UFMG Microscopy Center have provided the support I have needed to produce and complete my thesis and the CAPES has funded my studies.

Finally, I want to thank those that have been on my side with endless support throughout these years: my family. My mother, my father (in memoriam), stepfather and brother, for supporting me throughout all my studies at University. My husband, Bruno, for being patient. My uncles, aunts, cousins, sisters and brothers in law, father and mother in law, nephews. You make my life easier.

“By uniting we stand, by dividing we fall”

John Dickinson (1732–1808) The Liberty Song Memoirs of the Historical Society of Pennsylvania

SUMMARY

LIST OF FIGURES

LIST OF TABLES

RESUMO

Chapas espessas do aço inoxidável lean duplex (AILD) UNS S32304 foram soldadas por diferentes processos comumente empregados na fabricação de equipamentos e tubulações: Shielded Metal Arc Welding (SMAW), Gas Metal Arc Welding (GMAW) and Flux-cored arc welding (FCAW). O comportamento eletroquímico das diferentes regiões da junta soldada (zona de fusão (ZF), metal base (MB) e zona termicamente afetada (ZTA)) foi caracterizado tanto de forma independente, utilizando uma microcélula eletroquímica, quanto juntos, avaliando toda a área da junta soldada. Os testes eletroquímicos foram realizados em glicerina acidificada, um subproduto da indústria do biodiesel. O estudo da corrosão das juntas soldadas foi realizado utilizando técnicas como polarização potenciodinâmica cíclica, espectroscopia de impedância electroquímica e análise de Mott Schottky. Microscopia óptica (MO), microscopia eletrônica de transmissão (MET), microscopia eletrônica de varredura (MEV) foram utilizadas para caracterização das amostras. Os resultados foram correlacionados com as características microestruturais das amostras. O estudo de capacitância mostrou que os filmes passivos formadas nas juntas soldadas de AILD comportaram-se como semicondutores do tipo-n e do tipo-p acima e abaixo do potencial de banda plana, respectivamente. Além disso, as amostras soldadas pelo processo GMAW exibiram uma melhor resistência à corrosão quando comparadas aos outros processos de solda usando o mesmo metal de adição. Resultados para potencial de pite usando a técnica de microcélula e imagens de MEV mostraram que a ZTA é a zona mais crítica para a corrosão localizada para todas as amostras. Precipitados de Cr_2N não foram observados nas amostras sem solda; entretanto, foram identificados nos contornos de grão ou na fase ferrítica das amostras soldadas. Em geral, a resistência à corrosão da região de topo

da solda foi maior do que a região de raiz da solda. Basicamente, todas as amostras soldadas apresentaram resistência à corrosão semelhante ou superior em comparação com o metal base correspondente.

ABSTRACT

UNS S32304 Lean Duplex Stainless Steel (LDSS) thick plates were welded by different processes commonly employed in the manufacture of equipment and piping: shielded metal arc welding (SMAW), gas metal arc welding (GMAW) and flux cored arc welding (FCAW). The electrochemical behavior of different weldment zones (fusion zone (FZ), base metal (BM) and heat affected zone (HAZ)) was characterized both independently, using an electrochemical microcell, and together by testing the whole welded area. The electrochemical tests were performed in acidified glycerin, a byproduct of the biodiesel industry. The study of the corrosion behavior of the welded joints was performed using electrochemical techniques such as cyclic potentiodynamic polarization, electrochemical impedance spectroscopy and Mott-Schottky analysis. Optical microscopy, transmission electron microscopy and scanning electron microscopy were used for sample characterization. The results were correlated to the microstructural features of the materials. The capacitance study showed that the passive films formed on welded LDSS behaved as n-type and p-type semiconductors above and below the flat band potential, respectively. Furthermore, the samples welded by the Gas Metal Arc Welding process exhibited better corrosion resistance than others welding processes using the same filler metal. Results for pitting potential using microcell technique and SEM images showed that the HAZ was the most critical zone for pitting corrosion for all samples. No chromium nitride precipitation was observed in the specimens without welding, while many nitride precipitates were found at grain boundaries or ferrite grains in the welded specimens. These pits are believed to be closely related with the Cr_2N precipitates. In general, the corrosion resistance of the top regions of welds was higher in acidified glycerin than that of weld roots. Basically, all

the welded samples exhibited similar or a higher corrosion resistance, compared with the corresponding base metal.

1. INTRODUCTION

Duplex stainless steels (DSSs) are materials that exhibit a combination of high yield strength–toughness and a superior localized corrosion resistance, which are being widely used in chemical, petrochemical, marine, nuclear and paper industries. However the deterioration in corrosion resistance as a result of exposure to high temperatures, which can occur during welding, is a typical problem for users of DSS.

An improved understanding of the corrosion properties of DSS can provide direction for their application and reduce the costs associated with corrosion, for example, in industrial biodiesel plants. The biodiesel industry has experienced a significant number of failures (e.g. holes in pipes) caused by corrosion in acidified medium, which resulted in production losses and, consequently, economic losses.

To inhibit undesired reactions, both biodiesel and glycerin are neutralized by, in line, dosage of hydrochloric acid. From the perspective of corrosion, the neutralization stage plays a fundamental role in the process, because the hydrochloric acid solution is one of the most aggressive environments in industry. The majority of failures related to corrosion arise at the hydrochloric acid dosing points.

The most typical problems of welded DSS are associated with the heat-affected zone (HAZ), not with the fusion zone (FZ), since the properties of the FZ could be improved by using high-alloyed filler metal and N_2-containing shield gas. A great number of investigations have been carried out on the HAZ of DSSs, but few studies on the HAZ of multi-pass welds have been reported even though multi-pass welding is more

common during industrial fabrication, especially for plates or pipes. Although several studies related to the effect of heat input and thermal cycles on the microstructure of pipeline steels have been performed, corrosion of welded joints of DSS in biodiesel plant environments has not received much attention.

This research is a continuation of a project that evaluated the mechanical and metallurgical behavior of thick plates of UNS S32304 lean duplex stainless steel multipass-welded by processes commonly employed in the manufacture of equipment and piping: shielded metal arc welding (SMAW), gas metal arc welding (GMAW), and flux cored arc welding (FCAW). In this context, this work is aimed at evaluating the corrosion resistance of UNS S32304 LDSS plates welded using the SMAW, GMAW and FCAW processes in acidified glycerin, a by-product of biodiesel industry, which is a gap in literature.

In this thesis, three papers containing research work on corrosion of welded joints of UNS S32304 lean duplex stainless steel are presented, with an emphasis on the interrelation between microstructure (phase balance, weld oxide, element distribution and precipitates) and corrosion properties. The focus has been on multi-pass welding of thick material (22 mm) using slightly over-alloyed filler metals, ISO 23 7 N L and ISO 22 9 3 N L. The testing environment was acidified glycerin, a byproduct of the biodiesel industry. The electrochemical behavior of different weldment zones (fusion zone, base metal and heat affected zone (HAZ)) was characterized both independently, using an electrochemical microcell, and together by testing the whole welded area. The electrochemical and electronic properties of passive films formed on the UNS S32304

LDSS thick plates were also evaluated using techniques such as electrochemical impedance spectroscopy and Mott–Schottky analysis.

The main work in this thesis was carried out at Fontana Corrosion Center (FCC) at Ohio State University (OSU), USA. The first section consists of a review of literature about duplex stainless steels and their weldability and corrosion behavior. The second part consists of three papers which will be referred to in the text by chapter 4, 5 and 6.

Chapter 4: Pitting corrosion of welds in UNS S32304 lean duplex stainless steel.

Sicupira, D. C.; Frankel, G. S.; Lins, V. de F. C.

Materials and Corrosion, **2015**, DOI: 10.1002/maco.201508502.

Chapter 5: Electrochemical study of passive films formed on welded lean duplex stainless steel.

Sicupira, D. C.; Cardoso Junior, R.; Bracarense, A. Q.; Frankel, G. S.; Lins, V. de F.C.

Chapter 6: Cyclic polarization study of thick welded joints of lean duplex stainless steel in acidified glycerin.

Sicupira, D. C.; Cardoso Junior, R.; Bracarense, A. Q.; Frankel, G. S.; Lins, V. de F.C.

2. OBJECTIVES

2.1. General objective

Evaluate the corrosion resistance of UNS S32304 LDSS plates welded by various processes commonly employed in the manufacture of equipment and piping: shielded metal arc welding (SMAW), gas metal arc welding (GMAW) and flux cored arc welding (FCAW) in acidified glycerin, a by-product of the biodiesel industry.

2.2. Specific objectives

- Evaluate the electrochemical behavior of UNS S32304 steel in acidified glycerin by using the technique of electrochemical impedance spectroscopy.
- Determine the pitting potential of the whole sample using the potentiodynamic polarization testing.
- Determine the pitting potential and evaluate the repassivation ability using the technique of cyclic potentiodynamic polarization with microcell.
- Determine the pitting potential and evaluate the repassivation of the whole sample using cyclic potentiodynamic polarization.
- Evaluate the semiconducting properties of passive films by Mott-Schottky measurements.

- Perform steel surface characterization, before and after the electrochemical tests, using optical microscopy (OM), scanning electron microscopy (SEM) and transmission electron microscopy (TEM).

3. REVIEW OF LITERATURE

3.1. Biodiesel Production

Biodiesel is the name of a clean burning mono-alkyl ester-based oxygenated fuel made from natural, renewable sources such as new/used vegetable oils and animal fats [1]. Potential renewable raw materials for biodiesel are mainly vegetable oils, seeds and lignocelluloses [2].

Transesterification is one of the commonly adoptable methods to convert those vegetable oils as fuel [1]. Transesterification is the reaction of a fat or vegetable oil with an alcohol to form esters and glycerol. Among the alcohols that can be used in the transesterification process are methanol, ethanol, prophanol, buthanol and amyl alcohol. Since the reaction is reversible, excess alcohol is required to shift the equilibrium to the product side. A catalyst is usually used to improve the reaction rate and yield. Alkali-catalyzed transesterification is much faster than acid-catalyzed transesterification and is often used commercially [3,4].

Methyl route is the main industrial process used to produce biodiesel. This chemical reaction (Figure 1) is also known as methanolysis, and one mole of triglyceride reacts with three moles of methanol in the presence of sodium hydroxide (catalyst) to form the methyl ester (Biodiesel) as product and glycerol (glycerin) as byproduct [1].

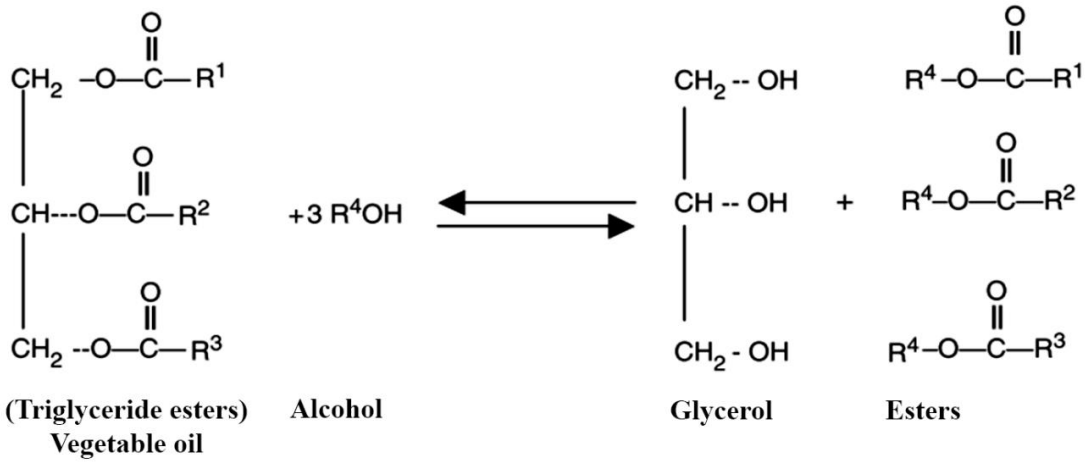

Figure 3.1: Representation of transesterification reaction (Adapted from [3]).

For a better understanding of the flow of glycerin in the plants of Petrobras Biocombustíveis - PBIO, the flowchart representing the glycerin circuit is shown below (Figure 3.2).

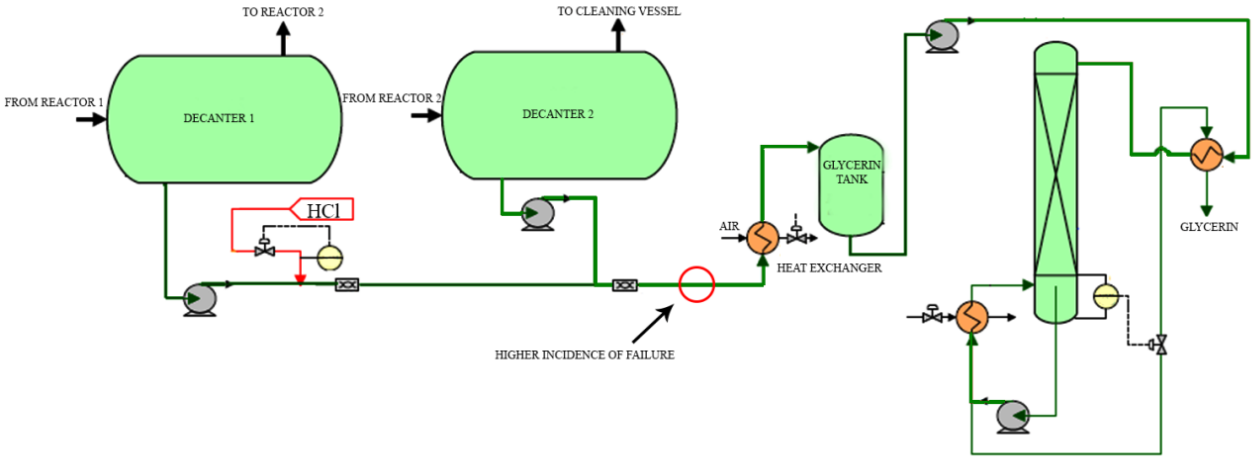

Figure 3.2: Flowchart representing the glycerin circuit in Biodiesel plants (Adapted from [5]).

The flow reacted in the first reactor goes to the first decanter to be separated into two phases - biodiesel and glycerin. The upper phase (biodiesel), which still has a significant

proportion of triglycerides, is sent to the second reactor. The lower phase, which has excess of methanol and catalyst, is stored prior to distillation [5].

To inhibit undesired reactions, both biodiesel and glycerin are neutralized by in line dosage of hydrochloric acid. From the perspective of corrosion, the neutralization stage plays a fundamental role in the process, because the hydrochloric acid is one of the most aggressive chemicals. The majority of failures related to corrosion occur at the hydrochloric acid dosing points [5].

According to ANP [6], Brazil is among the largest producers and consumers of biodiesel in the world, with a total capacity in March 2015 of 21,506.51 m^3/day. Since November 1, 2014, the sale of diesel BX - name of the mixture of diesel derived from petroleum and a percentage (7% currently) of biodiesel - is mandatory in all posts that resell diesel. Installed production capacity of biodiesel in Brazil (Petrobras Biofuel) is enough to absorb significant increases in mandatory minimum of biodiesel addition in fuels.

3.2. Stainless Steel and their Weldability

Stainless steel are alloyed with at least 12% chromium and become corrosion resistant by formation of a self-healing chromium oxide on the steel surface [7]. By varying the chromium, nickel, molybdenum, nitrogen, etc., composition of the steel it is possible to achieve different properties suitable for various applications. Mo is added for enhancing resistance against pitting and Ni for obtaining austenite, for instance [7,8].

Stainless steels may be divided into different groups on the basis of their microstructure. Three main types of microstructures exist in stainless steels, i.e., ferritic, austenitic and martensitic. These microstructures may be obtained by properly adjusting steel chemistry and processing. Of these, austenitic, ferritic and ferritic-austenitic (duplex) are the most commonly used.

3.2.1. Duplex stainless steel

Duplex stainless steels (DSS) are metallic alloys based on the Fe–Cr–Ni system, in which chemistry and thermo-mechanical processing confers a dual phase microstructure with similar amounts of ferrite (α) and austenite (γ), typically in a proportion of 50–50% [9-11], as shown in Figure 3.3.

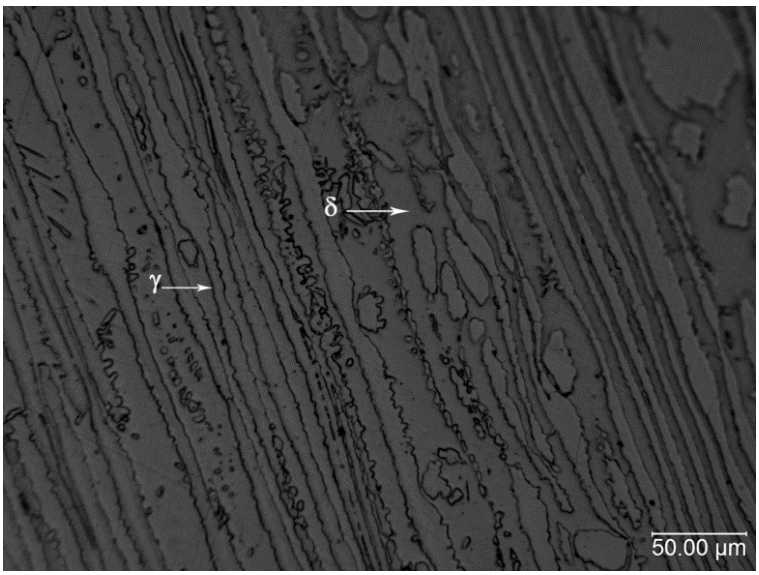

Figure 3.3: Optical microstructure of LDSS.

This equal phase balance offers unique, attractive grouping of high corrosion resistance, high mechanical strength and superior weldability in various atmospheres [11]. It is

known that DSS exhibits well-balanced characteristics of favorable mechanical strength of α phase and the high corrosion resistance of the γ phase [11,12]. DSSs offer several advantages over the common austenitic stainless steels and can be very attractive due to their almost double strength and equal pitting corrosion resistance [13]. Furthermore, with only about half of the nickel content of common austenitic steels, they are less sensitive to the price of nickel, which can be volatile [14]. These types of alloys are low carbon (less than 0.04%) and contain 20–30% Cr, 0–5%Mo, 1–8%Ni and 0.1–0.3%N, as well as some additions of Cu and W [11].

DSS is broadly used in chemical industries, power plants, petrochemical and offshore structural industries [11,12]. This wide usage is closely connected with the increasing demands for cost-saving materials having resistance to highly aggressive environments [11,15]. DSS has high resistance to chloride stress corrosion cracking; excellent pitting and crevice corrosion resistance in low pH and sour environments even in presence of chloride [10].

However, the deterioration in corrosion resistance as a result of exposure to high temperatures, which is the case during fabrication such as welding, is a typical problem to users of duplex stainless steels [11,13,16-21]. When DSS is welded, the thermal history may severely impair performance, especially local pitting corrosion resistance and toughness [22]. Such degradation result from the unbalanced duplex phase fraction with excess of ferrite phase and the precipitation of deleterious secondary phases such as chromium nitrides, secondary austenite (γ_2), sigma (σ), chi (χ) etc. The most typical problems of welded DSS are associated with the heat-affected zone (HAZ), and not with

the fusion zone (FZ) [16], since the properties of FZ can be modified by using high-alloyed filler metal and N_2 containing shield gas [18,23].

For duplex grade, the solidification is entirely as delta ferrite, and then the austenitic phase forms through a solid-state phase transformation [24]. During post solidification cooling, γ tends to precipitate first on the δ/δ boundary and then grow into the ferrite grain with Widmanstätten morphology. This phase is called primary austenite (γ_1), since it is formed just after the complete ferritic solidification [10]. However, for the fast cooling rate of welded joints, the ferrite–austenite transformation is suppressed and less austenite will be formed in the HAZ [24], resulting in a supersaturated ferrite, enriched with nickel, manganese and nitrogen [10]. Under this supersaturated condition, when this microstructure is reheated, the decomposition of ferrite phase can occur, resulting in the formation of a new austenite phase (γ_2) [21,25]. As cited by Sieurin and Sandström [9], multipass welding can cause diffusional transformation of ferrite to austenite in reheated areas, as well as precipitation of intermetallic phases.

It has been reported that chemical composition differences exist between the different austenite types, with the γ_2 having lower contents of Cr, Mo and N than γ_1 [10,15,21, 22]. A deleterious effect of γ_2 precipitation on the localized corrosion resistance of DSS has also been reported and has been associated with the chemical composition of that phase [15,21,22]. However, more recent results have shown that the reduced corrosion resistance of the reheated microstructure is associated with the presence of nitrides [10,24]. Ramirez *et al.* [26] reported that the formation of Cr_2N precipitates, containing a higher concentration of Cr, caused localized depletion areas in Cr around the Cr_2N, which led to increased localized corrosion susceptibility.

If the ferrite content is high in the weld metal as the result of rapid cooling, intensive nitrides precipitation occurs at δ/γ interfaces or within ferrite matrix because the ferrite becomes supersaturated in nitrogen (the solubility limit of the ferrite is exceeded at low temperature) and the nitrogen has insufficient time to partition into the austenite. This results in a competition between large ferrite grains with a low amount of allotriomorphic and Widmannstätten austenite and extensive chromium nitride formation, both intragranular and intergranular [15].

The mechanical and corrosion properties of DSSs are directly related to the microstructure, particularly the phase balance that results in the partitioning of alloying elements (Cr, Mo, N and Ni) [9-12,15,25,27]. Thus, the heat input and the chemical composition must be well considered in the design of welded DSS structures. Too low welding energy can lead to high ferrite contents and intense chromium nitride precipitation [15]. According to Davison and Redmond [14], austenite contents lower than 25% are unacceptable for most industrial applications. On the other hand, high heat inputs or long exposure to temperatures in the 600–1000°C range may cause precipitation of brittle intermetallic phases [28].

3.2.2. Lean duplex stainless steel

Volatility of the Ni price has focused interest in the development of low alloy duplex steels (generally low Ni or Mo contents), which are cheaper than standard 2205 DSS [29]. The nickel content of about 5% in the well-established duplex steel 2205 is partly

replaced by manganese and nitrogen and also the molybdenum content is reduced in the so-called lean DSS (LDSS) [13].

Those lean, low alloyed duplex steels, are characterized by equivalent mechanical strength and toughness compared to conventional duplex grades but have lower resistance to localized corrosion, although their corrosion resistance is comparable to that of austenitic steels like the widely used 304 and 316 grades [8, 29]. In particular, lean duplex grades, with lower nickel and molybdenum contents, have a competitive cost and are anticipated to be increasingly used for structural applications [30].

LDSSs have typical chemical composition of < 0.03 C, 21.5-24.5 Cr, 0.05-0.6 Mo, 3.0-5.5 Ni, < 2.5 Mn and 0.05-0.2 N (wt.%). One of the most common LDSS alloys is the UNS S32304 steel, which has a nominal composition of 23% Cr, 4% Ni, and additions of Mo, N and Mn [31].

Alvarez *et al.* [29] has discussed the differences in the corrosion properties of 2205 DSS and 2304 LDSS and attributed them to their different Mo contents. Since Mo is a ferritizer element, it tends to be localized in the ferrite and, thus, increases the corrosion resistance of this phase. The lower Mo content of 2304 explains why ferrite in this material corrodes during the tests, while the whole 2205 alloy remains fully immune.

LDSSs are widely used due to both the higher strength compared to austenitic and ferritic stainless steels and the lower cost of these materials by lowering the content of Mo and Ni [32]. More nitrogen is added to increase the pitting corrosion resistance, since the concentration of Mo is lower than in duplex steels [32]. The solubility of

nitrogen in ferrite drops rapidly with the decrease in temperature, consequently intense nitride precipitation was observed within the ferrite grains [11,18-20,24,26]. The possibility of chromium nitride formation during welding of DSS has been indicated in several studies [11,18-20,24,26], however the precipitation of the σ phase is kinetically very slow due to the low molybdenum content in LDSS [22]. Ramirez *et al.* [26] showed that chromium-rich nitrides precipitated at the interior of the ferrite grains and at ferrite/austenite interfaces after quenching from 1350°C. This chromium nitride precipitation has been shown to severely impair the corrosion resistance and the toughness of the DSSs [10,11,18-29,24,26,33]. Results obtained by different workers on the deleterious effects of Cr_2N on mechanical and corrosion properties are in general agreement [7,15,18,19,22,28,33,34].

It was also proposed that when the material in this condition is reheated, as in multipass welding, the most apparent changes in the microstructure are the dissolution of the intragranular nitrides and the precipitation of secondary austenite [10,25]. However, it has been proposed that the chemical composition of γ_2, with lower chromium, molybdenum, and nitrogen contents than the preexisting austenite (γ), compromises the corrosion resistance [10,26,33].

An increased amount of nitrogen is beneficial for austenite reformation [9]. The use of nitrogen as an alloy addition improves tensile properties, and pitting and crevice corrosion resistance. Nitrogen also causes austenite to form from the ferrite at a higher temperature, allowing for restoration of an acceptable balance of austenite and ferrite after a rapid thermal cycle in the heat-affected zone (HAZ) after welding [35]. In addition, it minimizes the extent of partitioning of elements, bringing homogenization

of chromium distribution in the two phases, ferrite and austenite [17, 27]. All these factors would result in a significant improvement in the integrity of the welded assembly and its corrosion resistance in particular [35]. This nitrogen advantage enables the use of duplex grades in the as-welded condition.

The weld microstructure is not only dependent on the chemical composition, but also on the welding parameters, which affect the thermal weld cycle [15]. The heat input should be sufficient to enable reasonable austenite formation in the weld and HAZ. A minimum of 0.2-0.5 kJ/mm is usually required in arc welding process, depending on grade and material thickness [17]. Duplex stainless steels have been welded by limiting the heat input to 1.0 or 3.5kJ/mm and the maximum interpass temperature to 100-150°C in order to avoid precipitation of detrimental phases in previous passes [17].

Higher nitrogen contents are extremely helpful with the lower heat input constraint, especially for the lower-alloyed grades such as the 2304 alloy [14]. It is still necessary to be concerned about preheat or a controlled interpass temperature for a multiple-pass weld that will slow the cooling rate enough to allow sufficient reformation of austenite to produce a good toughness and corrosion resistance [14].

3.3. Welding Processes

There are many methods available for joining stainless steel, but fusion welding, predominates. Fusion welding processes include all of those processes in which the melting or fusion of portions of the substrates, with or without added filler, plays a principal role in the formation of bonds to produce a weld [36]. All fusion welds contain

a distinct fusion zone (FZ), as well as heat-affected zone (HAZ) and unaffected base metal (BM). Here follows a brief description of the welding methods used in this thesis work. These welding methods are: (1) gas-metal arc welding (GMAW), (2) shielded-metal arc welding (SMAW), (3) flux-cored arc welding (FCAW).

The GMAW process employs a continuous consumable solid wire electrode and an externally supplied inert shielding gas [36]. The consumable wire electrode produces an arc with a workpiece made part of the electric circuit and provides filler to the weld joint. The externally supplied shielding gas protects the arc and the molten weld metal from air and also provides desired arc characteristics through its effect on ionization. In summary, the GMAW process offers flexibility and versatility, is readily automated and enables high deposition rates and efficiencies (80-90%). The greatest shortcoming of the process is that the power supplies typically required are expensive [36].

The SMAW process is also known as the stick welding process [36]. Metal coalescence is produced by the heat from an electric arc that is maintained between the tip of flux-covered, discontinuous consumable electrode and the surface of the base metal being welded. A core wire conducts the electric current from a constant-current power supply to the arc and provides most of the filler metal to the joint. The covering on a SMAW electrode provides a gaseous shield to protect the molten metal of the weld from the air. Advantages of SMAW are that it is simple, portable, and requires inexpensive equipment. Shortcomings of the process are that it offers only limited shielding protection relative to inert gas shielded processes, provides limited deposition rates compared to many other arc welding processes, and is usually performed manually, rather than automatically [36].

.

FCAW is similar to SMAW in that it is self-shielding, however, the gas and flux-generating flux is contained in the core of a roll-formed and/or drawn tubular wire, rather than on the outside of a core wire as a coating [36]. The cored wire serves as a continuous consumable electrode, with the filler in the core fulfilling the same functions as the coating in SMAW – providing self-shielding gases, slagging ingredients, arc stabilizers, and alloy additions and deposition rate enhancers. The FCAW process can also be operated in a gas-shielding gas mode (as performed in this work), in which case it is closely related to GMAW process. Both employ a continuous consumable electrode, both provide filler, and both use an externally provided gas to shield the arc and the weld metal [36].

3.4. Corrosion

According to McCafferty [37], corrosion is the destructive attack of a metal by its reaction with the environment. Corrosion is an electrochemical process that usually occurs not by direct chemical reaction of a metal with its environment but rather through the operation of coupled electrochemical half-cell reactions.

- Anodic Reactions

The loss of metal occurs as an anodic reaction and equation 1 shows the oxidation of iron.

$$Fe_{(s)} \rightarrow Fe^{2+}{}_{(aq)} + 2e^{-} \quad (3.1)$$

There is an increase in the oxidation number of the species that oxidizes and there is a loss of electrons at the anodic site (electrons are produced by the reaction).

- Cathodic Reactions

A given species undergoes reduction, i.e., there is a decrease in its oxidation number. There is a gain of electrons at the cathodic site (electrons are consumed by the reaction).

An example of a cathodic reaction is the reduction of hydrogen ions to form hydrogen gas:

$$2H^{+}_{(aq)} + 2e^{-} \rightarrow H_{2\,(g)} \tag{3.2}$$

This is the predominant cathodic reaction in acidic solutions.

Another common cathodic reaction is the reduction of dissolved oxygen to hydroxyl ions, which occurs in neutral or basic aerated solutions.

$$O_{2_{(g)}} + 2H_2O + 4e^{-} \rightarrow 4OH^{-}_{(aq)} \tag{3.3}$$

On a corroding metal surface, anodic and cathodic reactions occur in a coupled manner at different places on the metal surface.

For the occurrence of corrosion, four conditions are necessary [37]:

- An anodic reaction
- A cathodic reaction
- A conductive path of contact between anodic and cathodic sites
- The presence of an electrolyte

An electrolyte is a solution which contains dissolved ions capable of conducting a current. The most common electrolyte is an aqueous solution, i.e., water containing dissolved ions; but other liquids, such as liquid ammonia or ionic liquid, can also function as electrolytes [37].

The potentiodynamic polarization test, and the closely-related cyclic potentiodynamic polarization test, is an electrochemical technique that provides the corrosion behavior of a metal. This method determines the relative susceptibility to localized corrosion.

Microelectrochemical methods are powerful techniques to study localized corrosion processes on small areas of passive metals. Many papers have used microelectrode cells to study working areas in the µm-nm range [4,38]. Corrosion processes such as pitting, intergranular corrosion, stress corrosion cracking, crevice corrosion or galvanic corrosion have been mainly studied based on large-scale experiments (working electrode in the mm^2– cm^2 range) [13]. However, such processes are due to mechanisms on a smaller scale. Therefore, it is advisable to develop appropriate small-scale experimental devices that interrogate a small exposed surface area of the working electrode. Additionally, these experimental devices can be applied to cases in which a heterogeneous material is the focus of interest, as in the study of welded joints [4]. The main benefit of using microcells is directly related to the small size of the exposed working area, which is in the micrometer range, although some drawbacks for capillary microcells must be considered, as has been explained by Birbilis *et al.* [38].

3.4.1. Passivity of metals

As recognized, protective oxides or hydroxides can form on the surfaces of transition metals such as Fe, Cr, Ni, Mo and their alloys [39]. The oxide film with a thickness of several nanometers protects underlying metal/alloy from corrosive environment, commonly termed as the passive film. The protectiveness of passive film depends greatly on the Cr, Mo and N contents of the alloy [39,40].

The passivity of stainless steels is due to the formation of a protective layer on their surface that has been described as consisting of multilayer structures [40]. Recent studies also established that the passive oxide film formed on stainless steels consists primarily of chromium oxide, Cr_2O_3, and iron oxide, Fe_2O_3, as inner and outer layers, respectively [40-42]. The first being the barrier layer against cation transfer and the latter being an exchange layer with the electrolyte [43]. Generally, the passive films on metals are mainly made up of metallic oxides or hydroxides, which can be semiconductors [44]. Consequently, semiconducting properties are often observed on the surfaces of the passive metals [44]. Their electrical properties are expected to be crucially important in understanding the protective characteristics against corrosion [45].

It has been generally accepted that oxide film formed on stainless steel has n- or p-type semiconducting properties depending upon the applied potential [40]. In the last decade, increasing research of the electronic properties (especially the semiconducting behavior) of the passive films formed on stainless steels has given an important contribution to the understanding of the corrosion behavior of these alloys [45-47]. According to Bensalah *et al.* [47] the semi-conductive properties of the passive film depend on the contribution of each oxide and the concentration of each cation or anion vacancies inside these oxides. The passive film with a deficiency in metal ions or excess of cationic vacancies generally behaves as p-type (acceptors), while n-type (donors) is developed in the passive films either by cationic transport through interstitial diffusion or by anion diffusion into the metal [48].

Capacitance studies are useful for obtaining information on the electronic structure of a semiconductor and by the analysis of the Mott-Schottky plots it is possible to obtain the donor and acceptor densities [44]. It has been considered that a higher concentration of donors in the oxide layer favors the incorporation of ions, such as chlorides, into the anion vacancies of the oxide film and their diffusion through it [49,50]. This could favor the breakdown of the oxide film and lead to pitting [50]. Fattah-alhosseini and Vafaeian [45] in a recent work evaluated the electrochemical behavior of coarse-grained and fine-grained AISI 430 ferritic stainless steel in 0.1M HNO_3 solution. Using Mott–Schottky analysis, it was found that the calculated donor and acceptor densities decreased with grain refinement, suggesting that the passivation behavior was enhanced with decreasing grain size.

3.4.2. Pitting corrosion

There are two major types of corrosion: uniform corrosion and localized corrosion. In uniform corrosion, the metal is attacked more or less evenly over its entire surface. In localized corrosion, corrosion is limited to certain areas on the metal surface. Pitting corrosion is one of the prevalent forms of localized corrosion. In pitting corrosion, the metal is attacked at certain sites on the metal surface where the otherwise protective oxide film breaks down locally, usually due to the action of chloride ions as shown in Figure 3.4 [37].

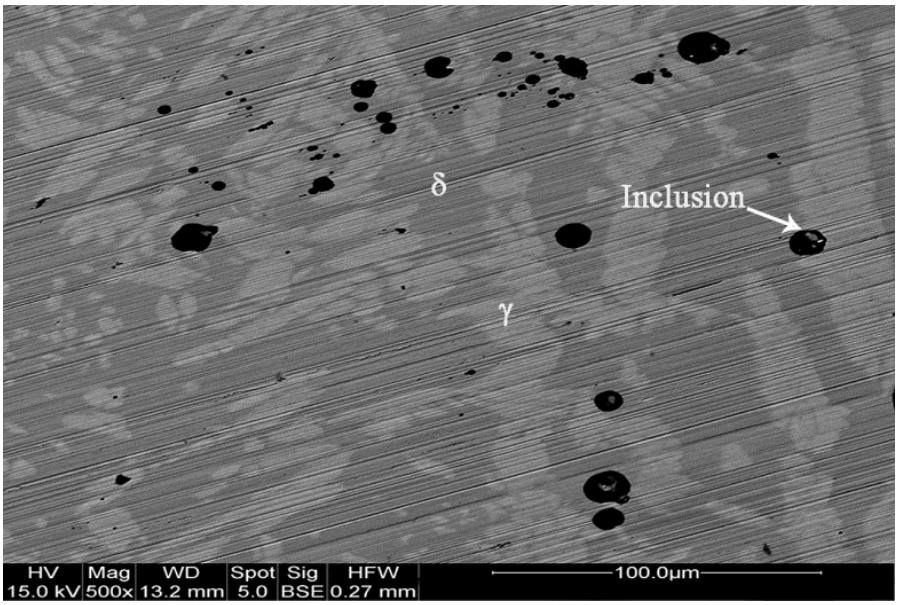

Figure 3.4: Pit formed on welded samples after polarization measurements in a chloride solution.

Pitting corrosion is a localized accelerated dissolution of metal that occurs as a result of a breakdown of the otherwise protective passive film on the metal surface and will only occur in the presence of aggressive anionic species, and chloride ions are usually, although not always, the main cause of this type of corrosion [50-52]. The tendency of a metal or alloy to undergo pitting is characterized by its pitting potential (E_{pit}) and the tendency to repassivate is characterized by its protection potential (E_{prot}), as illustrated in Figure 3.5 (Region I: Pitting initiates and propagates, region II: Pitting does not initiate but propagates if initiated at higher potentials, region III: Pitting will not initiate or propagate).

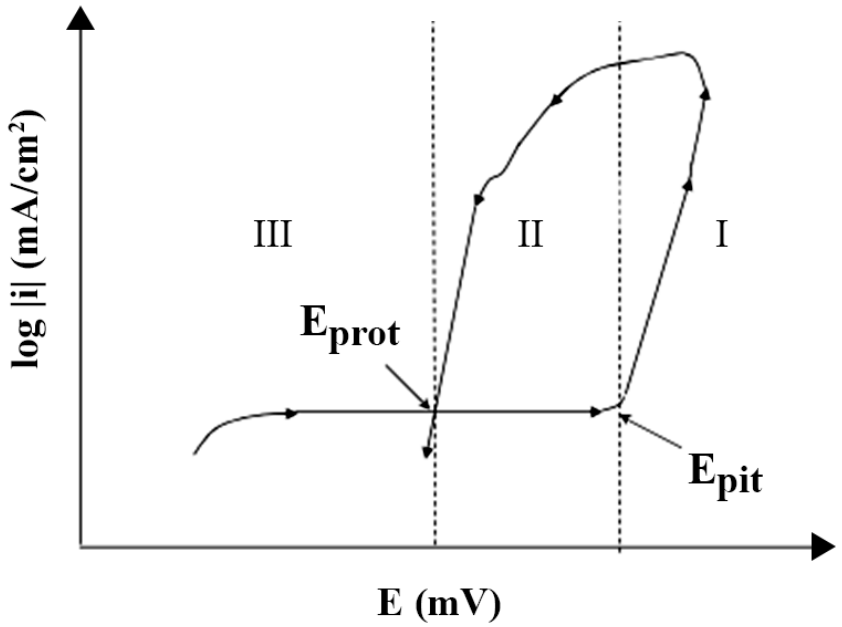

Figure 3.5: Schematic illustration of the pitting potential E_{pit} and the protection potential E_{prot}. The arrows show the direction of polarization (for a passive metal) (Adapted from [37]).

Pitting corrosion has been studied for several decades by many researchers and is one of the most difficult forms of corrosion to manage reliably [48]. Resistance to pitting corrosion is a major engineering design feature of many structures and components and despite this, chloride induced pitting remains a major form of failure [43]. Many variables are involved in the phenomenon; almost every feature of a metal/environment system has an effect on pitting. For example, the well known phenomenon of chloride induced pitting of many metals is naturally a function of the chloride concentration and the temperature, quite apart from the identity, the composition, and microstructural characteristics of the metal. In addition to the chloride concentration, however, the

presence of most other components of the environment has an effect on the pitting characteristics as well [50,51].

According to Frankel and Sridhar [53], the process of localized corrosion can be divided into a sequence of steps: initiation by the breakdown of the passive film; metastable growth of small pits (metastable in this context indicates that many pits cease to grow at this stage); stable growth of localized corrosion sites that can grow quite large; and finally – if conditions permit – repassivation or cessation of attack. Localized corrosion is known to initiate above a critical potential (E_{pit}) and repassivate below another (E_{prot}) lower potential. There is a lot of literature on these characteristic potentials and they form an important component of the knowledge of pitting [15,54-56].

It has been suggested that localized corrosion or pitting in passive metals results from a variety of mechanisms. Theories for passive film breakdown and pit initiation have been categorized in three main mechanisms that focus on passive film penetration, film breaking, or adsorption [52]. These three mechanisms of pit initiation are not necessarily mutually exclusive as shown in Figure 3.6.

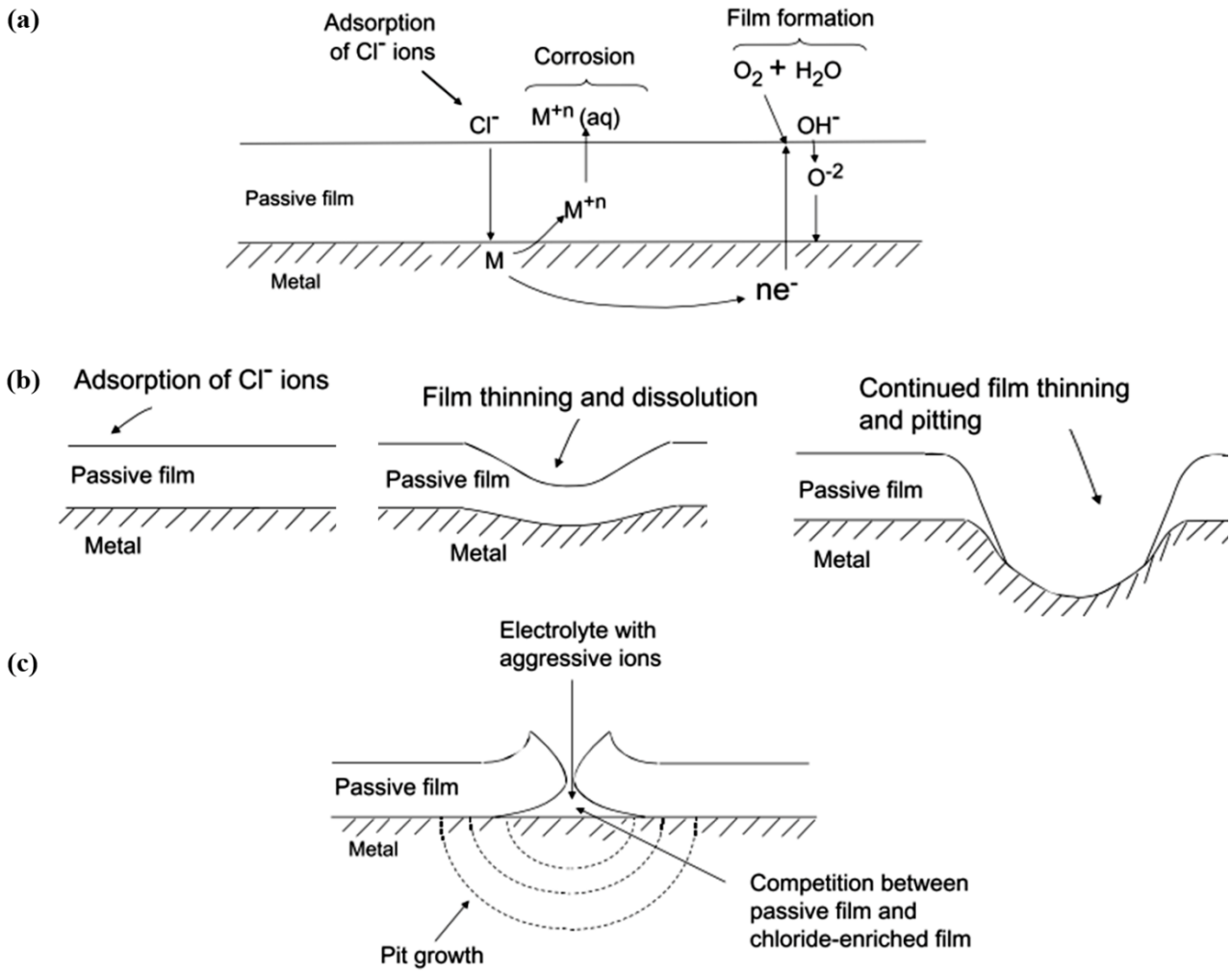

Figure 3.6: Schematic drawn representing pit initiation by (a) penetration, (b) adsorption and thinning, and (c) film breaking (Adapted from [37]).

The penetration mechanism involves the transfer of anions through the oxide film to the metal surface, where they start their specific action. As discussed by Hoar [57], penetration process is evidently preceded by adsorption of anions at the film/solution interface, more specifically, by the replacement of adsorbed water by adsorbed anions.

A point defect model for the breakdown of passivity have been developed involving the action of vacancies within the passive film. According to Macdonald [49] Cl^- ions adsorb and incorporate into the anion vacancies of the oxide film and diffuse through it.

This alters the cation vacancy concentration and promotes film breakdown by cation vacancy condensation, which leads to pitting.

The film breakdown mechanism requires cracks or flaws in the film which give access of anions to the metal surface. According Frankel [52], surface tension effects may lead to mechanical stresses at weak sites or flaws and cause the local breakdown events, which rapidly heal in nonaggressive environments.

It has been proposed by some authors [24,41,43,57,58] that adsorption of aggressive anions (Cl^-) reduce the surface tension of the passive film such that cracks would arise, allowing anions to reach the metal surface. The ionic film breakdown starts with the competition for adsorption, at the film/electrolyte interface, between hydroxyl and chloride ions [24,41,50]. According to Marcus et al. [43], if Cl^- are adsorbed on the oxide surface, the Me–Cl^- (or MeO(H)–Cl^-) surface complexes are less strongly bound to the oxide matrix and the activation energy for their transfer to the electrolyte is decreased. As a consequence, the localized dissolution rate is increased and film growth is poisoned. This leads to thinning of the passive layer. After depassivation, Cl^- also competes for adsorption on the metal surface and hinders repassivation, leading to the formation of enlarged nanopits [43].

3.4.3. Corrosion of welded joints of DSS

In general, the considerable concentration of Cr, Mo and N gives the DSS resistance to pitting in chloride-containing solutions [15]. A common way to rank the pitting susceptibility in DSS is using the pitting resistance equivalent number (PREN). The

pitting corrosion resistance is higher for a higher PREN. The following equation is widely used [19,20,27]

$$PREN = \%Cr + 3.3\%Mo + 20\%N \quad (3.4)$$

The PREN of the two single phases (δ and γ) can vary, resulting in different corrosion resistance for each single phase [8,19]. PREN for each phase should be measured to predict the weaker phase, in which the pitting corrosion should occur [15,19]. In fact, it is frequently reported that the main alloying elements, i.e. chromium, molybdenum, nickel and nitrogen, are not evenly distributed in ferrite and austenite. Chromium and molybdenum enrich in ferrite, whereas nickel and nitrogen are concentrated in austenite [18,19,27]. According to Chen *et al.* [19], as the cooling rate decreases, the content of Cr and Mo increases and the Ni content decreases in δ phase. The alloying element concentration of each phase is diffusion-controlled during the cooling stage of the welding thermal cycle [19], thus, the lower the cooling rate the higher diffusion of the alloying elements during the thermal cycle [55]. The diffusion coefficient of nitrogen, which is an interstitial element, is about four orders of magnitude greater than that of substitutional elements such as Cr, Mo and Ni between 1350 and 800°C [19]. Kim et al. [59] reported that nitrogen addition in the shielding gas increased the corrosion resistance because it reduced the elemental partitioning of Cr and Mo between the two phases. In another work, Kim *et al.* [60] found that the addition of N_2 gas in the Ar shielding gas also strengthens the reformation of the γ-phase during the solidification, which affects positively the corrosion resistance. As γ-phase content is increased, the precipitation of Cr_2N is reduced at the intergranular and intragranular site of the δ-phase.

The PREN expression neglects the pH, the effect of microstructure, surface state, temperature, amount of inclusions and precipitates in the metal microstructure, all of which certainly influences the beneficial role played by the alloying elements on the pitting corrosion resistance [8]. These often forgotten precautions when working with PREN are especially important in the case of DSS, as these elements are not evenly distributed between the two phases, and even more so if heat treatment is not optimized or if it induces the precipitation of deleterious phases such as sigma [8]. Tan *et al.* [18] have demonstrated that the pitting corrosion resistance of a specimen was closely related to the PREN value of the ferrite phase. Pitting occurred in the ferrite phase for all the specimens, indicating that ferrite phase is less resistant than the austenite phase. Zhang *et al.* [61] found some pits in the γ phase for the as-annealed specimen, which indicates that the γ phase is a weak phase for the as-annealed specimen. According to them [61] this can be explained by the difference in the pitting resistance equivalent numbers (PRENs) between the two phases in the DSS. The δ phase of the as-annealed specimens was enriched in the elements Cr and Mo, and the γ phase was enriched in the elements Ni and Mn. The PREN of the γ phase was lower than that of the δ phase in this case.

According to Chen *et al*. [19], as the cooling rate increases, PREN of ferrite phase decreases while that of austenite phase increases. At lower cooling rate, there is more time for Cr and Mo to concentrate in ferrite phase. Due to the lower PREN value of ferrite phase than that of austenite phase, ferrite phase is less resistant and pitting will occur in ferrite phase. In a work performed by Mesquita *et al.* [8], the effect of Mo was evaluated. According to them [8], pits are preferentially nucleated in the usually less

resistant ferrite phase in the absence of Mo (lower PREN for ferrite phase), and in the presence of Mo (higher PREN for ferrite phase), however, ferrite gets much more corrosion resistant so that it overtakes the usually more resistant austenitic phase.

A great number of investigations have studied the effect of alloying elements, especially N, which is most effective in the formation of austenite [16,18,19,25,27]. According to Hsieh *et al.* [28] both nitrogen and nickel are effective austenite formers; however, the effect of nitrogen on the reformation of austenite is much greater than that of nickel. Contrary to the resistance at the initiation of the corrosion, the Ni content has an influence on the propagation rate of the corrosion [62]. According to Cui and Lundin [62], nickel is effective in promoting repassivation and chromium is the essential element in forming this passive film. When these two elements are at low levels, the passive film is rather weak in its resistance to corrosion attack.

Bhatt *et al.* [35] found that in the presence of 5 and 10% nitrogen in the shielding gas during welding, the ferrite contents decreases to 35 and 29%, respectively, resulting in an improved pitting corrosion resistance of the weldments obtained by using a gas tungsten arc. Concerning the Mo, Mesquita *et al.* [8] discussed the stronger beneficial effect on the corrosion resistance of ferrite compared to austenite. The overall corrosion resistance of Mo-containing DSS grades is increased.

The pitting corrosion resistance of 2304 DSS after autogenous plasma-arc welding has been investigated by Tan *et al.* [24]. In this study, the as-welded joint displayed impaired pitting corrosion resistance and pitting preferentially occurred at ferrite grains in the HAZ near the fusion line. In another study in welded joints of 2304 DSS, Chen *et*

al. [19] found that pitting also occurred in the ferrite phase for all simulated HAZ specimens and is influenced by Cr_2N and inclusions. According to their results, the pitting corrosion resistance of the HAZ in 2304 DSS decreased with the cooling rate.

Cr_2N is often found to precipitate in the ferrite phase [10,11,18-20,24,26,33,61]. These precipitates resulted in depletion in Cr in the adjacent matrix region. The chromium-depleted zones provide a favorable site for pitting corrosion nucleation, as reported by several authors [11,18-20,24,26,33,61]. The pitting corrosion resistance can be maintained when the austenite content does not fall below 25% due to the decrease of the precipitation of Cr_2N. However with nitrogen and nickel contents lower than 0.15 and 5.5% (for example in the case of the steel studied), respectively, the reformation of austenite is limited, even if the cooling time is increased, and will result in the formation of Cr_2N [28].

On various DSSs, many efforts have been made to find the optimum phase balance for the highest resistance against pitting corrosion [11,15,19,28,63]. Tan *et al.* [18] reported that a typical problem in the heat affected zone (HAZ) of as-welded low nickel DSS is the precipitation and/or dissolution of nitrides within ferrite and at ferrite–austenite interfaces with the generation of γ_2. A great number of investigations have been carried out on the HAZ of DSS [23,25,64].

The Cr_2N formed in the as-welded UNS S31803 duplex stainless steel was analyzed by Zhang *et al.* [65] using transmission electron microscopy (TEM). The Figure 3.7 indicates a rod-like Cr_2N, which precipitated intragranularly or along the ferrite grain boundaries.

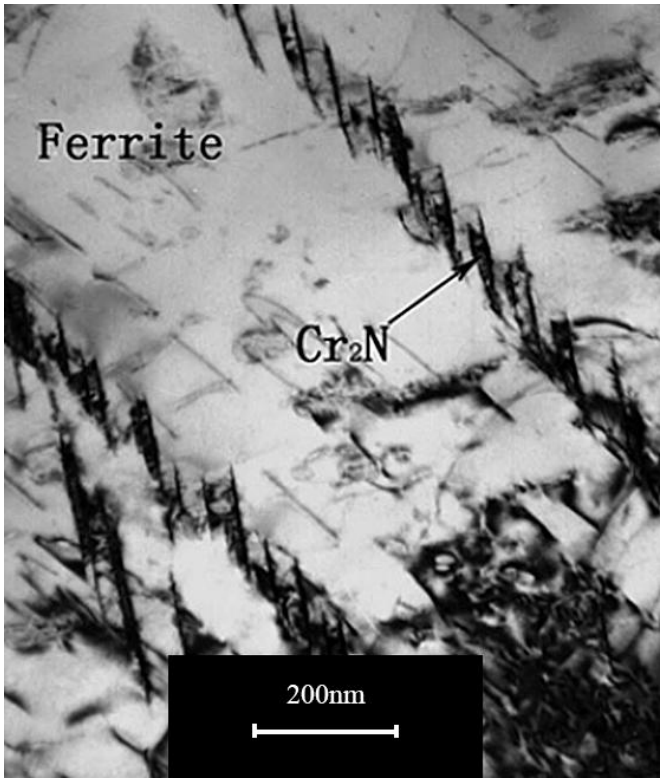

Figure 3.7: TEM of Cr_2N in the as-welded metal UNS S31803 [65].

3.5. References

[1] Salvi, B.L.; Panwar, N.L. *Renewable and Sustainable Energy Reviews*, **2012**, *16*, 3680.

[2] Hassan, M. Hj.; Kalam, Md. A. *Procedia Engineering*, **2013**, *56*, 39.

[3] Agarwal, A.K. *Progress in Energy and Combustion Science*, **2007**, *33*, 233.

[4] Garcia, C.M.; Teixeira, S.; Marciniuk, L.L.; Schuchardt, U. *Bioresource Technology*, **2008**, *99*, 6608.

[5] Torres, C.E.A.S. *MSc. Thesis*, Belo Horizonte, Brazil, **2013**.

[6] ANP – Agência Nacional Do Petróleo, Gás Natural e Biocombustíveis. *Superintendência de Refino, Processamento de Gás Natural e Produção de Biocombustíveis*, **2015**.

[7] Lo, K.H.; Shek, C.H.; Lai, J.K.L. *Materials Science and Engineering: R: Reports*, **2009**, *65*, 39.

[8] Mesquita, T.J.; Chauveau, E.; Mantel, M.; Kinsman, N.; Roche, V.; Nogueira, R.P. *Materials Chemistry and Physics*, **2012**, *132*, 967.

[9] Sieurin, H.; Sandström, R. *Materials Science and Engineering: A*, **2006**, *418*, 250.

[10] Chehuan, T.; Dreilich, V.; De Assis, K.S.; De Sousa, F. V.V.; Mattos, O. R. *Corrosion Science*, **2014**, *86*, 268.

[11] Ha, H.-Y.; Jang, M.-H.; Lee, T.-H.; Moon, J. *Corrosion Science*, **2014**, *89*, 154.

[12] Asif M, M.; Shrikrishna, K.A.; Sathiya, P.; Goel, S. *Journal of Manufacturing Processes*, **2015**, *18*, 92.

[13] Westin, E.M.; Olsson C.-O.A.; Hertzman S. *Corrosion Science*, **2008**, *50*, 2620.

[14] Davison, R.M.; Redmond, J.D. *Materials & Design*, **1991**, *12*, 187.

[15] Kang, D.H.; Lee, H.W. *Corrosion Science*, **2013**, *74*, 396.

[16] Garzón, C.M.; Ramirez, A.J. *Acta Materialia*, **2006**, *54*, 3321.

[17] Westin, E.M. *PhD. thesis*, Stochholm, Sweden, **2010.**

[18] Tan, H.; Wang, Z.; Jiang, Y.; Yang, Y.; Deng, B.; Song, H.; Li, J. *Corrosion Science***, 2012**, *55*, 368.

[19] Chen, L.; Tan, H.; Wang, Z.; Li, J.; Jiang, Y. *Corrosion Science*, **2012**, *58*, 168.

[20] Jiang, Y.; Tan, H.; Wang, Z.; Hong, J.; Jiang, L.; Li, J. *Corrosion Science*, **2013**, *570*, 252.

[21] Nowacki, J.; Łukojć, A. *Journal of Materials Processing Technology*, **2005**, *164–165*, 1074.

[22] Zanotto, F.; Grassi, V.; Merlin, M.; Balbo, A.; Zucchi, F. *Corrosion Science*, **2015**, *94*, 38.

[23] Nowacki, J.; Łukojć, A. *Materials Characterization*, **2006**, *56*, 436.

[24] Tan, H.; Wang, Z.; Jiang, Y.; Han, D.; Hong, J.; Chen, L. *Corrosion Science*, **2011**, *53*, 2191.

[25] Ramirez, A.J.; Brandi, S.D.; Lippold, J.C. *Science and Technology of Welding and Joining*, **2004**, *9*, 301.

[26] Ramirez, A. J.; Lippold, J.C.; Brandi, S.D. *Metallurgical and Materials Transactions A*, **2003**, *34A*, 1575.

[27] Weber, L.; Uggowitzer, P. J. *Materials Science and Engineering: A*, **1998**, *242*, 222.

[28] Hsieh, R.-I.; Liou, H.-Y.; Pan, Y.-T. *Journal of Materials Engineering and Performance*, 2**001**, *10*, 526.

[29] Alvarez, S. M.; Bautista, A.; Velasco, F. *Corrosion Science*, **2011**, *53*, 1748.

[30] Pilhagen, J.; Sandström, R. *Materials Science and Engineering: A*, **2014**, *602*, 49.

[31] Aguiar, I.; Pérez Escobar, D.; Santos, D. B.; Modenesi, P. J. *Revista Matéria*, **2015**, *20*, 212.

[32] Sarlak, H.; Atapour, M.; Esmailzadeh, M. *Materials and Design*, **2015**, *66*, 209.

[33] Liou, H.-Y.; Hsieh, R.-I.; Tsai, W.-T. *Materials Chemistry and Physics*, **2002**, *7*, 33.

[34] Ha, H.-Y.; Kwon, H.-S. *Electrochimica Acta*, **2007**, *52*, 2175.

[35] Bhatt, R.B.; Kamat, H.S.; Ghosal, S.K.; De, P.K. *Journal of Materials Engineering and Performance*, **1999**, *8*, 591.

[36] Messler Jr., R. W. Principles of welding: Processes, physics, chemistry, and metallurgy. *John Wiley & Sons*, **1999**, NY, USA.

[37] McCafferty, E. Introduction to corrosion Science. *Springer*, **2012**, VA, USA.

[38] N. Birbilis, R. G. Buchheit, *J. Electrochem. Soc.* **2005**, *152*, B140.

[39] Chan, K. W.; Tjong, S. C. *Materials*, **2014**, *7*, 5268.

[40] Hakiki, N. E. *Corrosion Science*, **2011**, *53*, 2688.

[41] Sato, N. *Corrosion Science*, **1990**, *31*, 1.

[42] Zheng, Z. J.; Gao, Y.; Gui, Y.; Zhu, M. *Journal of Solid State Electrochemistry*, **2014**, *18*, 2201.

[43] Marcus, P.; Maurice, V.; Strehblow, H. H. *Corrosion Science*, **2008**, *50*, 2698.

[44] Di Paola, A. *Electrochimica Acta*, **1989**, *34*, 203.

[45] Fattah-alhosseini, A.; Vafaeian, S. *Journal of Alloys and Compounds*, **2015**, *639*, 301.

[46] Gadala, I. M.; Alfantazi, A. *Applied Surface Science*, **2015**, *357*, 356.

[47] BenSalah, M.; Sabot, R.; Triki, E.; Dhouibi, L.; Refait, Ph.; Jeannin, M. *Corrosion Science*, **2014**, *86*, 61.

[48] Pieretti, E. F.; Manhabosco, S. M.; Dick, L. F P.; Hinder, S.; Costa, I. *Electrochimica Acta*, **2013**, *124*, 150.

[49] Macdonald, D. D. *Journal of the Electrochemical Society*, **1992**, *139*, 3434.

[50] Soltis, J. *Corrosion Science*, **2015**, *90*, 5.

[51] Burstein, G. T.; Liu, C.; Souto, R. M.; Vines, S. P. *Corrosion Engineering, Science and Technology*, **2004**, *39*, 25.

[52] Frankel, G. S. *Journal of the Electrochemical Society*, **1998**, *145*, 2186.

[53] Frankel, G. S.; Sridhar, N. *MaterialsToday*, **2008**, *11*, 38.

[54] Mohammadi, F.; Eliyan, F. F.; Alfantazi, A. *Corrosion Science*, **2012**, *63*, 323.

[55] Garcia, C.; Martin, F.; de Tiedra, P.; Blanco, Y.; Lopez, M. *Corrosion Science*, **2008**, *50*, 1184.

[56] Yang, Y.; Yan, B.; Li, J.; Wang, J. *Corrosion Science*, **2011**, *11*, 3756.

[57] Hoar, T.P. *Corrosion Science*, **1967**, *7*, 341.

[58] Baker, M. A.; Castle, J. E. *Corrosion Science*, **1992**, 33, 1295.

[59] Kim, S.-T.; Jang, S.-H.; Lee, I.-S.; Park, Y.-S. *Corrosion Science*, **2011**, *53*, 1939.

[60] Kim, H.-J.; Jeon, S.-H.; Kim, S.-T.; Park, Y.-S. *Corrosion Science*, **2015**, *91*, 140.

[61] Zhang, Z.; Zhao, H.; Zhang, H.; Yu, Z.; Hu, J.; He, L.; Li, J. *Corrosion Science*, **2015**, *93*, 120.

[62] Cui, Y.; Lundin, C. D. *Materials & Design*, **2007**, *28*, 324.

[63] Tsuge, H.; Tarutani, Y.; Kudo, T. *Corrosion - NACE*, **1988**, *18*, 305.

[64] Bettini, E.; Kivisäkk, U.; Leygraf, C.; Pan, J. *Electrochimica Acta*, **2013**, *113*, 280.

[65] Zhang, Z.; Wang, Z.; Jiang, Y.; Tan, H.; Han, D.; Guo, Y.; Li, J. *Corrosion Science*, **2012**, *62*, 42.

[66] Williams, D. B.; Carter, C. B. Transmission Electron Microscopy. A Textbook for Materials Science, *Springer*, **2009**, 2ed, NY, USA.

[67] Brett, C. M. A.; Brett, A. M. O. Electrochemistry: Principles, Methods, and Applications, *Oxford University Press*, **1993**, 1ed.

[68] Jorcin, J.-B.; Orazem, M. E.; Pébère, N., Tribollet, B. *Electrochimica Acta*. **2006**, *51*,1473.

[69] Orazem, M. E.; Tribollet, B. Electrochemical impedance spectroscopy, *John Wiley & Sons*, **2008**, New Jersey, USA.

[70] Belkaid, S.; Ladjouzi, M. A.; Hamdani, S. *Journal of Solid State Electrochemistry*, **2011**, *15*, 525.

4. PITTING CORROSION OF WELDS IN UNS S32304 LEAN DUPLEX STAINLESS STEEL

Dalila C. Sicupira[a,b], G.S. Frankel[b], Vanessa de F. C. Lins[a]

[a] Chemical Engineering Department, Federal University of Minas Gerais, 6627, Antônio Carlos Avenue, Pampulha, Belo Horizonte, MG 31270-901, Brazil

[b] Fontana Corrosion Center, Dept. of Materials Science and Engineering, The Ohio State University, Columbus, OH 43210, USA

Abstract

The pitting corrosion of welded joints of lean duplex stainless steel (LDSS) UNS S32304 was studied. LDSS S32304 thick plates were welded by different processes commonly employed in the manufacture of equipment and piping: shielded metal arc welding, gas metal arc welding and flux cored arc welding. The electrochemical behavior of different weldment zones (fusion zone, base metal and heat affected zone (HAZ)) was characterized both independently, using an electrochemical microcell, and together by testing the whole welded area. The electrochemical testing was performed in acidified glycerin, a process fluid of the biodiesel industry. The HAZ was the most susceptible zone for pitting corrosion for all samples. The results were correlated to the microstructural features of the materials. Finally, the results from the microcell and whole weld approaches were compared. According to the results, the gas metal arc welding process with 2209 as filler metal was found to be the optimum for application of 2304 duplex stainless steels in the acidified glycerin environment.

Keywords: pitting corrosion, LDSS, welding process, microcell.

DOI: 10.1002/maco.201508502, Materials and Corrosion, 2015.

4.1. Introduction

Duplex stainless steel (DSS) alloys can be cost-effective alternatives to austenitic grades with equivalent corrosion resistance, especially in applications in which the high yield strength can be utilized in the design to decrease the wall thickness of pipelines and equipment [1,2]. The number of applications for DSS has increased steadily and new alloys are continuously developed. Lately, the main focus has been on lean duplex grades (LDSS), and the fluctuating alloying element prices (especially Ni and Mo) during the last decade has accelerated the development and the amount of applications for these steels [1,2].

The weldability of modern DSS is satisfactory, although the heat-affected zone and the weld metal in general exhibit higher ferrite content and coarser grains than the base material [3]. Compared with the earlier generation of duplex steels, weldability has been improved appreciably by the introduction of nitrogen as an alloying element. However, the precipitation of secondary phases that include intermetallic phases (σ, χ) and nonmetallic compounds (Cr_2N, CrN) exerts a detrimental influence on the corrosion properties because they can induce the segregation of alloying elements and the formation of chromium-depleted zones [4-8]. The formation of δ-ferrite is other

parameter that is also a concern because of its susceptibility to attack in corrosive environments [7].

The most typical problems of welded DSS are associated with the heat-affected zone (HAZ), not with the fusion zone (FZ), since the properties of the FZ could be improved by using high-alloyed filler metal and N_2-containing shield gas. A great number of investigations have been carried out on the HAZ of DSSs [4,7,9-17]. Few studies on the HAZ of multi-pass welds have been reported even though multi-pass welding is more common during industrial fabrication, especially for plates or pipes of medium thickness. The corrosion over time becomes preferential and increasingly localized, accelerating to cause continuous weakening and thinning of a pipeline, for example, and thus making it more susceptible to dangerous ruptures [10].

The pitting corrosion resistance of 2304 duplex stainless steels after autogenous plasma-arc welding and subsequent short-time post-weld heat treatment at different temperatures was investigated by Tan *et al.* [18]. As-welded joints displayed impaired pitting corrosion resistance and pitting preferentially occurred at ferrite grains in the HAZ near the fusion line. Chen *et al.* [19] found that the pitting corrosion resistance of the HAZ in 2304 duplex stainless steels decreased with cooling rate and pitting occurred in the ferrite phase, and also that the pitting corrosion resistance of the HAZ in duplex stainless steels may be influenced by Cr_2N and inclusions.

Microelectrochemical methods are powerful techniques to study localized corrosion processes on small areas of passive metals. Many papers have used microelectrode cells to study working areas in the μm-nm range [13-16,20]. Corrosion processes such as

pitting, intergranular corrosion, stress corrosion cracking, crevice corrosion or galvanic corrosion have been mainly studied based on large-scale experiments (working electrode in the mm^2– cm^2 range) [1,2,10,21-25]. However, such processes are due to mechanisms on a smaller scale. Therefore, it is advisable to develop appropriate small-scale experimental devices that interrogate a small exposed surface area of the working electrode. Additionally, these experimental devices can be applied to cases in which a heterogeneous material is the focus of interest, as in the study of welded joints [16]. The main benefit of using microcells is directly related to the small size of the exposed working area, which is in the micrometer range, although some drawbacks for capillary microcells must be considered, as has been explained by Birbilis *et al.* [20].

Improved the understanding of the corrosion resistance of LDSS can minimize costs related to corrosion in different types of industries in which it may be used, for example, in the biodiesel industry. In Brazil, biodiesel is typically produced by a transesterification process using a methyl route, and a basic catalyst [26]. At a point in the process, hydrochloric acid aqueous solution is added to neutralize the catalyst. The biodiesel industry has experienced a significant number of failures (holes in pipes) caused by corrosion in acidified medium, which cause production losses and, consequently, economic losses. Although several studies related to the effect of heat input and thermal cycles on the microstructure of pipeline steels have been performed [1,9-11,27], there are few studies related to corrosion of LDSS in biodiesel plants.

In this context, the objective of this work is to evaluate the corrosion resistance of LDSS UNS S32304 plates welded by various processes commonly employed in the manufacture of equipment and piping: shielded metal arc welding (SMAW), gas metal

arc welding (GMAW) and flux cored arc welding (FCAW) in acidified glycerin, a by-product of biodiesel industry, which is a gap in literature. Samples of the FZ, HAZ, base metal (BM), and the whole weld were evaluated.

4.2. Materials and Methods

4.2.1. Sample preparation

Measurements were performed on welded joints of UNS S32304 type LDSS with composition Ni: 3.63 wt.%, Cr: 22.45, Mn: 1.35, S: 0.0004, Si: 0.39, P: 0.028, Mo: 0.44, N: 0.113 and C: 0.019. The LDSS UNS S32304 was provided by Aperam South America in the form of plates of 22 mm nominal thickness, 350 mm long and 180 mm wide. For each welding process, two filler metals with different chemical compositions, (23%Cr 7%Ni) and (22%Cr 9%Ni 3%Mo) were evaluated.

This work is a continuation of a project [28] in which the welded samples were prepared. The details of the welding parameters are presented in Tables IV.1 and IV.2. The filler metal compositions are shown in Table IV.3.

Table IV.1: Welding process, consumable and gas of protection used [26].

Identification	**EN Specification**	**Filler metal**	**Diameter (mm)**	**Shielding Gas**
SMAW 2307	E Z 23 7 N L R	23%Cr7%Ni	3.25	-
SMAW 2209	E 22 9 3 N L R 3 2	22%Cr9%Ni3%Mo	4.00	-
GMAW 2307	G 23 7 NL	23%Cr7%Ni	1.00	Star GoldTM SS[a]

GMAW 2209	G 22 9 3 NL	22%Cr9%Ni3%Mo	1.00	Star GoldTM SS[a]
FCAW 2307	T 23 7 N L P	23%Cr7%Ni	1.20	75%Ar+25%CO_2
FCAW 2209	T 22 9 3 N L P	22%Cr9%Ni3%Mo	1.20	75%Ar+25%CO_2

[a]Star Gold SS: Ar+CO_2+N_2 supplied by Praxair.

Table IV.2: Welding parameters [26].

Identification	**Passes**	**Current (A)**	**Voltage (V)**	**Speed (cm/ min)**	**Heat input (kJ/mm)**	**T interpasses (°C)**
SMAW 2307	Root	85	25.0	11.3	1.13	-
	Others	135	31.1	14.8	1.70	100-150
SMAW 2209	Root	140	29.0	12.1	2.01	-
	Others	160	28.7	15.9	1.73	100-150
GMAW 2307	Root	210	29.0	13.6	2.69	-
	Others	213	29.0	23.1	1.60	100-150
GMAW 2209	Root	195	29.0	15.3	2.21	-
	Others	212	29.0	23.3	1.58	100-150
FCAW 2307	Root	208	29.0	23.2	1.56	-
	Others	210	29.0	23.2	1.58	100-150
FCAW 2209	Root	210	29.0	23.3	1.57	-
	Others	210	29.0	22.9	1.59	100-150

Table IV.3: Chemical composition of the filler metals used (wt. %) [26].

Welding process	**Filler metal**	**C**	**Mn**	**Si**	**P**	**S**	**Cr**	**Ni**	**Mo**	**Cu**	**N**
SMAW	2307	0.028	0.78	0.96	0.017	0.014	22.6	7.62	0.36	0.26	0.14
SMAW	2209	0.027	0.79	0.99	0.019	0.012	21.92	9.31	3.15	0.06	0.14
GMAW	2307	0.03	0.88	0.86	0.017	0.01	23.82	8.92	0.31	0.095	0.13
GMAW	2209	0.029	1.47	0.57	0.02	0.009	21.94	9.20	3.12	0.14	0.14
FCAW	2307	0.024	0.92	0.96	0.018	0.011	23.7	8.93	0.3	0.095	0.12
FCAW	2209	0.022	1.06	0.91	0.022	0.013	21.66	9.2	2.94	0.18	0.15

The welded samples were cut transversely to the welding direction, to make possible the evaluation of the FZ, HAZ, and BM regions, and also of both the root (R) and top (T) regions of the welded joints. The specimens sizes were approximately 5 x 30 x 5 mm, as shown in Figure 4.1.

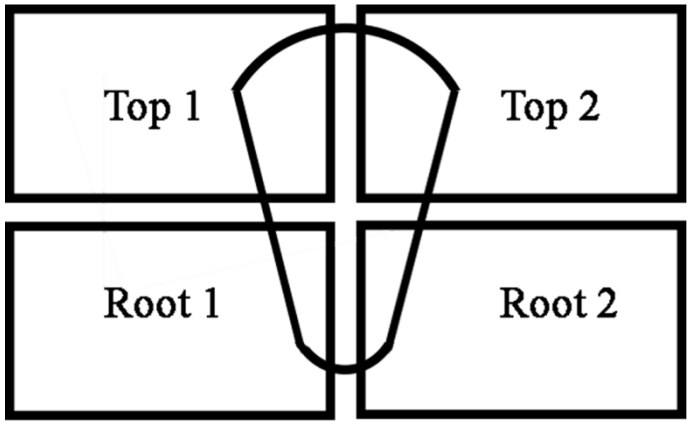

Figure 4.1: Representation of cutting samples for localized corrosion test.

Electrical contact was made by welding a copper wire on the back of the samples, which were then mounted in epoxy resin. The samples were ground to 600 grit and stored in a desiccator. Before each experiment, the edge between the sample and epoxy was sealed by black wax to minimize crevice corrosion. The acidified glycerin solution was prepared based on the composition supplied by Petrobras Biocombustível (PBIO). The base electrolyte was 49% glycerin + 29% methanol + 17% water + 3% sodium chloride (%wt.). The tests were carried out in acidified glycerin at pH 5.8.

4.2.2. Microstructure analysis

Microstructural examination of specimens was conducted using a light optical microscope (Olympus PME 3, LECO). The specimens were first prepared by polishing to a 1µm finish, and electrolytically etching in 10% oxalic acid electrolyte at 6 V for 60s.

4.2.3. Potentiodynamic polarization testing

Potentiodynamic polarization testing was performed using a Gamry Reference 600 potentiostat. A conventional three-electrode cell was used, the working electrodes being prepared from the LDSS welded samples with an exposed surface of approximately 1 cm^2. The reference was a saturated calomel electrode (SCE) and a Pt mesh was used as the counter electrode. The tests were performed under constant stirring and at a temperature of 65±1°C to simulate the operational conditions of the pipes.

The open circuit potential (OCP) in acidified glycerin solution (pH=5.8) was measured for 1 h and the potentiodynamic polarization curves were then measured at a scan rate 0.167 mV/s. After that, microstructural observations were carried out using scanning electron microscopy (SEM, Sirion XL-30, FEI).

4.2.4. Electrochemical microcell testing

The local electrochemical behavior of specimens was studied at room temperature using the electrochemical microcell technique. This technique utilized a glass micro-capillary filled with the electrolyte, as shown in Figure 4.2.

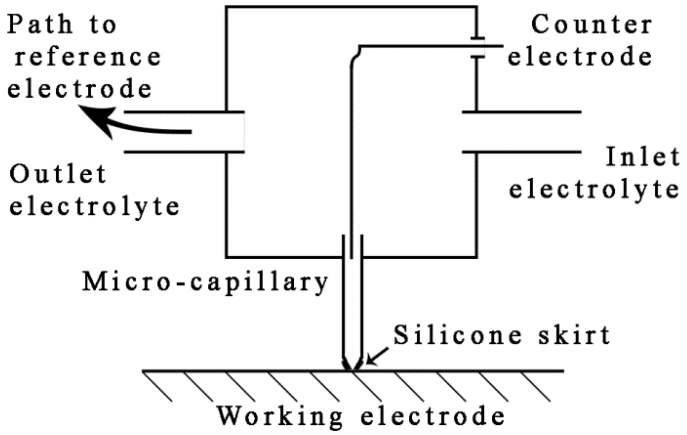

Figure 4.2: Schematic drawing of the microcell (Adapted from [18]).

The micro-capillary tip was sealed to the sample surface with a layer of silicone rubber. The entire setup was placed in a Faraday cage. The diameter of the tip was 200 μm, the counter electrode was a platinum wire and a saturated calomel electrode (SCE) as reference.

The tests were carried out in acidified glycerin at pH 5.8. The open circuit potential (OCP) was allowed to stabilize for a period of 5 min and the cyclic potentiodynamic polarization curves were then measured at a scan rate 5 $mV.s^{-1}$. The short stabilization and relatively fast scan rate were used to minimize the test duration and thereby avoid any issues with cell leakage, or the establishment of concentration gradients in the capillary. As discussed by Birbilis and Buchheit [20] the nominal cell resistance (responsible for IR–drop) is comparatively high with respect to other systems, with values approaching 10 kΩ recorded. However, since the absolute currents measured during testing were typically below 10^{-7} A, the ohmic drop was negligible, less than 1 mV. The scanning direction was reversed when the current density reached 5 $mA.cm^{-2}$. Three replicate tests of each measurement were performed and the most typical of the results are presented. After testing, optical microscopy was used to observe the corrosion morphology.

4.3. Results and discussion

Figure 4.3 shows the microstructure of the base metal (a) and top samples welded by SMAW (b), GMAW (c) and FCAW (d) processes using 2209 as the filler metal. The base metal, as shown in figure 4.3(a), exhibits the typical microstructural features of DSS: island-like γ phase, surrounded by the continuous matrix of the δ-ferrite phase. In general, similar microstructures were observed for each welded sample analyzed. The FZ structure consists of austenite grains in the form of Widmanstätten plate precipitates and secondary austenite (γ_2) within a matrix of ferrite. As expected, the samples showed higher proportions of austenite in the FZ than in HAZ. Inclusions are present in the FZ, which were suggested previously [28] to be (Mn, Si)-oxides. The HAZ also exhibited

chromium nitrides, primarily in the interior of the ferrite grains (Fig. 4.3(b-d)). LDSSs contain high concentrations of nitrogen, which plays an important role for improving the crevice and pitting corrosion of the austenite phase in chloride environments. However, nitrogen has a lower solubility in ferrite than in austenite and increasing nitrogen additions can cause chromium nitride precipitation and the subsequent formation of γ_2, especially in the HAZ in welded joints due to the influence of welding thermal cycle [19, 29-32]. According to Ramirez *et al.* [32] heterogeneous nucleation of intragranular austenite (primary and secondary) on the intragranular nitrides is the dominant nucleation mechanism for these particles in the HAZ of the DSS. Chromium nitride stability is such that the larger precipitates serve as a substrate for heterogeneous intragranular γ_2 nucleation, but at the same time the intragranular nitrides that are dissolving within the same colony supply the required nitrogen for the transformation. Previous work [28] indicated that it was not possible to observe any noticeable microstructure difference between the 2307 and 2209 consumables. However, the GMAW process showed a higher proportion of γ in the FZ, probably due to the nitrogen addition to the shielding gas, see table IV.1

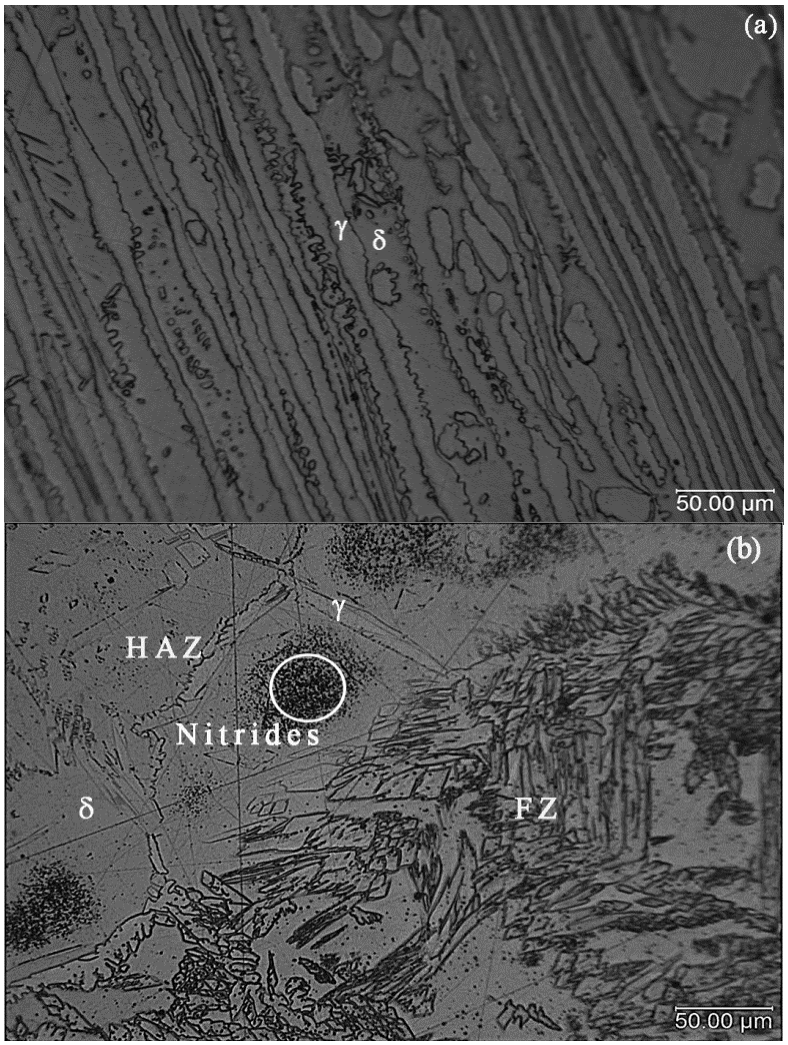
(a)
γ
δ
50.00 µm
(b)
γ
HAZ
Nitrides
δ
FZ
50.00 µm

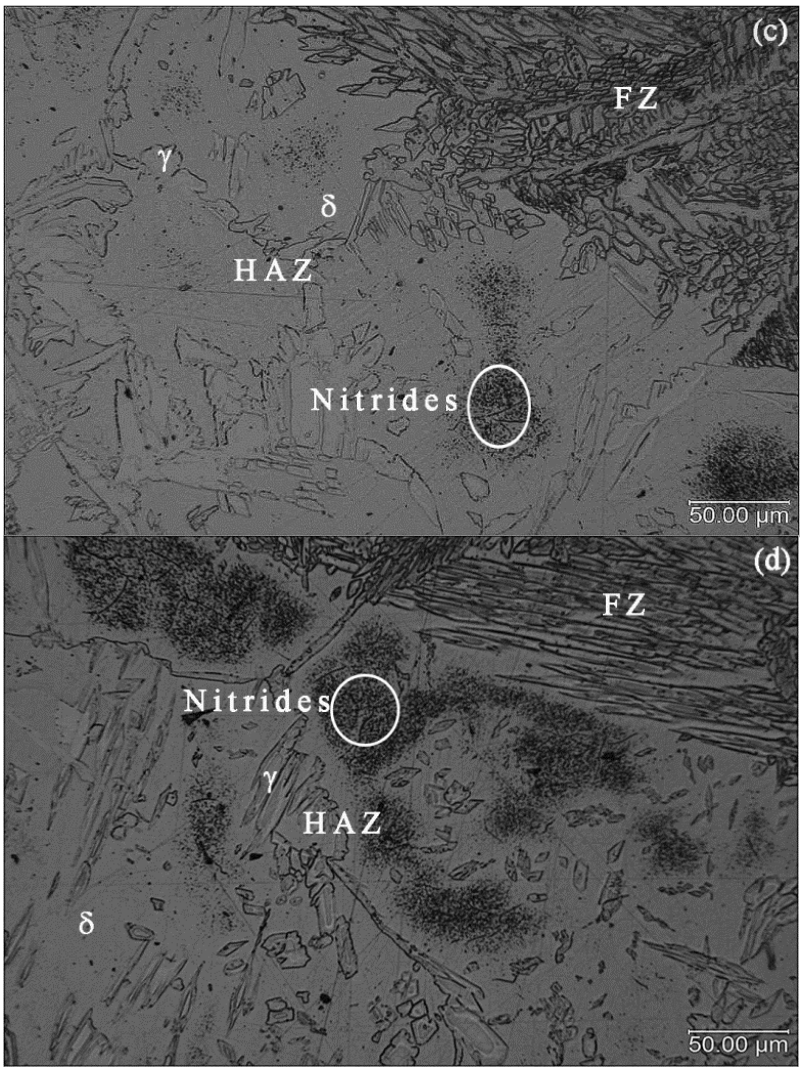

Figure 4.3: Optical microstructure of base metal (a) and top samples welded by different processes showing HAZ and FZ, 2209 as filler metal: (b) SMAW (c) GMAW (d) FCAW.

The OCP and breakdown potential (E_b) were evaluated by potentiodynamic polarization testing of the whole weld. Root (R) and top (T) regions of each welded sample were analyzed. Figure 4.4 (a-c) shows the results obtained for samples welded by SMAW, GMAW and FCAW processes, respectively. The OCP values and breakdown potentials of as-received and welded samples are also presented in Figure 4.5.

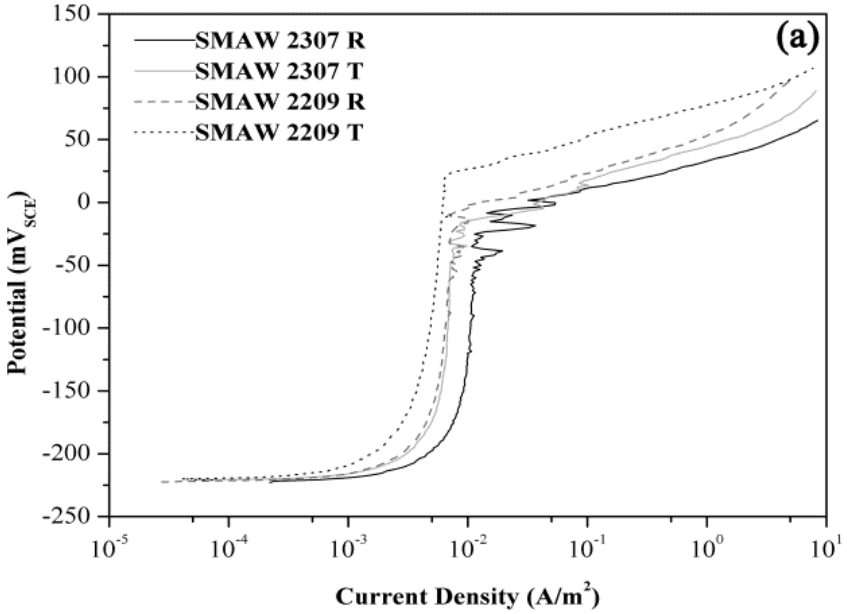
(a)
SMAW 2307 R
SMAW 2307 T
SMAW 2209 R
SMAW 2209 T
Potential (mV$_{SCE}$)
Current Density (A/m^2)

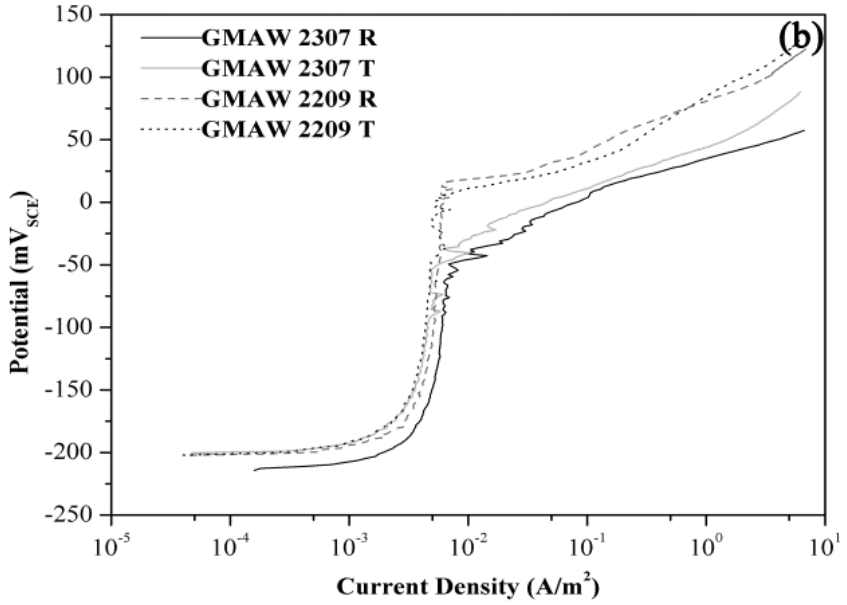
(b)
GMAW 2307 R
GMAW 2307 T
GMAW 2209 R
GMAW 2209 T
Potential (mV$_{SCE}$)
Current Density (A/m^2)

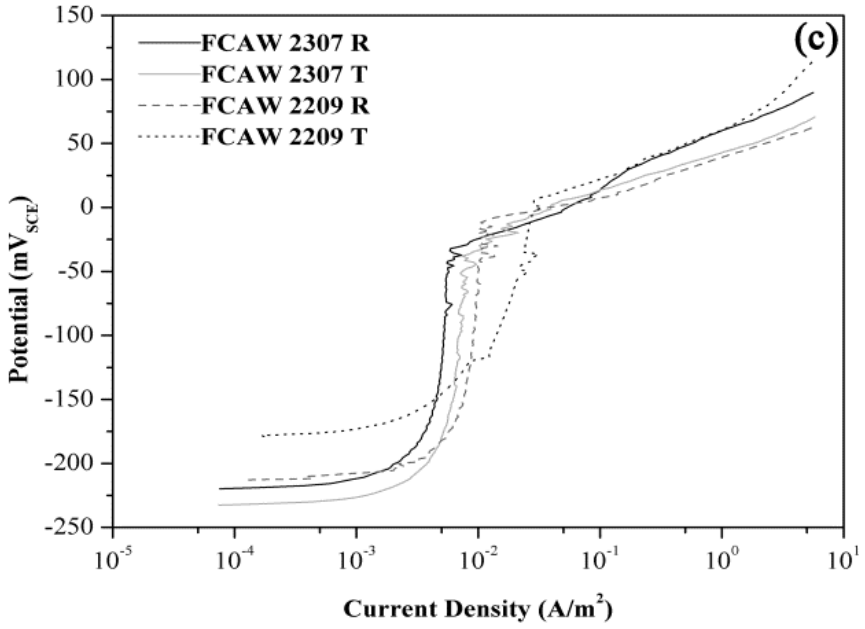

Figure 4.4: Potentiodynamic polarization curves for (a) SMAW (b) GMAW and (c) FCAW process. R denotes root, T denotes top; 2307 and 2209 refer to the filler metal.

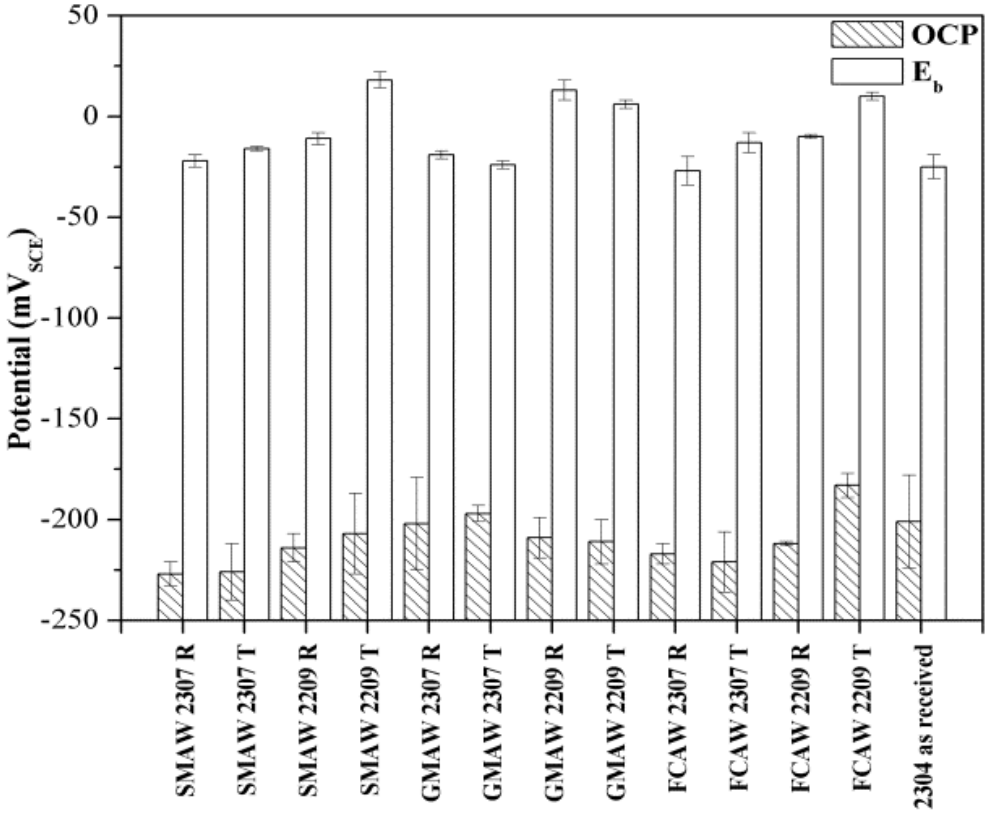

Figure 4.5: Experimental data for welded samples.

The OCP values of the welded samples were approximately -0.2V_{SCE} in the acidified glycerin. Wide passive regions were observed for all the samples tested, which is evidence of their excellent pitting corrosion resistance in this chloride-containing environment. As the potential reached about 0 mV SCE, the current density increased sharply, indicating the initiation and growth of pitting corrosion. The effect of the δ fraction was observed in the E_b levels of the samples. As described by Cardoso Junior *et al.* [28], GMAW welded joints showed higher levels of γ than the others. It is noted that the δ phase is less noble phase than the γ phase in the HAZ of welded samples.

Comparing the E_b values for the whole welded joints and for the as-received LDSS alloy in Figure 4.5, welding resulted in no significant decrease in pitting corrosion resistance. To investigate the pitting corrosion of the joints in more detail, pitting morphologies were observed by SEM, and are shown in Figure 4.6 (a-c).

Both ferrite and austenite phase were corroded, showing similar pitting corrosion resistance of ferrite phase and austenite phase (Fig. 4.6). It is easy to see that the BM and HAZ were more susceptible than the FZ as more and larger pits are evident in Fig. 4.6a and 4.6c. This enhanced susceptibility of the HAZ to pitting corrosion was found for all welded joints, and it resulted from two aspects of the microstructure evolution during welding. The Cr and Mo contents are diluted by an increase in the δ volume fraction, so the Cr and Mo content of ferrite phase in the HAZ is lower than in the parent metal and Cr_2N is often found to precipitate in the ferrite phase [7,11,18,19,31, 33-36].

In general, top samples showed higher values of E_b comparing with root samples, due to higher filler metal dilution for root regions. However, this difference is not noticeable for the GMAW process. Among the investigated welded samples, the pitting corrosion resistance after the same welding thermal cycle was the best for GMAW, which indicated the best weldability considering the corrosion resistance.

Two types of pits can be observed in Fig. 4.6. One type initiated in the vicinity of big inclusions, as shown in Fig. 4.6b. There were not many of this type of pit and these inclusions could be found in either the δ or γ phase. The interfaces between the inclusions and the adjacent matrix are incoherent and enriched in dislocations, and have been deemed to trigger pitting corrosion in chloride-based media [25,35,36]. The second type of pit was formed mostly in the δ/γ interface (Fig. 4.6c).

It is well-known that the partitioning behavior of alloying elements and the microstructure play an important role in determining the pitting resistance of duplex stainless steels [35]. Fig. 4.6c shows that the pits in the HAZ are mostly located in the ferrite/austenite interface and develop into the ferrite. This occurs because the gap of corrosion resistance in both phases is reduced due to the diffusion of the phase-stabilizing elements [35]. Furthermore, as revealed in Figure 4.3, a large amount of Cr_2N was precipitated in the HAZ. These precipitates cause Cr depletion in the adjacent region. The incoherent boundaries and chromium-depleted zones lower E_{corr} and E_b and provide a favorable site for pitting corrosion nucleation. The pits shown in Fig. 4.6c were believed to be closely related with the Cr_2N precipitates.

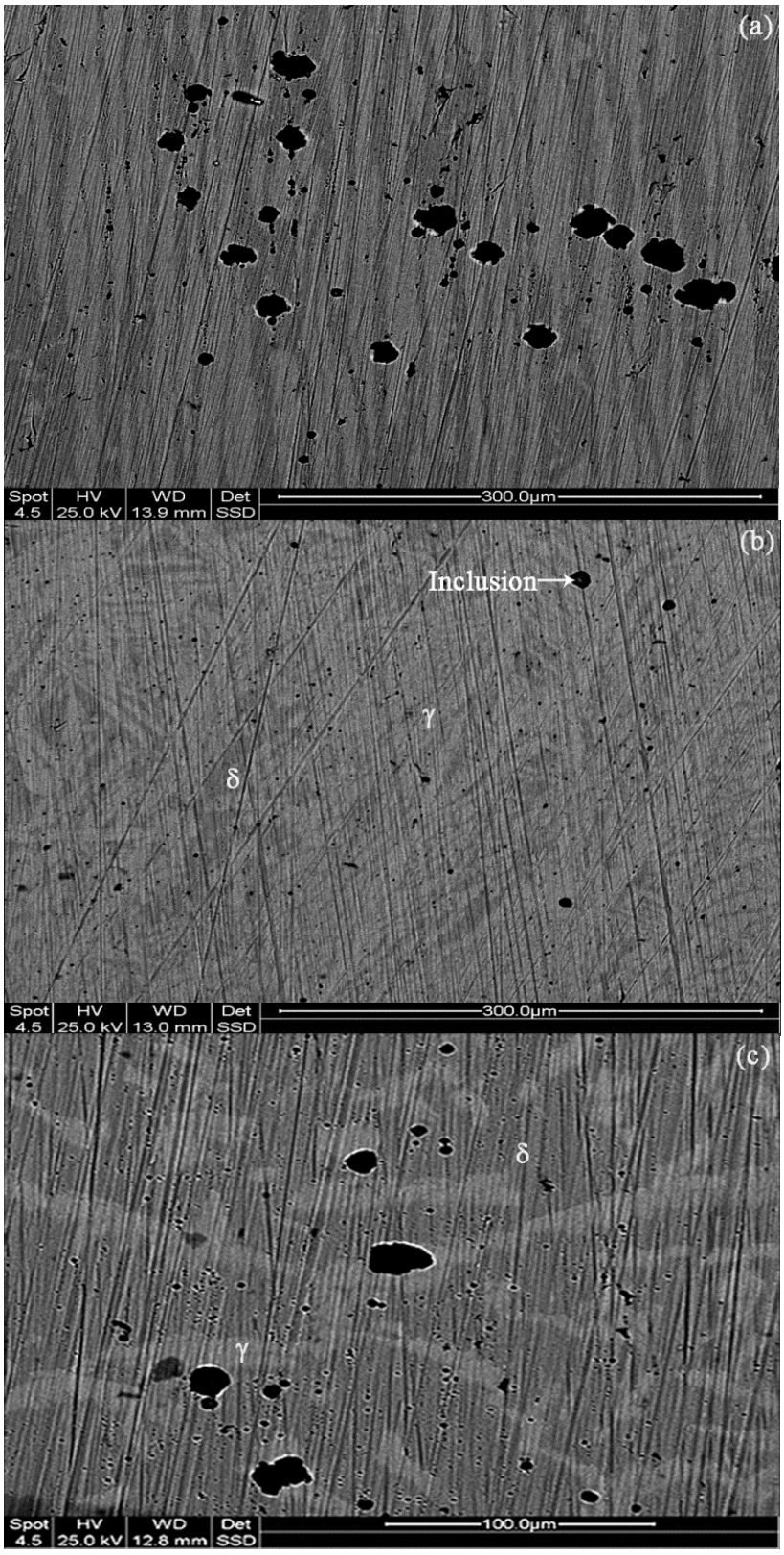

Figure 4.6: Pit morphologies of welded samples after polarization measurements (FCAW 2307 root region): (a) BM (b) FZ (c) HAZ.

The different regions (BM, HAZ and FZ) of each welded sample were tested with the microcell and the OCP and breakdown potentials (E_b) were evaluated by cyclic polarization. Root (R) and top (T) regions of each welded sample were also analyzed. Figures 4.7, 4.8 and 4.9 show the results obtained for samples welded by SMAW, GMAW and FCAW processes, respectively. The OCP values and breakdown potentials of as-received and samples welded by SMAW, GMAW and FCAW process are summarized in Figure 4.10 (a-c), respectively.

Pitting of LDSS is always associated with the breakdown of the passive film. The protective role of the passive film depends on its composition and structure, so it is expected that the changes in microstructure and composition due to welding will affect the pitting corrosion behavior. In general, the OCP values for the as-received sample were more negative than those for welded samples (Figure 4.10 (a-c)). Furthermore, by comparing different regions of the welded samples, OCP values in the FZ region were more positive than those in the HAZ region, suggesting that the FZ has better corrosion resistance than the HAZ region.

Each of the cyclic potentiodynamic polarization curves of the welded samples in Figures 4.7-4.9 exhibits spontaneous passivity above the OCP followed by a breakdown at which point the current increases rapidly. Upon reversal of the scan direction, each curve also shows a large positive hysteresis loop, with repassivation occurring near or even below the original OCP. The existence of a large hysteresis loop and low repassivation potential indicates that pit repassivation was difficult and that these materials have a high likelihood of forming pits during long time exposure to the acidified glycerin solution containing chloride. Samples welded with the filler metal

2209 exhibited more-noble pitting potential than those welded with 2307, which is attributed to the higher Ni content and Mo presence in the 2209 filler metal. Therefore, although the content of Ni and Mo extends the passive region and strengthens the passive layers [37] it does not promote the repassivation of the pits.

The HAZ regions of these welds exhibit a lower corrosion resistance in this environment than the FZ, and higher or similar E_b than for BM. The lower E_b values in the HAZ compared to the FZ might be the result of the large amount of Widmanstätten austenite (WA) in the FZ that seemed to resist pitting or localized corrosion [31], and also, the higher content of chromium nitrides in the HAZ; chromium nitride particles are believed to be nucleation sites for pitting [30,31]. According to Lindou *et al.* [9] pitting corrosion resistance of DSS HAZ may be influenced by chromium nitrides and inclusions. The region adjacent to these precipitates can be depleted in Cr and also enriched in dislocations similar to inclusions as mentioned above [13,25]. The incoherent and chromium-depleted zones can lower E_{corr} and E_b and trigger pitting corrosion in chloride-based media. According to Tsuge *et al.* [38] the nitrogen content required for achieving the same pitting resistance in both ferrite and austenite in duplex stainless steel is approximately 0.18% and, in regions with lower nitrogen content, the austenite would be less resistant to pitting. This could explain why the HAZ showed E_b higher than or similar to BM. The BM has higher austenite content than the HAZ region, and for the case of low nitrogen UNS S32304, austenite was more attacked than ferrite, see Fig. 4.6a and 4.6c. For the SMAW and FCAW welding processes, the top samples showed higher E_b than root samples. This can be explained by the smaller dilution of the filler metal for the top of the welded samples. However, the opposite was true for samples welded by GMAW process where the root was more corrosion resistant

than the top. GMAW does not involve slag formation, which can protect the fusion zone against loss of beneficial nitrogen, especially the top region. A decreased amount of nitrogen is detrimental for austenite reformation, and because of that, gas protection containing nitrogen was used for the GMAW process. The high nitrogen content also favors the formation of WA and the large amount of WA seemed to resist pitting or localized corrosion [31]. This is demonstrated in the SEM micrograph shown in Figure 4.6b, in which WA was unaffected. From the observations described above, it is evident that samples welded using filler metal 2209 had a better anodic behavior than the filler metal 2307, mostly due to the content and stabilizing role of Mo and Ni. After testing, the localized corrosion morphology was found in all cases to be small and globular pits (Figure 4.11). Considering experiments performed on the whole weld and with the microcell technique, the same tendency was observed. Top samples had higher E_b than root samples for the SMAW and FCAW welding process and, in the case of samples welded by the GMAW process, the root was more resistant than the top. Furthermore, the highest pitting corrosion resistance was obtained for GMAW with the filler metal 2209.

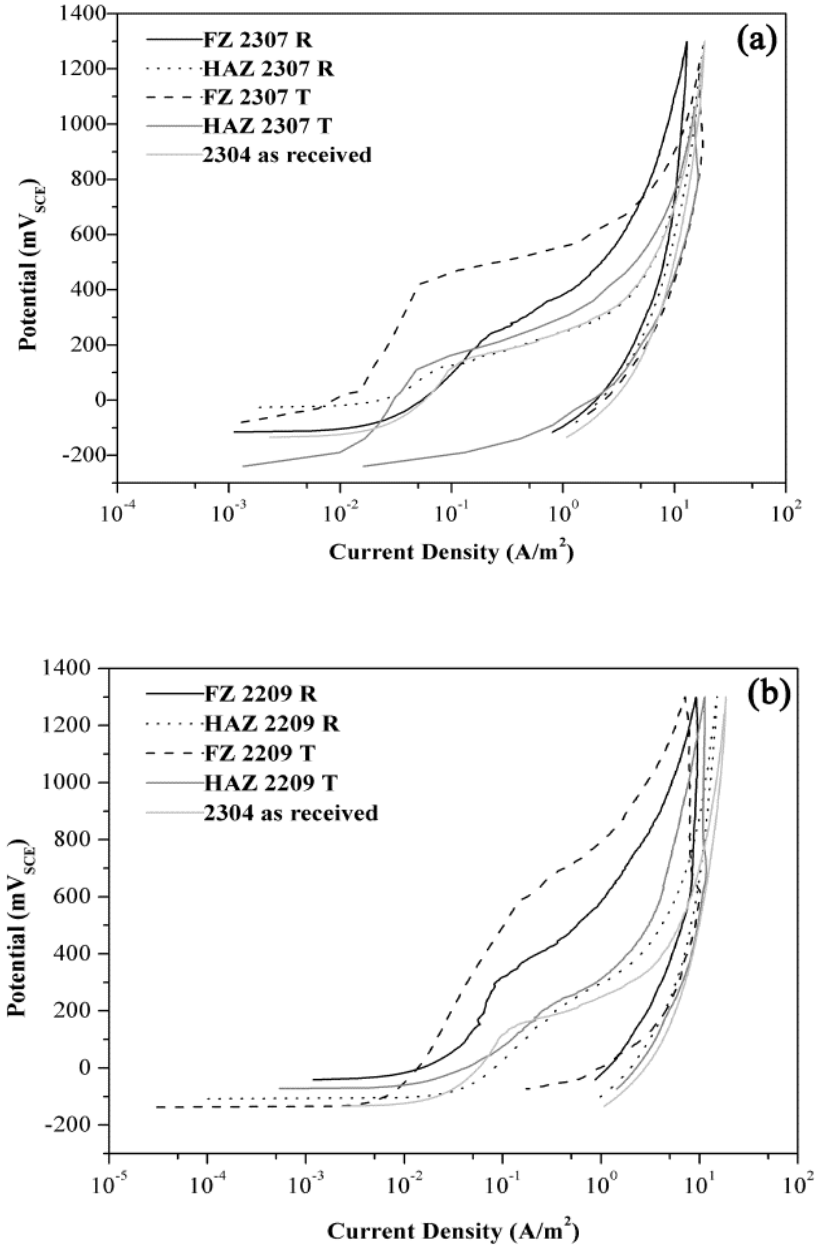

Figure 4.7: Cyclic potentiodynamic polarization curves for SMAW process: (a) 2307 as filler metal and (b) 2209 as filler metal.

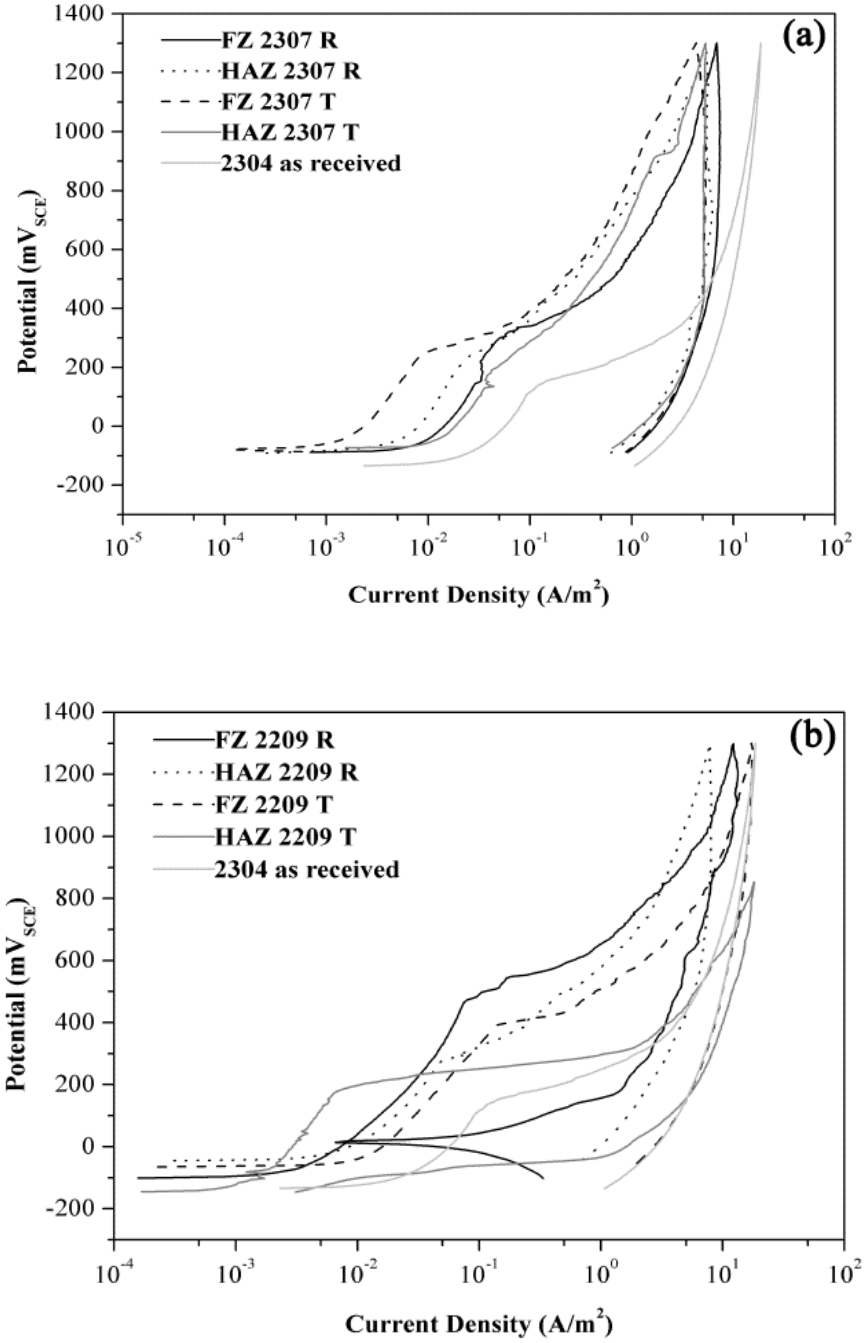

Figure 4.8: Cyclic potentiodynamic polarization curves for GMAW process: (a) 2307 as filler metal and (b) 2209 as filler metal.

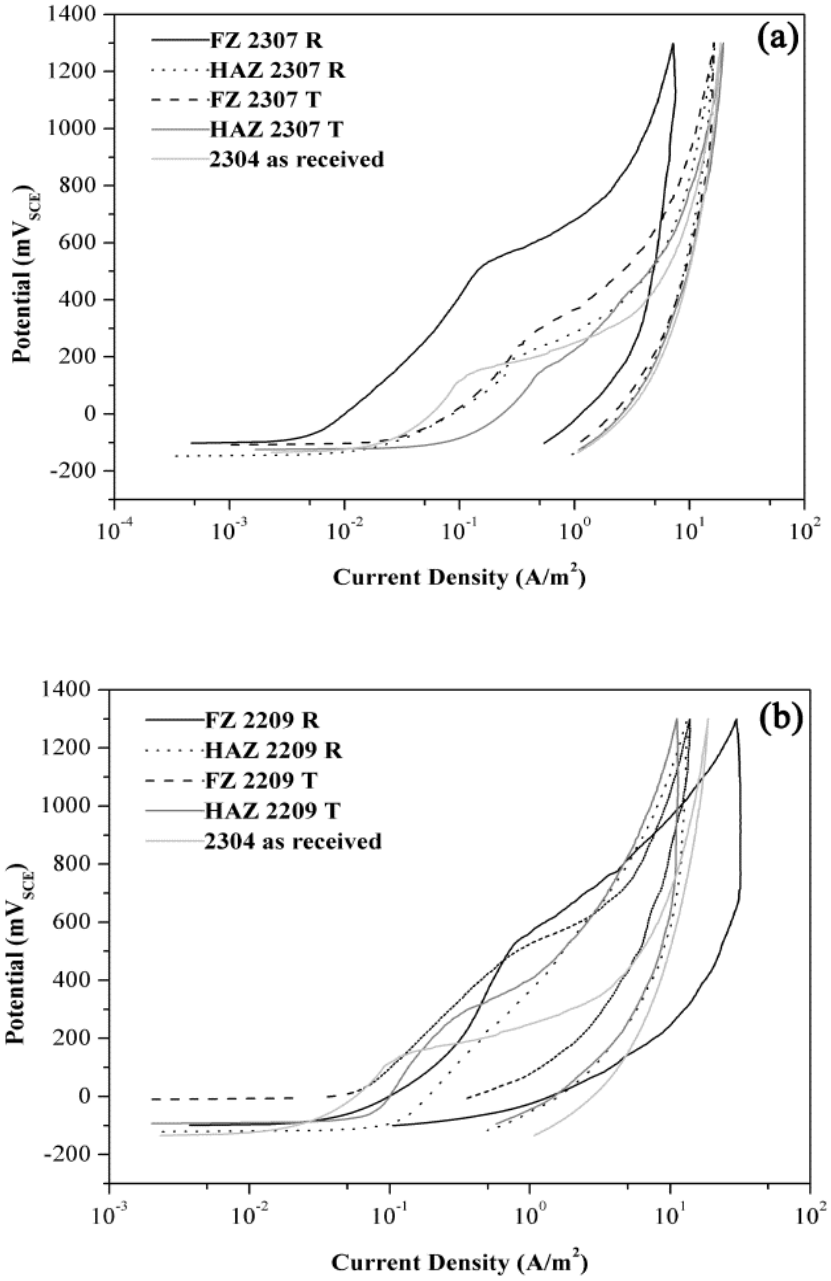

Figure 4.9: Cyclic potentiodynamic polarization curves for FCAW process: (a) 2307 as filler metal and (b) 2209 as filler metal.

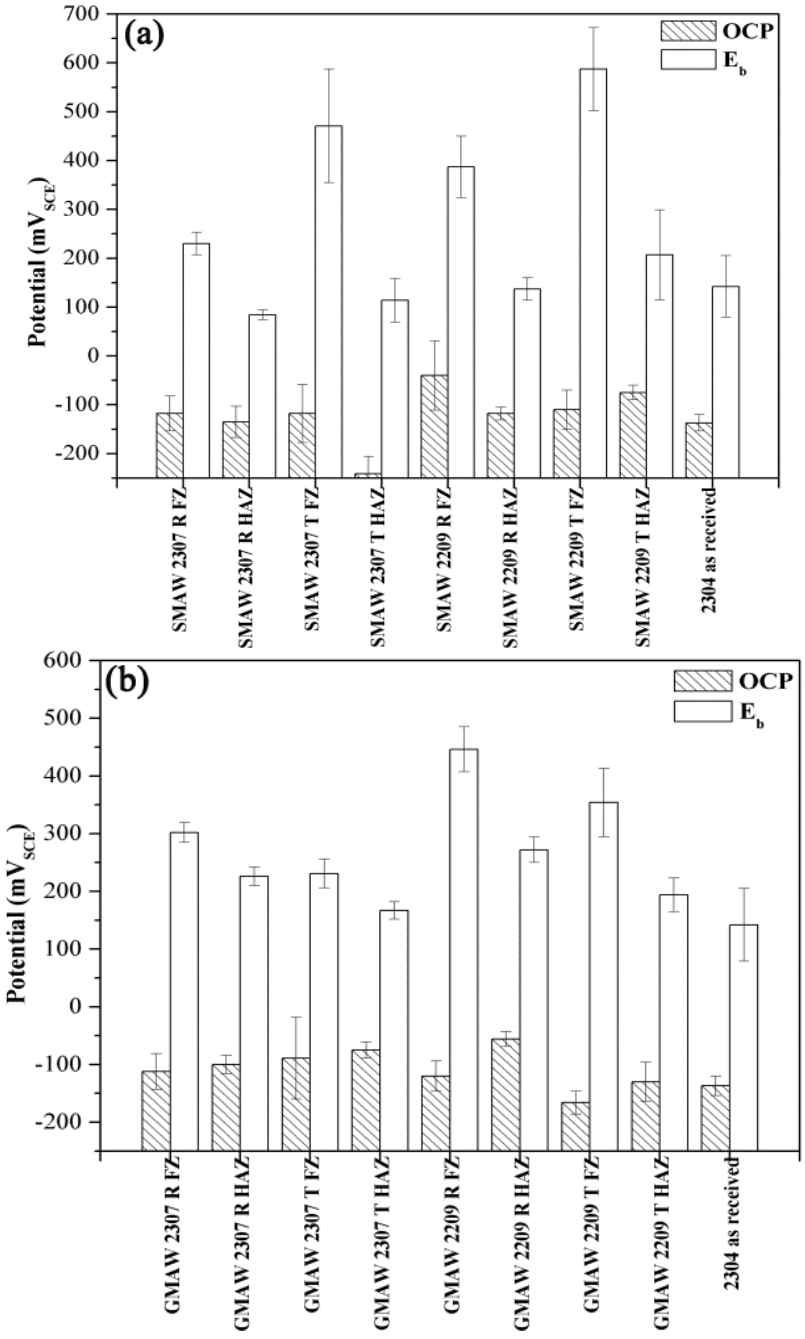
(a)
OCP
E_b
Potential (mV_{SCE})
700
600
500
400
300
200
100
0
-100
-200
SMAW 2307 R FZ
SMAW 2307 R HAZ
SMAW 2307 T FZ
SMAW 2307 T HAZ
SMAW 2209 R FZ
SMAW 2209 R HAZ
SMAW 2209 T FZ
SMAW 2209 T HAZ
2304 as received
(b)
OCP
E_b
Potential (mV_{SCE})
600
500
400
300
200
100
0
-100
-200
GMAW 2307 R FZ
GMAW 2307 R HAZ
GMAW 2307 T FZ
GMAW 2307 T HAZ
GMAW 2209 R FZ
GMAW 2209 R HAZ
GMAW 2209 T FZ
GMAW 2209 T HAZ
2304 as received

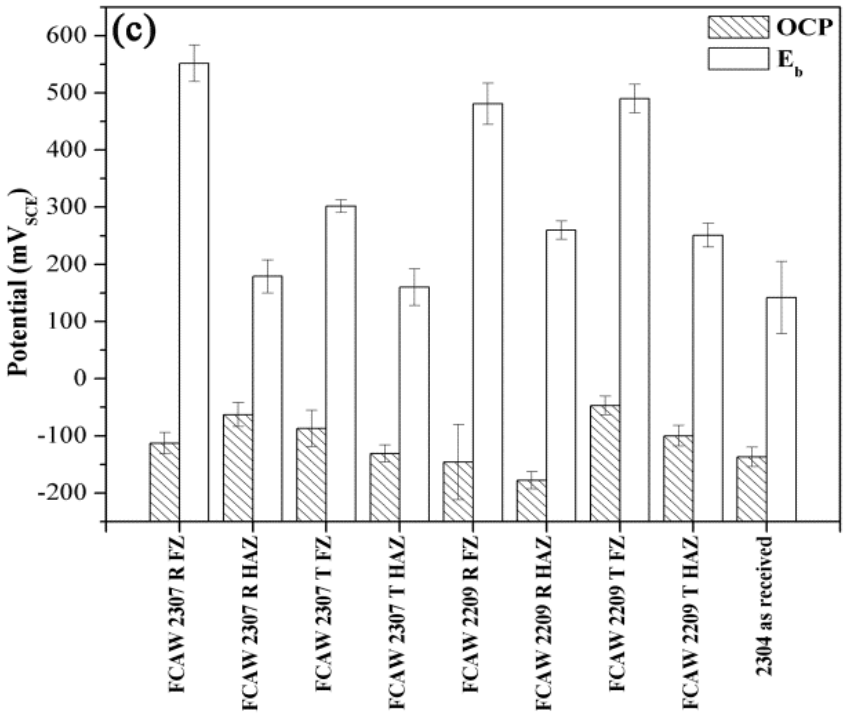

Figure 4.10: Experimental data for samples welded by the SMAW (a), GMAW (b), and FCAW process (c).

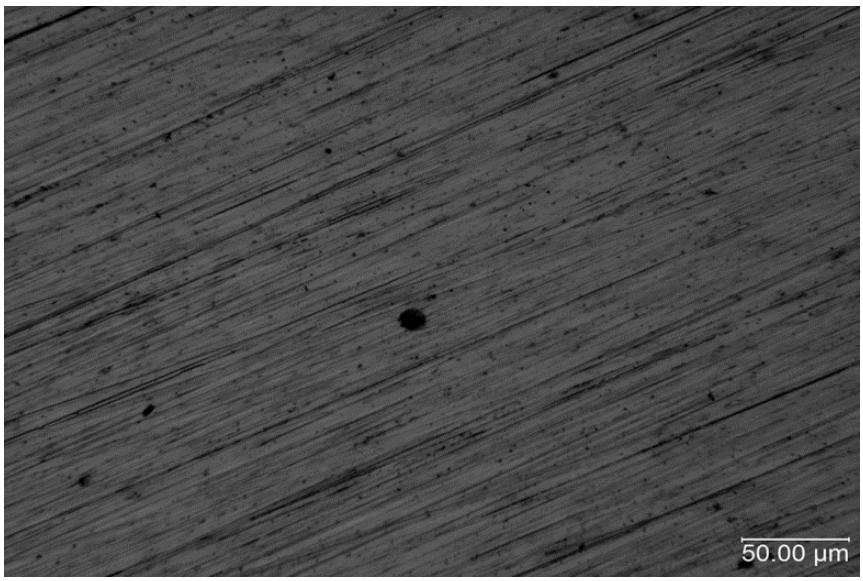

Figure 4.11: Pit morphology for SMAW 2307 FZ top sample. Similar results were obtained for the others.

4.4. Conclusions

Welded joints of lean duplex stainless steel fabricated under different conditions were tested in acidic glycerin. Based on the results, is possible to conclude:

- Welds made with 2209 filler metal showed better microstructure and pitting corrosion resistance than with 2307 filler metal, indicating that higher-alloyed specimen exhibited better welding performance, for both whole samples and the WZ tested by the microcell technique.
- No chromium nitride precipitation was found on the as-received specimens, while many nitrides precipitates were found at grain boundaries or ferrite grains on the as-welded specimens.
- The breakdown potential (E_b) for the GMAW welding process was higher than the E_b obtained for the other welding processes.
- For SMAW and FCAW welding processes, top samples showed higher E_b than root samples. However, in the case of samples welded by GMAW process, the root was more resistant than the top, for both cases whole sample and microcell technique.
- After testing, two types of pits were observed. One type was found to initiate in the vicinity of big inclusions and the second was formed within the δ or γ phase.
- The pitting susceptibility is comparable in the HAZ and the BM. Thus, welding thermal cycles do not affect substantially the values of E_b in the HAZ.
- The pitting corrosion resistance of the FZ was improved after welding as a consequence of the enrichment of alloying elements in these regions from the filler metals.

- Considering corrosion resistance and microstructure phase balance, GMAW welding process with 2209 as filler metal is the best welding process for 2304 duplex stainless steels.

4.5. References

[1] E.M. Westin, C.-O.A. Olsson, S. Hertzman, *Corros. Sci.* **2008**, *50*, 2620.

[2] A. Burkert, J. Lehmann, A. Burkert, J. Mietz, P. Gümpel, *Mater. Corros*. **2014**, *65*, 1080.

[3] H. Sieurin, R. Sandström, *Mater. Sci. Eng. A.* **2006**, *418*, 250.

[4] C.M. Garzón, A.J. Ramirez, *Acta Mater.* **2006**, *54*, 3321.

[5] J.-O. Nilsson, P. Kangas, T. Karlsson, A. Wilson, *Metall. Mater. Trans. A* **2000**, *31A*, 35.

[6] B. Deng, Z. Wang, Y. Jiang, T. Sun, J. Xu, J. Li, *Corros. Sci.* **2009**, *51*, 2969.

[7] Y. Jiang, H. Tan, Z. Wang, J. Hong, L. Jiang, J. Li, *Corros. Sci.* 2013, *70*, 252.

[8] T. Suter, H. Böhni, *Electrochem. Commun.* **2001**, *47*, 191.

[9] L. Chen, H. Tan, Z. Wang, J. Li, Y. Jiang, *Corros. Sci.* **2012**, *58*, 168.

[10] F. F. Eliyan, A. Alfantazi, *Corros. Sci.* **2013**, *74*, 297.

[11] H. Tan, Z. Wang, Y. Jiang, Y. Yang, B. Deng, H. Song, J. Li, *Corros. Sci.* 2012, *55*, 368.

[12] J. Pilhagen, R. Sandström, *Mater. Sci. Eng., A*, 2014, *602*, 49.

[13] V. Vignal, H. Krawiec, O. Heintz, R. Oltra, *Electrochim. Acta* **2007**, *52*, 4994.

[14] H. Krawiec, V. Vignal, R. Oltra, *Electrochem. Commun.* **2004**, *6*, 655.

[15] T. Suter, H. Böhni, *Electrochem. Commun.* **2001**, *47*, 191.

[16] C. Garcia, F. Martin, P. Tiedra, Y. Blanco, M. Lopez, *Corros. Sci.* **2008**, *50*, 1184.

[17] S. Schmigalla, S. Krasnorutskyi, M. Zinke, A. Heyn, *Mater. Corros*. **2015**, *66*, 442.

[18] L. Chen, H.Tan, Z.Wang, J. Li, Y. Jiang, *Corros. Sci.* **2012**, *58*, 168.

[19] H. Tan, Z. Wang, Y. Jiang, D. Han, J. Hong, L. Chen, L. Jiang, J. Li. *Corros. Sci.* **2011**, *53*, 2191.

[20] N. Birbilis, R. G. Buchheit, *J. Electrochem. Soc.* **2005**, *152*, B140.

[21] D.M. Garcia-Garcia, J. Garcia-Anton, A. Igual-Murioz, E. Blasco-Tamarit, *Corros. Sci.* **2006**, *48*, 2380.

[22] P. Ferro, A. Tiziani, F. Bonollo, *Weld. J.* **2008**, *87*, 298.

[23] V. Muthupandi, P.B. Srinivasan, *Mater. Sci. Eng., A* **2003**, *358*, 9.

[24] I. A. Chaves, R. E. Melchers, *Corros. Sci.* **2011**, *53*, 4026.

[25] Y. Yang, B. Yan, J. Li, J. Wang, *Corros. Sci.* **2011**, *53*, 3756.

[26] J.C Bergmann, D.D Tupinambá, O.Y.A Costa, J.R.M Almeida, C.C Barreto, B.F Quirino, *Renewable and Sustainable Energy Rev.* **2013**, *21*, 411.

[27] F. Mohammadi, F. F. Eliyan, A. Alfantazi, *Corros. Sci.* **2012**, *63*, 323.

[28] R. Cardoso Junior, A. Q. Bracarense, F. R. Campos, C. S. Souza, D. M. Silveira, V. F. C. Lins, *Soldagem e Inspeção* **2012**, *17*, 306.

[29] E. Bettini, U. Kivisäkk, C. Leygraf, J. Pan, *Electrochim. Acta* **2013**, *113*, 280.

[30] D.H. Kang, H.W. Lee, Corros. Sci. **2013**, *74*, 396.

[31] H.Y. Liou, R.I. Hsieh, W.T. Tsai, *Mater. Chem. Phys.* **2002**, *74*, 37.

[32] A. J. Ramirez, S. D. Brandi, J. C. Lippold, *Sci. Technol. Weld. Joining* **2004**, *9*, 301.

[33] A. J. Ramirez, J. C. Lippold, S. D. Brandi. *Metall. Mater. Trans. A* **2003**, *34*, 1575.

[34] T. Chehuan, V. Dreilich, K. S. de Assis, F. V.V. de Sousa, O. R. Mattos. *Corros. Sci.* **2014**, *86*, 268.

[35] Z. Zhang, Z. Wang, Y. Jiang, H. Tan, D. Han, Y. Guo, J. Li, *Corros. Sci.* **2012**, *62*, 42.

[36] Z. Zhang , H. Zhao , H. Zhang , Z. Yu , J. Hu , L. He , J. Li, *Corros. Sci.* **2015**, *93*, 120.

[37] E. Blasco-Tamarit, A. Igual-Munõz, J. Garcia-Anton, D. Garcia-Garcia, *Corros. Sci.* **2006**, *48*, 863.

[38] H. Tsuge, Y. Tarutani, and T. Kudo, *Corrosion* **1988**, *44*, 305.

5. ELECTROCHEMICAL STUDY OF PASSIVE FILMS FORMED ON WELDED LEAN DUPLEX STAINLESS STEEL

Dalila C. Sicupira[a,c*], Ronaldo C. Junior[b], Alexandre Q. Bracarense[b], G.S. Frankel[c], Vanessa de F. C. Lins[a]

[a] Chemical Engineering Department, Universidade Federal de Minas Gerais, 6627, Antônio Carlos Avenue, Pampulha, Belo Horizonte, MG 31270-901, Brazil, Fax:+55 31 34091789, e-mail address: dsicupira@ufmg.br

[b] Mechanical Engineering Department, Universidade Federal de Minas Gerais, 6627, Antônio Carlos Avenue, Pampulha, Belo Horizonte, MG 31270-901, Brazil

[c] Fontana Corrosion Center, Dept. of Materials Science and Engineering, The Ohio State University, Columbus, OH 43210, USA

Abstract

Duplex stainless steel (DSS) has been considered as an excellent alternative for applications where high corrosion resistance and high mechanical strength are required. The use of this material can minimize costs related to corrosion in different industries, for example, in the biodiesel industry. The objective of this study is to evaluate the corrosion resistance of thick welded joints of UNS S32304 lean duplex stainless steel (LDSS) fabricated by different welding processes, in acidified glycerin, a byproduct of the biodiesel industry. The electrochemical behavior of the passive films formed on UNS S32304 LDSS was evaluated using Electrochemical Impedance Spectroscopy and

Mott-Schottky measurements. The capacitance study shows that the passive films formed on welded DSS behave as n-type and p-type semiconductors above and below the flat band potential, respectively. Furthermore, the samples welded by the Gas Metal Arc Welding process exhibited better corrosion resistance than other welding process using the same filler metal.

Keywords: corrosion, duplex stainless steel, welding.

5.1. Introduction

Duplex stainless steels (DSS) are being widely used as alternatives to austenitic stainless steels and nickel-based alloys [1-3]. They represent an important class of steels with a combination of mechanical strength and corrosion resistance in chloride-ion-containing environments [2]. They have been used as structural materials in power plants, petrochemical industries and marine construction [4]. Their good properties are attributed to the duplex microstructure, which consists of approximately equivalent amounts of austenite (γ) and ferrite (δ) [5-7].

Recently, lean duplex stainless steels (LDSS) were developed [1]. Despite it has the advantage of being cheaper than DSS due to the partial substitution of nickel by manganese and nitrogen, there are still difficulties in welding of LDSS [1].

One of the most common LDSS alloys is UNS S32304, which has a nominal composition of 23% Cr, 4% Ni, and additions of Mo, N and Mn [8]. Among these, the

alloying elements Cr, Mo and N are usually associated with the localized corrosion resistance of stainless steels.

The use of slightly over-alloyed filler metal such as ISO 23 7 N L or ISO 22 9 3 N L can, generally, results in a good weldability of this type of LDSS [1]. However, the fusion welding process causes changes in the ferrite/austenite phase balance in DSS and favors the precipitation of intermediate phases in the welded joints [11]. As consequence of this phenomenon, corrosion resistance and mechanical properties of these materials are dramatically impaired, particularly in the heat affected zone (HAZ) [11-13].

The protective passive film formed on the surface of these materials gives them a high corrosion resistance. This protective layer has been described as consisting of multilayer structures [14,15]. Recent studies also established that the passive oxide film formed on stainless steels consists primarily of chromium oxide, Cr_2O_3, and iron oxide, Fe_2O_3, as inner and outer layers, respectively [14,15]. The first, acting as a barrier layer against cation transfer and the latter, an exchange layer with the electrolyte [16]. Generally, the passive films of metals are mainly made up of metallic oxides or hydroxides which can be semiconductors [17]. Consequently, semiconducting properties are often observed on the surfaces of the passivity metals [17].

Recently, increasing research of the electronic properties of the passive films formed on stainless steels has been an important contribution to the understanding of the protective behavior against corrosion of these alloys [18-20]. Depending upon the applied potential, the oxide film formed on stainless steel has n- or p-type semiconducting

properties [18]. Capacitance studies are very useful for giving information on the electronic structure of a semiconductor and by the analysis of the Mott-Schottky plots it is possible to obtain the donors and acceptors densities for n- or p-type semiconductors, respectively [17]. The donors and acceptors in semi-conducting passive layers are defects, including cation vacancies, anion vacancies and cation interstitials. In a recent work by Fattah and Vafaeian [18], the electrochemical behavior of coarse-grained and fine-grained AISI 430 ferritic stainless steel in 0.1 M HNO_3 solution has been investigated. Mott–Schottky analysis revealed that the passive films behave as n-type and p-type semiconductors and the calculated donor and acceptor densities were smaller for the refined grain, indicating that the passivation behavior improved with decreasing the grain size.

An improved understanding of the corrosion properties of LDSS can increase their application and reduce the costs associated with corrosion, for example, in industrial biodiesel plants. The biodiesel industry has experienced a significant number of failures (e.g. holes in pipes) caused by corrosion in acidified medium, which resulted in production losses and, consequently, economic losses. Although several studies related to the effect of heat input and thermal cycles on the microstructure of pipeline steels have been performed [21,22], corrosion of welded joints of DSS in biodiesel plant environments has not received much attention.

The aim of the present work is to study the electrochemical and electronic properties of passive films formed on UNS S32304 LDSS thick plates multipass-welded by processes commonly employed in the manufacture of equipment and piping: shielded metal arc welding (SMAW), gas metal arc welding (GMAW), and flux cored arc welding

(FCAW). The testing environment was acidified glycerin, a byproduct of the biodiesel industry, and the techniques used were Electrochemical Impedance Spectroscopy (EIS) and Mott–Schottky analysis.

5.2. Experimental Procedures

5.2.1. Materials

The UNS S32304 LDSS was provided by Aperam South America in the form of plates of 22 mm nominal thickness, 350 mm long and 180 mm wide. The chemical composition of the steel used in this work is presented in Table V.1. Multipass welding was employed using SMAW, GMAW and FCAW processes. The details of the welding parameters are presented in Tables V.2 and V.3. For each welding process, two filler metals with different chemical compositions, (23%Cr 7%Ni) and (22%Cr 9%Ni 3%Mo) were evaluated. The filler metal compositions are shown in Table V.4.

Table V.1: Chemical composition of base metal [23].

Element	**C**	**Mn**	**Si**	**P**	**S**	**Cr**	**Ni**	**Mo**	**Cu**	**N**	**O**
Content (%wt)	0.019	1.3	0.39	0.028	0.00040	22	3.6	0.44	0.50	0.11	0.0033

Table V.2: Filler metal and shielding gas specification [23].

Identification	**EN Specification**	**Filler metal**	**Diameter (mm)**	**Shielding Gas**
SMAW 2307	E Z 23 7 N L R	23%Cr7%Ni	3.25	-
SMAW 2209	E 22 9 3 N L R 3 2	22%Cr9%Ni3%Mo	4.00	-
GMAW 2307	G 23 7 NL	23%Cr7%Ni	1.00	Star GoldTM SS[a]
GMAW 2209	G 22 9 3 NL	22%Cr9%Ni3%Mo	1.00	Star GoldTM SS[a]
FCAW 2307	T 23 7 N L P	23%Cr7%Ni	1.20	75%Ar+25%CO_2
FCAW 2209	T 22 9 3 N L P	22%Cr9%Ni3%Mo	1.20	75%Ar+25%CO_2

[a]Star GoldTM SS: Ar+CO_2+N_2 supplied by Praxair.

Table V.3: Welding parameters [23].

Identification	Passes	Current (A)	Voltage (V)	Speed (cm/min)	Heat input (kJ/mm)	T Interpass (°C)
SMAW 2307	Root	85	25.0	11.3	1.13	-
	Others	135	31.1	14.8	1.70	100-150
SMAW 2209	Root	140	29.0	12.1	2.01	-
	Others	160	28.7	15.9	1.73	100-150
GMAW 2307	Root	210	29.0	13.6	2.69	-
	Others	213	29.0	23.1	1.60	100-150
GMAW 2209	Root	195	29.0	15.3	2.21	-
	Others	212	29.0	23.3	1.58	100-150
FCAW 2307	Root	208	29.0	23.2	1.56	-
	Others	210	29.0	23.2	1.58	100-150
FCAW 2209	Root	210	29.0	23.3	1.57	-
	Others	210	29.0	22.9	1.59	100-150

Table V.4: Chemical composition of the filler metals (%wt.) [23].

Welding process	Filler metal	C	Mn	Si	P	S	Cr	Ni	Mo	Cu	N
SMAW	2307	0.028	0.78	0.96	0.017	0.014	22.6	7.62	0.36	0.26	0.14
SMAW	2209	0.027	0.79	0.99	0.019	0.012	21.92	9.31	3.15	0.06	0.14
GMAW	2307	0.03	0.88	0.86	0.017	0.01	23.82	8.92	0.31	0.095	0.13
GMAW	2209	0.029	1.47	0.57	0.02	0.009	21.94	9.20	3.12	0.14	0.14
FCAW	2307	0.024	0.92	0.96	0.018	0.011	23.7	8.93	0.3	0.095	0.12
FCAW	2209	0.022	1.06	0.91	0.022	0.013	21.66	9.2	2.94	0.18	0.15

The sample preparation for electrochemical tests was described by the authors in a previous work [24].

5.2.2. Microstructure analysis

Before the electrochemical measurements, microstructural examination of specimens was conducted using an optical microscope (Olympus PME 3, LECO). After polishing, the specimens were then electrolytically etched in 10% oxalic acid electrolyte at 6 V for 60 s.

5.2.3. Electrochemical measurements

The EIS measurements were performed at a temperature of 65±1°C and under constant stirring to simulate the operational conditions in the pipes. A conventional three-electrode cell was used, the working electrodes being prepared from the LDSS welded samples with an exposed surface of approximately 1 cm^2. The reference was a saturated calomel electrode (SCE) and a Pt mesh was used as the counter electrode.

EIS was performed in acidified glycerin solution prepared based on the composition supplied by Petrobras Biocombustível (PBIO). The base electrolyte was 49% glycerin, + 29% methanol + 17% water + 3% sodium chloride (%wt). The pH was adjusted to 5.8 using additions of HCl and NaOH solutions. A Gamry Reference 600 potentiostat applied sinusoidal signals in the frequency range of 100 kHz - 5 mHz with amplitude of 10 mV. Before the measurements, the open circuit potential in acidified glycerin solution was measured for 1 h. The acquired impedance spectra are presented as

Nyquist plots and interpreted in terms of equivalent electrical circuits. All tests were performed in triplicate.

Mott–Schottky analysis was carried out on the passive films at a frequency of 1 kHz using a 10 mV sinusoidal signal and steps of 50 mV, in the anodic direction, form the initial potential of -1.0 V_{SCE} to the final potential of 1.0 V_{SCE}.

5.3. Results

5.3.1. Microstructure

Figure 5.1 shows optical micrographs of the weld fusion zone (FZ) without etching and figures 5.2 and 5.3 show FZ and heat affected zone (HAZ) etched in oxalic acid, respectively, for UNS S32304 samples welded by the different processes.

Inclusions in the FZ were evident (Fig. 5.1), which was described previously [23] to be (Mn, Si)-oxides for the majority of the samples and also Al-oxides and Ti-oxides for the case of GMAW and FCAW processes, using 2209 as filler metal, respectively. More inclusions were observed for the processes in which slags are generated, SMAW and FCAW, compared to the slag-free GMAW process. According to previous work [23], there are fewer inclusions in the root region than in the top region. Micro-crevice formation between inclusion and metallic matrix has been suggested to result in pit initiation [32].

The FZ structure (Fig. 5.2) consists of austenite grains in the form of Widmanstätten plates precipitates within a matrix of ferrite, and showed higher proportions of austenite than in the HAZ, as expected. There was also visible secondary phase precipitation in the ferrite matrix in both the HAZ and FZ. Two morphologies of secondary austenite precipitates (small white needle and island types), and some chromium nitrides colonies (dark etched phase) formed mainly within the ferrite grains. According to Ramirez *et al.* [25] inclusions in the FZ, act as the nucleation sites for intragranular austenite. However, the amount of inclusions in the DSS FZ usually is not high enough to justify all the intragranular austenite precipitation. In the case of the HAZ, due to the low levels of inclusions, the nucleation of intragranular austenite from inclusions is rare.

The microstructure of the FZ exhibits an austenite content of 43-54% in the top region and 38-59% in the root region. Among the samples, the FZ of GMAW samples showed higher austenite content, probably influenced by the N_2 addition to the shielded gas during welding. The microstructure of the HAZ exhibits austenite content of 18-24% in the top region and 17-27% for root region. The microstructure in the FZ and HAZ was similar for both consumables using a given weld process, indicating that both are suitable for welding UNS S32304 steel. However the microstructure of the HAZ for SMAW process was different from the others. Due to an experimental deviation, the SMAW samples were welded with a slightly large heat input, which resulted in higher proportions of austenite compared to the others for the same consumable (see Table V.3). This fact suggests that the microstructure is strongly influenced by the welding heat input, as described by some authors [7,25,26]. The slow cooling rate (with large heat input) can lead to high reformed austenite content in DSSs. Generally, a relatively large heat input (slow cooling rate) is beneficial to the microstructure of welded joints

with more austenite reformation during cooling stage and without the precipitation of chromium nitrides, thus affecting the corrosion behavior and some mechanical properties of the HAZ [7,25,26]. The corrosion behavior of the SMAW samples was affected by this experimental deviation during welding. As the austenite content increases, the possibility of chromium nitride precipitation decreases [26].

In order to increase the pitting corrosion resistance, more nitrogen is added for LDSS, since the concentration of Mo is lower than in standard DSS. It has been indicated in several studies the possibility of chromium nitride formation under rapid cooling conditions during welding of DSS [2,6,7,13,25-28]. In the present work, it was possible to see the presence of chromium nitride in the as-welded specimen after electrolytic etching in oxalic acid. Nitride precipitation was observed at the regions free of austenite within the ferrite grains due to the low solubility of nitrogen in ferrite with decrease in temperature. Ramirez *et al.* [25] showed that chromium-rich nitrides precipitated at the interior of the ferrite grains and ferrite/austenite interfaces after quenching from 1350°C. And also, in reheated condition, as in multipass welding, the precipitation of secondary austenite, γ_2 can occurs as consequence of the dissolution of the intragranular nitrides.

This chromium nitride precipitation has been shown to compromises the corrosion resistance and the toughness of DSS [2,6,7,13,25-28]. However, the initiation of localized corrosion caused by nitride particles depends on their distribution, amount and size, as well as their surrounding region [28].

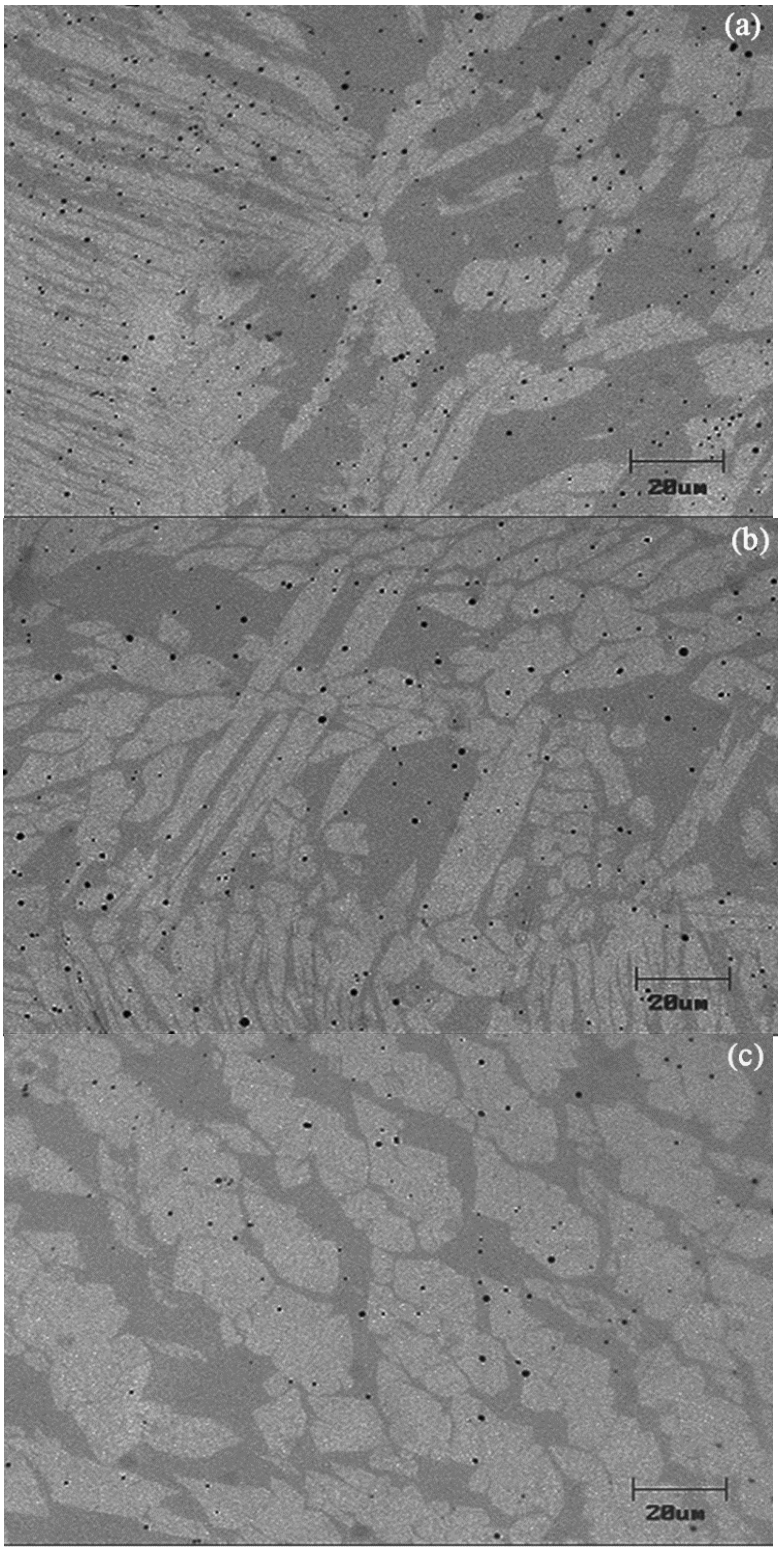
(a)
20um
(b)
20um
(c)
20um

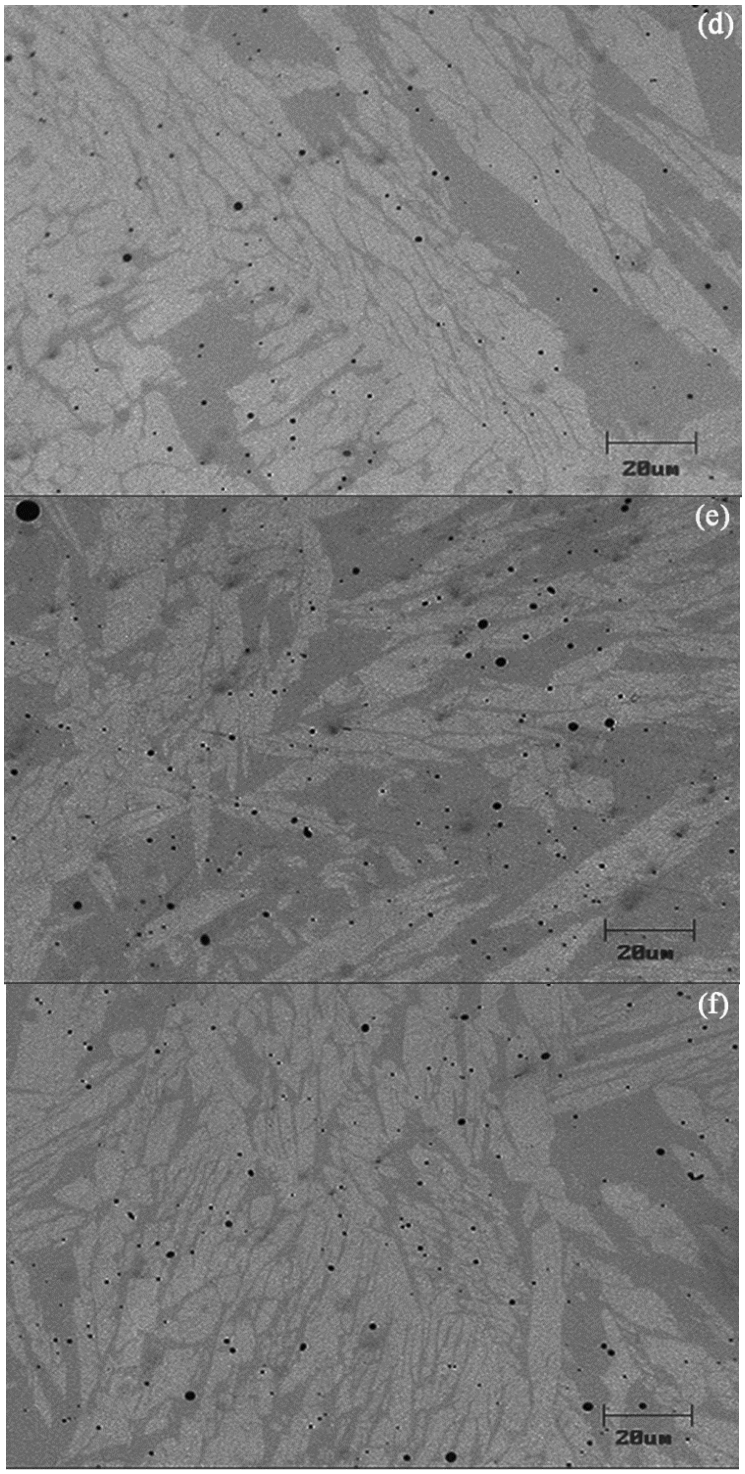

Figure 5.1: Optical microstructure of the FZ root region without etching, showing inclusions (a) SMAW 2307 (b) SMAW 2209 (c) GMAW 2307 (d) GMAW 2209 (e) FCAW 2307 (f) FCAW 2209.

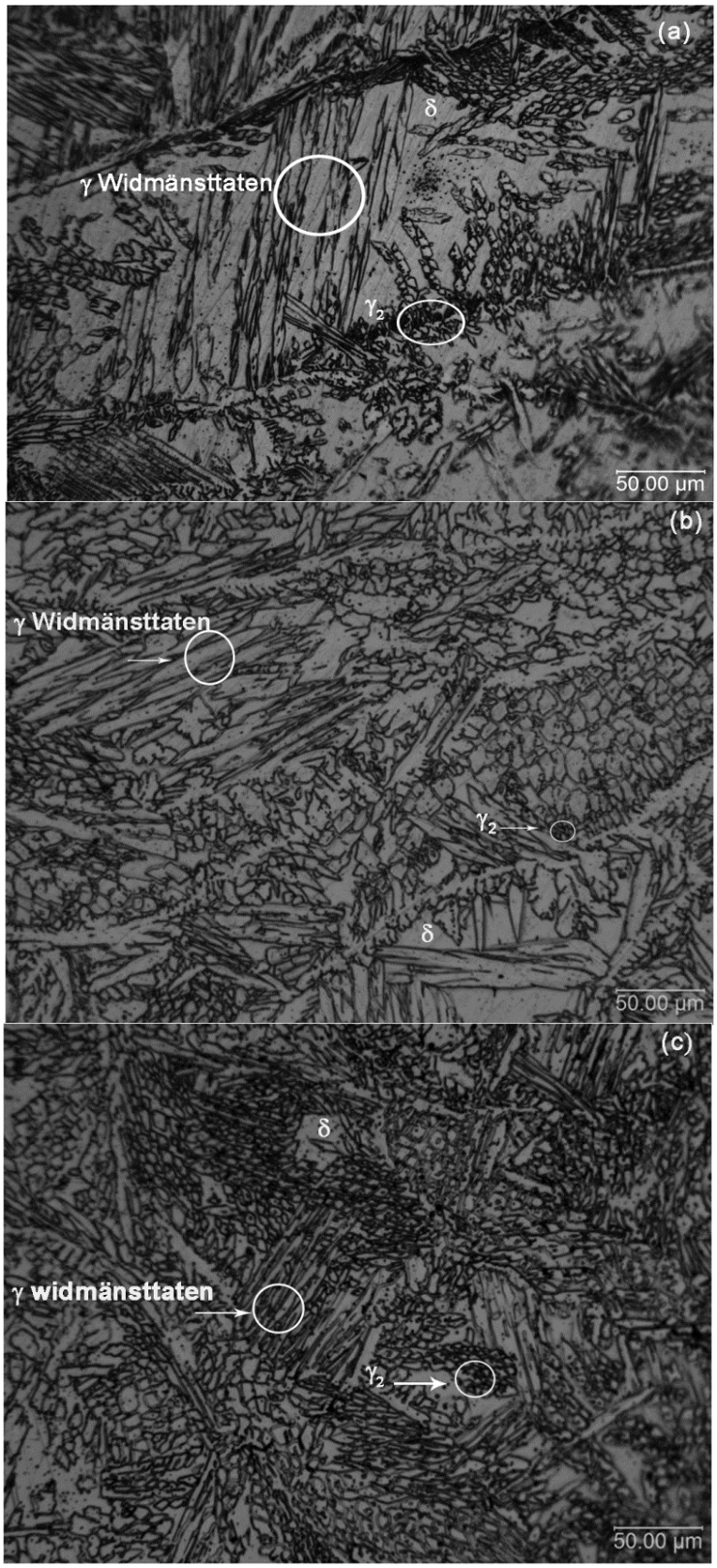

Figure 5.2: Optical microstructure of the top region FZ for samples welded by different processes, showing ferrite phase (matrix) and austenitic phase (island) (2307 as filler metal.(a) SMAW (b) GMAW (c) FCAW.

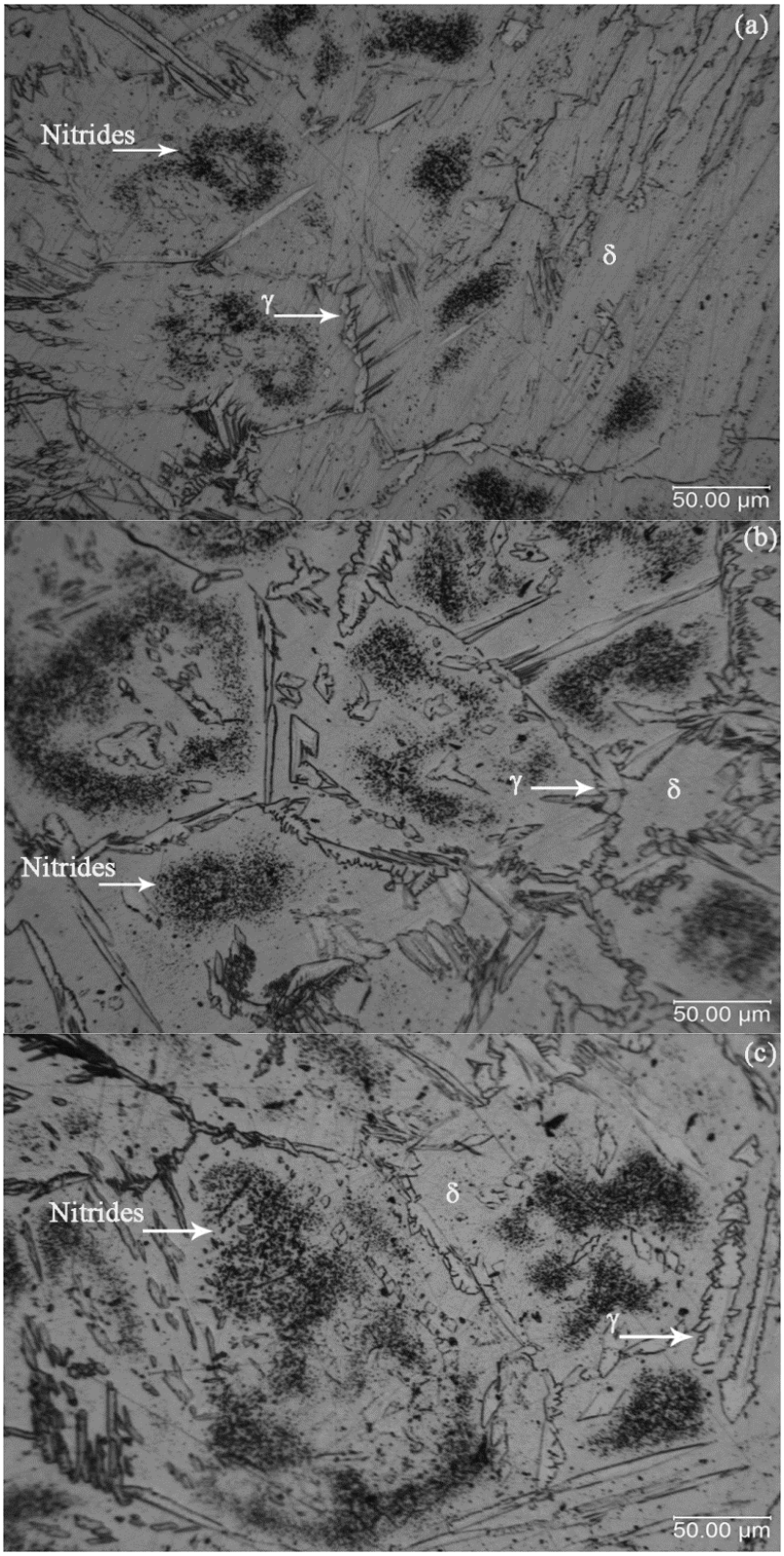

Figure 5.3: Optical microstructure of the top region HAZ for samples welded by different processes showing ferrite phase (matrix) and austenitic phase (island), 2307 as filler metal: (a) SMAW (b) GMAW (c) FCAW.

Figures 5.2 and 5.3 show that the welded joints had high proportions of austenite in the FZ. However, in the HAZ, as expected, lower levels of γ were identified. Secondary austenite and chromium nitrides can also be found inside the ferritic grains in the HAZ.

5.3.2. Electrochemical impedance analysis

Figures 5.4 (a-c) show the Nyquist plots for welds made in UNS S32304 with the SMAW, GMAW and FCAW processes, respectively, in acidified glycerin. Samples from the weld top and root welded with either filler metal exhibited similar EIS results in the acidified glycerin solution for welds made by the SMAW and FCAW processes (Figure 5.4a and 5.4c). However, differences were evident for samples made by the GMAW process (Figure 5.4b), as discussed below.

The impedance data were analyzed using equivalent electrical circuits and using the ZView program (Scribner Assoc.) to fit the experimental data. The Nyquist plots of all samples exhibited only one time constant and they took the form of flattened semi-circles centered below the real impedance axis. This behavior is typical of solid metal electrodes that show a frequency dispersion of the capacitive properties [29-31]. It has long been known that the impedance of solid electrodes usually deviates from ideal capacitive behavior, which is generally attributed to distributed surface reactivity, surface inhomogeneity, roughness or fractal geometry, electrode porosity, and to current and potential distributions associated with electrode geometry [29,30]. This type of behavior can be modeled using a constant phase element (CPE) [29-32].

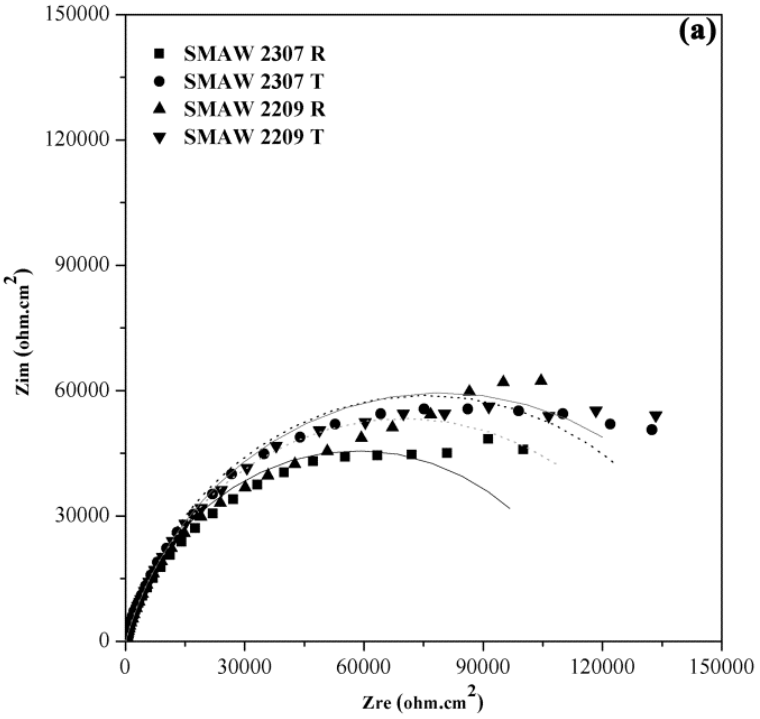
(a)
SMAW 2307 R
SMAW 2307 T
SMAW 2209 R
SMAW 2209 T
Zim (ohm.cm2)
Zre (ohm.cm2)
0
30000
60000
90000
120000
150000

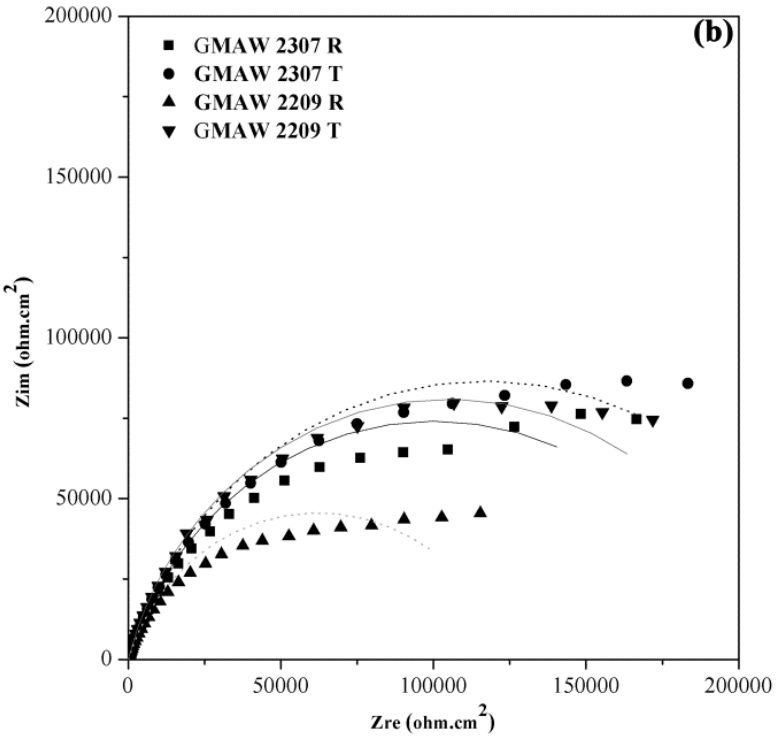
(b)
GMAW 2307 R
GMAW 2307 T
GMAW 2209 R
GMAW 2209 T
Zim (ohm.cm2)
Zre (ohm.cm2)
0
50000
100000
150000
200000

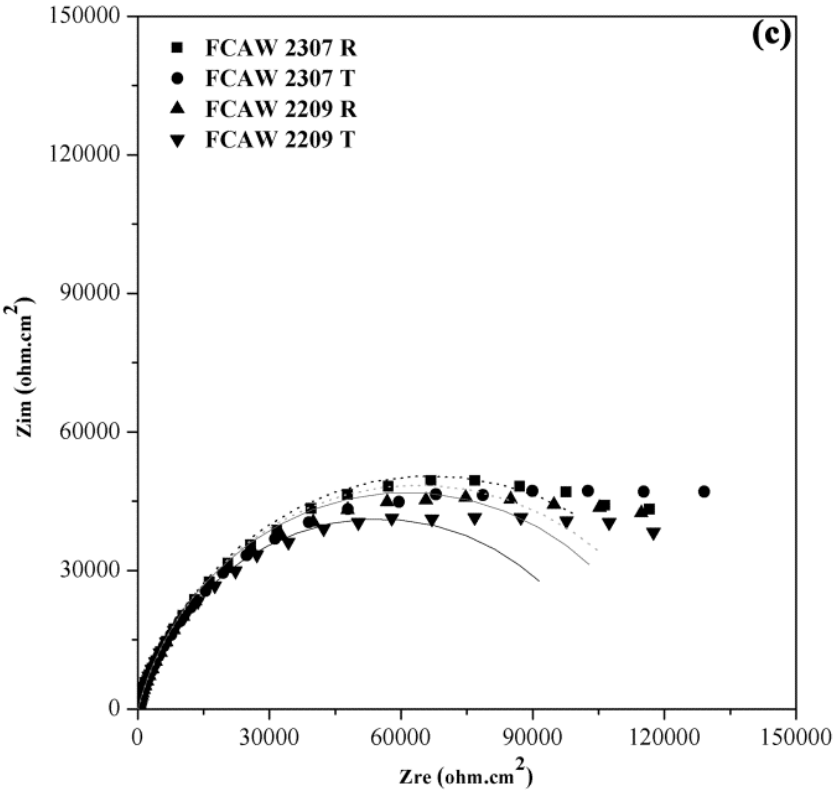

Figure 5.4: EIS results for samples welded by (a) SMAW (b) GMAW (c) FCAW process. Continuous lines are fitting results. T – top of weld, R – root of weld.

The impedance of a CPE, Z_{CPE}, is defined as [29-31]:

$$Z_{CPE} = \frac{1}{Q(j\omega)^n} \tag{5.1}$$

in which Q is the CPE magnitude ($\Omega^{-1}cm^{-2}s^n$), j^2=-1, n is the CPE exponent, and ω is the angular frequency. The magnitude of n is $0 \leq n \leq 1$ but is often close to 1 and the CPE behaves as a capacitor when n=1. The plot of the imaginary part of the impedance as a function of frequency gives a straight line with a slope equal to n [29-31].

The data in Figure 5.4 (a-c) can be fitted well by the single time constant equivalent circuit $R_s(QR_{ct})$ represented in Figure 5.5: R_s is the electrolyte solution resistance, R_{ct} is the charge transfer resistance associated with the charge transfer process between the metal and the solution, which occurs through the protective passive film. CPE represents the sum of capacitances related to the passive film and the electrical double layer. The diameter of the semi-circle impedance loop corresponds to R_{ct}. The CPE parameters n and Q obtained are in the range of usual values reported for passive film on stainless steel in chloride-containing solutions [33,34].

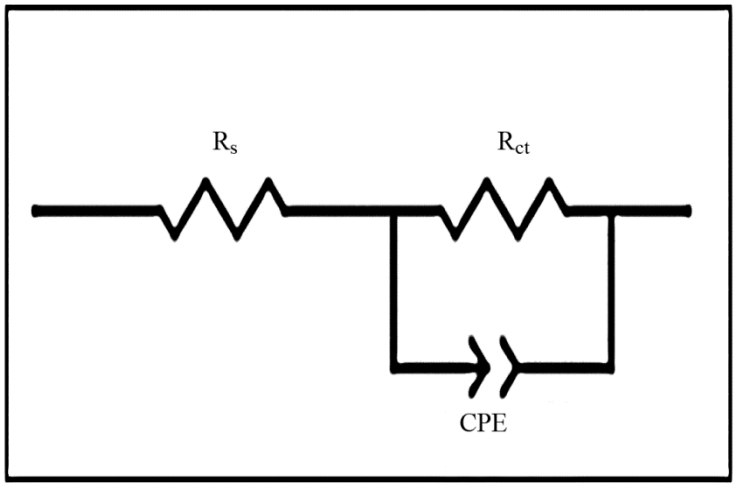

Figure 5.5: Equivalent circuits diagrams used for the modelling of the impedance data.

For the GMAW samples, the impedance magnitudes at the lowest frequencies were higher for the samples with 2307 filler metal than for 2209, as shown in Fig. 5.6. According to Cardoso Junior *et al.* [23] samples welded by GMAW process with 2307 filler metal had lower inclusion content and higher austenite content than for samples with 2209 filler metal, which can explain this behavior.

The effects of inclusions on the corrosion process have been investigated in detail. According to Stewart and Williams [35] inclusions are the dominant pit nucleation sites, and the lifetime of a metastable pit is directly related to the size of the inclusion particle. Baker and Castle [32] suggest that non-metallic inclusions in steel are a combined matrix of TiO_2-MnO-$A1_2O_3$-Cr_2O_3. The oxides of Ti, A1 and Cr are resistant to attack from the bulk solution, but, MnO will dissolve with Mn^{2+}. The presence of manganese oxide at the inclusion and its dissolution by H^+ could lead to metal passivity breakdown and pit initiation.

The values of R_{ct} determined by fitting of the data to the equivalent circuit in Figure 5.5 are presented in Figure 5.6. Also included is as-received UNS S32304. In general, the top region values have higher impedance than those from the root for both 2307 and 2209 filler metal. The differences are small, but the standard deviations indicate that they are significant. This suggests that top samples are more resistant to corrosion in acidified glycerin, i.e., the passive film becomes more protective in this case. Both filler metals used in this work were over-alloyed and the top of the welded sample has a lower dilution of the consumable, which likely explains this difference. Furthermore, the root region has higher content of secondary austenite than top region [23]. Molybdenum, chromium and nitrogen contents are lower in γ_2 than in the primary austenite, and as a result, welds containing γ_2 have poorer corrosion resistance than welds without γ_2 [3,36]. However, this correlation is not simple and would not be directly associated with the presence of γ_2 islands. Indeed, the mere presence of γ_2 does not necessarily imply in a higher susceptibility to localized corrosion [27].

Overall, for samples welded with either filler metal, R_{ct} was highest for the GMAW process followed by SMAW and FCAW processes (Figure 5.6). This behavior may be related to the higher values of inclusions in the FZ of samples welded by SMAW and FCAW processes in comparison to GMAW. Another factor that might influence the behavior of samples welded with GMAW process is the presence of N_2 in the shielding gas in that case. N incorporation in the passive film and N enrichment at the film/metal interface have been observed in high nitrogen alloys [37]. N-incorporation and higher Cr content in the passive film can improve pitting corrosion resistance [37].

An important result is that the as received samples showed similar or lower corrosion resistance in acidified glycerin compared to the welded samples.

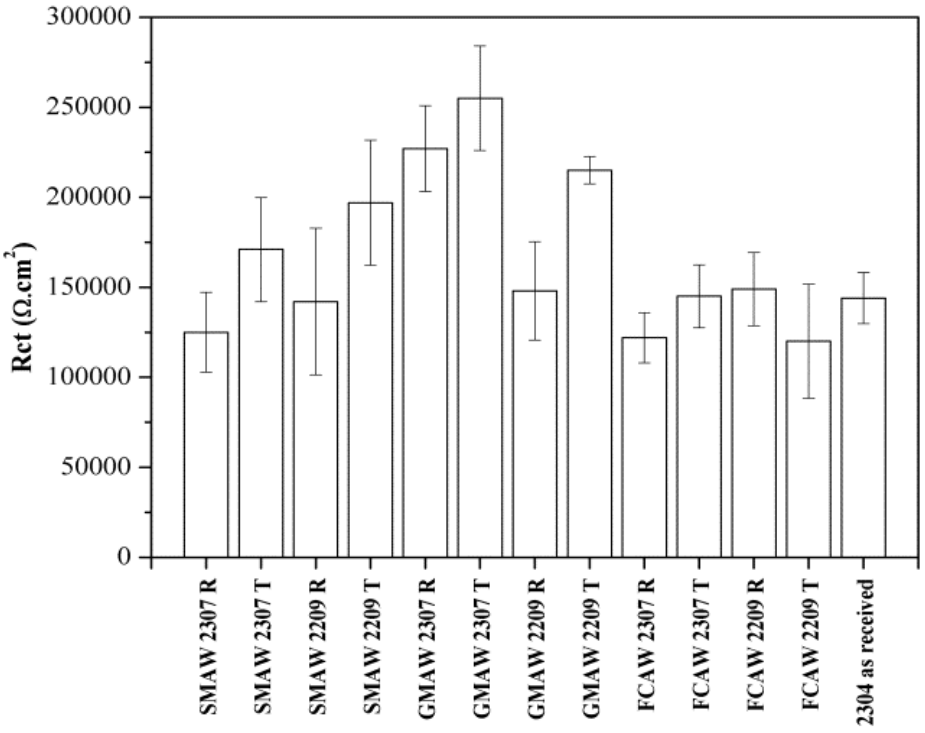

Figure 5.6: R_{ct} values of EIS experimental data. T – top of weld, R – root of weld.

5.3.3. Mott–Schottky analysis

It has been suggested that the formation and breakdown of the passive films on stainless steels are in part controlled by the electronic properties of the oxide film [14]. However, it is important to describe the electronic properties of the passive films together with microstructure and composition to understand the mechanisms behind passivity and localized corrosion.

It is well known that there are relationships between the semi-conducting properties and the corrosion resistance of a passive film. These semi-conducting properties can be determined by Mott–Schottky analysis. When exposed to an aqueous solution; the passive films behave as extrinsic semiconductors due to the presence of defects. These defects can be electron acceptors in the case of p-type doping, or electron donors, resulting in n-type doping [18]. The passive film with a deficiency in metal ions or excess of cationic vacancies generally behaves as p-type, while a passive film with excess of anionic vacancies or interstitials cations behave as n-type semiconductor [38].

The Mott–Schottky results are reported as the inverse square of an interfacial capacitance C as function of potential E [20]. According to the Mott–Schottky theory, the space charge capacitances of n-type and p-type semiconductors are given by [17,38]:

$$\frac{1}{C^2} = \frac{2}{\varepsilon\varepsilon_0 e N_q}\left(E_{FB} - E + \frac{kT}{e}\right) \tag{5.2}$$

Where C is the capacitance of the film/electrolyte interface, $C = -1/2\pi fZim$, where f is the test frequency and Z_{im} is the imaginary component of the interfacial impedance, E is the applied potential, ε denotes the dielectric constant of the passive film, usually taken as 15.6 for stainless steel [18], ε_0 is the vacuum permittivity ($8.8542*10^{-14}$ F/cm), N_q is the density of electron donors or acceptors for doping an n-type or p-type semiconductor, respectively, e is the elementary charge ($1.6029*10^{-19}$ C), k is the Boltzmann constant, T is the absolute temperature and E_{FB} is the flat-band potential. The flat band potential can be determined from the extrapolation of the linear portion to C^{-2} =0 [18].

A positive slope of the C^{2-} versus E plot results from the electrochemical behavior of a n-type semiconductor which is characteristic of a Fe^{2+}-rich oxide, while, a negative slope, indicates a p-type semiconductor behavior, related to the presence of Cr^{3+}-rich oxide [18, 38].

Fig. 5.7 shows the Mott–Schottky plots of the passive films formed on UNS S32304 in acidified glycerin. It should be noted that the capacitance results are in good agreement with the fact that the passive films have a duplex character and behave as n-type and p-type semiconductors above and below the flat band potential, respectively. These behaviors are in reasonable agreement with the results obtained in other works in acidic solutions and is assumed to be result of the semiconducting properties of the iron oxide and chromium oxide present in the passive films [14,18,20].

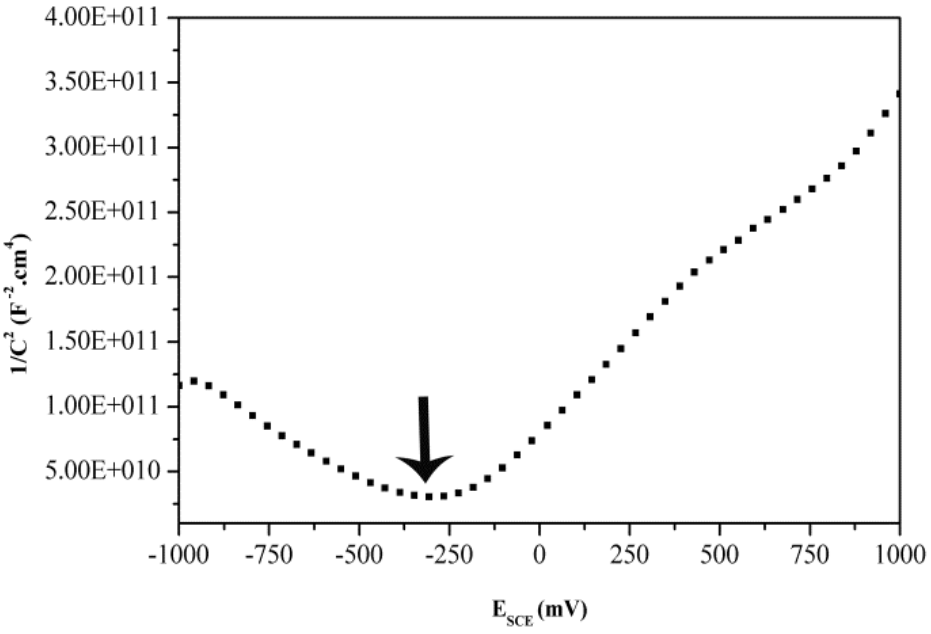

Figure 5.7: Mott–Schottky plots of UNS S32304 LDSS.

It has been proposed in the literature that the different passive oxide layers show variable semiconductor properties depending on the predominant defect present in the passive film. According to Bensalah *et al*. [20], the type of defects, i.e. donors or acceptors, depends on the composition of the oxide film. Thus a Cr-rich layer, Cr_2O_3 or $FeCr_2O_4$, but also MoO_2 and NiO exhibit p-type semiconductor behavior, while a Fe-rich layer, Fe_2O_3, MoO_3, and Fe(OOH) exhibit n-type behavior. Therefore the semi-conductive properties of the passive film depend on the contribution of each oxide and the concentration of the cationic or anionic vacancies inside these oxides.

Donor and acceptor densities have been determined from the positive and negative slopes in the main passive region, respectively and through the equation 5.2. Fig. 5.8 shows the calculated donors and acceptor densities for the passive films. The orders of

magnitude are around 10^{22} - 10^{23} cm^{-3} and are comparable to those reported for other stainless steels in acidic solutions [17,18].

The donor and acceptor densities of the passive film formed on the SMAW and FCAW samples were higher than those formed on the samples welded by GMAW, except for SMAW 2209, reflecting the better passive behavior of the GMAW samples and SMAW 2209. As received samples showed donor and acceptor densities close to that for GMAW process. A higher concentration of donors at the oxide layer favors the incorporation of ions, such as chlorides, into the anions vacancies of the oxide film and their diffusion through it [39,40]. This can favor the breakdown the oxide film and lead to pitting [40]. These results are consistent with EIS measurements that revealed an increase of the charge transfer resistance (R_{ct}) for the GMAW samples and SMAW 2209. The presence of N_2 in the shielding gas seems to influence the behavior of samples welded by the GMAW process and the higher heat input used for SMAW 2209 also affected the behavior of this sample. According to Fig. 5.8, GMAW shows the lowest donor and acceptor densities, hindering the incorporation of ions.

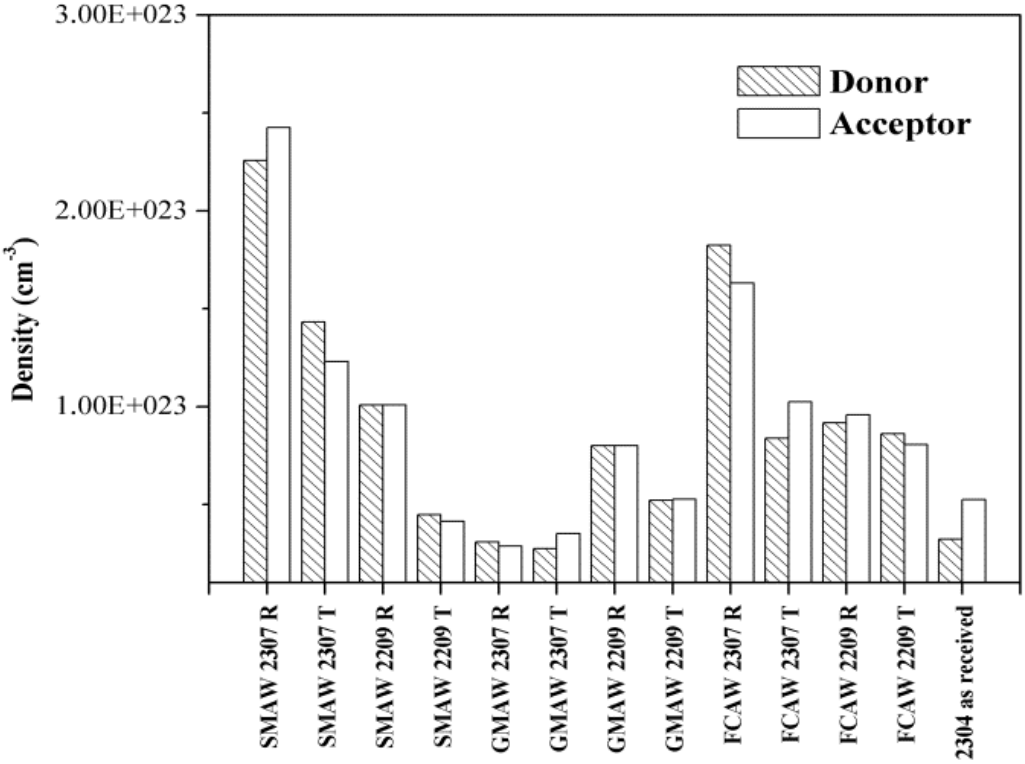

Figure 5.8: Donor and acceptor densities of welded and as received samples.

5.4. Conclusions

- The results of the impedance measurements confirm the semiconducting nature of the passive films investigated.
- The capacitance study shows that the passive films formed on welded DSS behave as n-type and p-type semiconductors above and below the flat band potential, respectively.
- Comparing values of R_{ct} and donor/acceptor densities, in general, top region of joints showed higher values of polarization resistance and lower values of donor/acceptor densities than the root region of welded joints.

- The highest values of R_{ct} and the lowest values of donor/acceptor densities in acidified glycerin were obtained for the lean duplex joints welded using GMAW process and 2307 consumable.
- Considering corrosion resistance, samples welded by GMAW process, compared to others for the same consumable, showed better corrosion resistance in acidified glycerin of a biodiesel plant.

5.5. References

[1] E.M. Westin, C.-O.A. Olsson, S. Hertzman, *Corros. Sci.* **2008**, *50*, 2620.

[2] H. Tan, Z. Wang, Y. Jiang, Y. Yang, B. Deng, H. Song, J. Li, *Corros. Sci.* **2012**, *55*, 368.

[3] C.M. Garzon, A.J. Ramirez, *Acta Mater.* **2006**, *54*, 3321.

[4] M. Asif M, K.A. Shrikrishna, P. Sathiya, S. Goel, *J. Manuf. Proces.* **2015**, *18*, 92.

[5] J. Pilhagen, R. Sandström, *Mater. Sci. Eng., A.* **2014**, *602*, 49.

[6] L. Chen, H. Tan, Z. Wang, J. Li, Y. Jiang, *Corros. Sci.* **2012**, *58*, 168.

[7] Y. Jiang, H.Tan, Z. Wang, J. Hong, L. Jiang, J. Li, *Corros. Sci.* **2013**, *570*, 252.

[8] I. V. Aguiar, D. P. Escobar, D. B. Santos, P. J. Modenesi, *Revista Matéria*, **2015**, 20, 212.

[9] D.H. Kang, H.W. Lee, *Corros. Sci.* **2013**, *74*, 396.

[10] H.-Y. Ha, M.-H. Jang, T.-H. Lee, J. Moon, *Corros. Sci.* **2014**, *89*, 154.

[11] V. Muthupandi, P. Bala Srinivasan, S. K. Seshadri, S. Sundaresan, *Mater. Sci. Eng, A.* **2003**, *358*, 9.

[12] P. Ferro, A. Tiziani, *J. Mater. Sci.* **2012**, *47*, 199.

[13] D.M. Garcia-Garcia, J. Garcia-Anton, A. Igual-Murioz, E. Blasco-Tamarit, *Corros. Sci.* **2006**, *48*, 863.

[14] N.E. Hakiki, *Corros. Sci*. **2011**, *53*, 2688.

[15] Z.J. Zheng, Y. Gao, Y. Gui, M. Zhu, *J. Solid State Electrochem*. **2014** , *18*, 2201.

[16] Marcus, V. Maurice, H. H. Strehblow, *Corros. Sci*. **2008**, *50*, 2698.

[17] A. Di Paola, *Electrochim. Acta*. **1989**, *34*, 203.

[18] A. Fattah-alhosseini, S. Vafaeian, *J. Alloys Compd*. **2015**, *639*, 301.

[19] I.M. Gadala, A. Alfantazi, *Appl. Surf. Sci.* **2015**, *357*, 356.

[20] M. BenSalah, R. Sabot, E. Triki, L. Dhouibi, Ph. Refait, M. Jeannin, *Corros. Sci*. **2014**, *86*, 61.

[21] F.F. Eliyan, A. Alfantazi, *Corros. Sci.* **2013**, *74*, 297.

[22] F. Mohammadi, F.F. Eliyan, A. Alfantazi, *Corros. Sci.* **2012**, *63*, 323.

[23] R. Cardoso Junior, A.Q. Bracarense, F.R. Campos, C.S. Souza, D.M. Silveira, V.F.C. Lins, *Soldagem e Inspeção*. **2012**, *17*, 306.

[24] D.C. Sicupira, G.S. Frankel, V.F.C. Lins, *Mater. Corros.* **2015**, DOI: 10.1002/maco.201508502.

[25] A.J. Ramirez, J.C. Lippold, S.D. Brandi. *Metallurg. Mater. Trans. A.* **2003**, *34*, 1575.

[26] H.-Y. Liou, R.-I. Hsieh, W.-T. Tsai, Mater. *Chem. Phys*. **2002**, *74*, 37.

[27] T. Chehuan, V. Dreilich, K.S. Assis, F.V.V. Sousa, O.R. Mattos, *Corros. Sci.* **2014**, *86*, 268.

[28] E. Bettini, U. Kivisäkk, C. Leygraf, J. Pan, *Electrochim. Acta*. **2013**, *113*, 280.

[29] J.-B. Jorcin, M. E. Orazem, N. Pébère, B. Tribollet, *Electrochim. Acta*. **2006**, *51*,1473.

[30] M.E. Orazem, B. Tribollet, *Electrochemical impedance spectroscopy*, Hoboken, Wiley, New Jersey **2008**.

[31] S. Belkaid, M.A. Ladjouzi, S. Hamdani, *J. Solid State Electrochem*. **2011**, *15*, 525.

[32] M.A. Baker, J.E. Castle, *Corros. Sci.* **1992,** *33*, 1295.

[33] M. Hoseinpoor, M. Momeni, M.H. Moayed, A. Davoodi, *Corros. Sci.* **2014,** *80*, 197.

[34] M. Azzi, M. Benkahoul, J.E. Klemberg-Sapieha, L. Martinu, *Surf. Coat. Technol*. **2010**, *205*, 1557.

[35] J. Stewart, D.E. Williams, *Corros. Sci*. **1992**, *33*, 457.

[36] N.A. McPherson, Y. Li, T.N. Baker, *Sci. Technol. Weld. Join.* **2000**, *5*, 235.

[37] H.-Y. Ha, T.-H. Lee, S.-J. Kim, *Electrochim. Acta*, **2012**, *80*, 432.

[38] E.F. Pieretti, S.M. Manhabosco, L.F.P. Dick, S. Hinder, I. Costa, *Electrochim. Acta*. **2013**, *124*, 150.

[39] D.D. Macdonald, *J. Electrochem. Soc*. **1992**, *139*, 3434.

[40] J. Soltis, *Corros. Sci*. **2015**, *90*, 5.

6. CYCLIC POLARIZATION STUDY OF THICK WELDED JOINTS OF LEAN DUPLEX STAINLESS STEEL IN ACIDIFIED GLYCERIN

Dalila C. Sicupira[a,c*], Ronaldo C. Junior[b], Alexandre Q. Bracarense[b], G.S. Frankel[c], Vanessa de F. C. Lins[a]

[a] Chemical Engineering Department, Universidade Federal de Minas Gerais, 6627, Antônio Carlos Avenue, Pampulha, Belo Horizonte, MG 31270-901, Brazil, Fax:+55 31 34091789, e-mail address: dsicupira@ufmg.br

[b] Mechanical Engineering Department, Universidade Federal de Minas Gerais, 6627, Antônio Carlos Avenue, Pampulha, Belo Horizonte, MG 31270-901, Brazil

[c] Fontana Corrosion Center, Dept. of Materials Science and Engineering, The Ohio State University, Columbus, OH 43210, USA

Abstract

The corrosion behavior of thick welded joints of UNS S32304 lean duplex stainless steel (LDSS) has been studied using cyclic polarization curves in acidified glycerin. LDSS S32304 thick plates were welded by different processes commonly employed in the manufacture of equipment and piping: shielded metal arc welding, gas metal arc welding and flux cored arc welding. The electrochemical behavior of different weldment zones (fusion zone, base metal and heat affected zone (HAZ)) was characterized. Transmission electron microscopy and scanning electron microscopy (SEM) were used for sample characterization. SEM images showed that the HAZ was the most critical zone for pitting corrosion for all samples. The results were correlated to

the microstructural features of the materials. In general, the corrosion resistance of the top regions of welds was higher in acidified glycerin than the weld root for welds fabricated with two different filler metals. Basically, all the welded samples exhibited similar or higher corrosion resistance, compared with the corresponding base metal.

Keywords: corrosion, duplex stainless steel, welding process, acidified glycerin.

6.1. Introduction

Duplex stainless steels (DSSs) are materials that exhibit a combination of high yield strength, toughness and localized corrosion resistance, and they are being widely used in chemical, petrochemical, marine, nuclear and paper industry [1]. The best properties are obtained with approximately equal amount of austenite (γ) and ferrite (α) phases [2].

Volatility of the Ni price has led to development of low alloy duplex steels (generally low Ni or Mo contents) [3]. The nickel content is partly replaced by manganese and nitrogen and also the molybdenum content is reduced in the so-called lean DSS (LDSS) [4].

Exposure to high temperatures, for example during welding, can result in deterioration in corrosion resistance of DSS [2-14]. During welding, DSS undergoes microstructural changes that impact on their mechanical and corrosion properties, especially local pitting corrosion resistance and toughness [2-14]. The degradation results from the unbalanced duplex phase fraction with excess of ferrite phase and the precipitation of deleterious secondary phases such as chromium nitrides, secondary austenite (γ_2), sigma

(σ), chi (χ), etc. [2-9]. A great number of investigations have been carried out on welded DSS joints [1-12]. Although multipass welding is more common during industrial fabrication, the study of multipass welding is scarcely reported, especially for plates or pipes of medium thickness or more.

The localized corrosion resistance of stainless steels is usually associated with the alloying elements Cr, Mo and N, whereas Ni mainly acts to stabilize the austenite phase [13-15]. A great number of investigations have studied the effect of alloying elements, especially N, which is most effective [6,8,13,16,17]. According to Hsieh *et al.* [18], a higher content of nitrogen and nickel favors the reformation of austenite. However, the effect of the nitrogen on the reformation of austenite is much greater than that of nickel. Hsieh *et al.* [18] also showed that the effect of manganese on the formation of austenite can be negligible. Bhatt *et al.* [19] found that the presence of 5 and 10% nitrogen in the shielding gas, decreases the ferrite contents to 35 and 29%, respectively, resulting in an improved pitting corrosion resistance of the weldments obtained by gas tungsten arc. According to Mesquita *et al.* [15] the general corrosion resistance of Mo-containing DSS grades is increased. Mo has a stronger beneficial effect on the corrosion resistance of ferrite compared to austenite.

The pitting corrosion resistance of 2304 DSS after autogenous plasma-arc welding was investigated by Tan *et al.* [20]. In this study, the as-welded samples showed impaired pitting corrosion resistance and pitting preferentially occurred at ferrite grains in the heat affected zone (HAZ) near the fusion line. In another study in welded joints of 2304 DSS, Chen *et al.* [8] found pits occurring in the ferrite phase for all simulated HAZ

specimens and is influenced by Cr_2N and inclusions. According to their results, the pitting corrosion resistance of the HAZ in 2304 DSS decreased with the cooling rate.

In this context, the objective of this work is to evaluate the corrosion resistance of UNS S32304 LDSS thick plates welded by three different welding processes in acidified glycerin, a byproduct of biodiesel industry.

6.2. Experimental Procedures

6.2.1. Materials

Measurements were performed on the whole welded joints of UNS S32304 LDSS. The chemical composition is shown in the Table VI.1. Three different welding processes were used: shielded metal arc welding (SMAW), gas metal arc welding (GMAW) and flux cored arc welding (FCAW). For each welding process, two filler metals with different chemical compositions, (23%Cr 7%Ni) and (22%Cr 9%Ni 3%Mo) were evaluated. The electrochemical behavior of different weldment zones (fusion zone (FZ), base metal (BM) and heat affected zone (HAZ)) was characterized in the top and root of the specimens.

Table VI.1: Chemical composition of the base metal [21].

Element	**C**	**Mn**	**Si**	**P**	**S**	**Cr**	**Ni**	**Mo**	**Cu**	**N**	**O**
Content (%wt)	0.019	1.3	0.39	0.028	0.00040	22	3.6	0.44	0.50	0.11	0.0033

This work is a continuation of a project [21], in which the samples were welded. The filler metal compositions, the welding parameters and the sample preparation for electrochemical tests were described by the authors in a previous work [22].

6.2.2. Microstructure characterization

A Tecnai G2-20 - SuperTwin FEI - 200kV transmission electron microscope (TEM) was used for identification of the precipitates. After the polarization tests, microstructural observations were carried out using scanning electron microscopy (SEM, Quanta 200F, FEI).

6.2.3. Electrochemical measurements

The tests were performed at a temperature of 65±1°C and under constant stirring to simulate the operational conditions in the pipes of biodiesel plants. A conventional three-electrode cell was used, the working electrodes being prepared from the LDSS welded samples with an exposed surface of approximately 1 cm^2. The reference was a saturated calomel electrode (SCE) and a Pt mesh was used as the counter electrode.

Cyclic potentiodynamic polarization tests were performed in real acidified glycerin from a biodiesel plant with approximate concentration 49.5% glycerin, 29% methanol, 17% water, 3% NaCl, and 1.5% organic materials, pH=6.2 and conductivity of 4.9 ms/cm. An Ivium compactstat potentiostat was used to measure the open circuit potential (OCP) for 1 h and the cyclic potentiodynamic polarization curves were then measured at a scan rate 0.167 mV/s from the open circuit potential (OCP) until the

current density reached 5 $mA.cm^{-2}$ at which point the scanning direction was then reversed. Three replicate tests of each measurement were performed.

6.3. Results

6.3.1. Microstructure

According to previous investigations [22], similar microstructures were observed for each welded sample analyzed. The fusion zone (FZ) structure consists of austenite grains in the form of Widmanstätten plate precipitates and secondary austenite (γ_2) within a matrix of ferrite, and also, samples showed higher proportions of austenite in the FZ than in HAZ. The HAZ exhibited chromium nitrides primarily in the interior of the ferrite grains. Nitride precipitation is more likely to occur in the ferrite phase because the solubility of nitrogen in ferrite drops rapidly with the decrease in temperature. Figure 6.1 shows nitride colonies within the ferrite grains in the HAZ of UNS S32304.

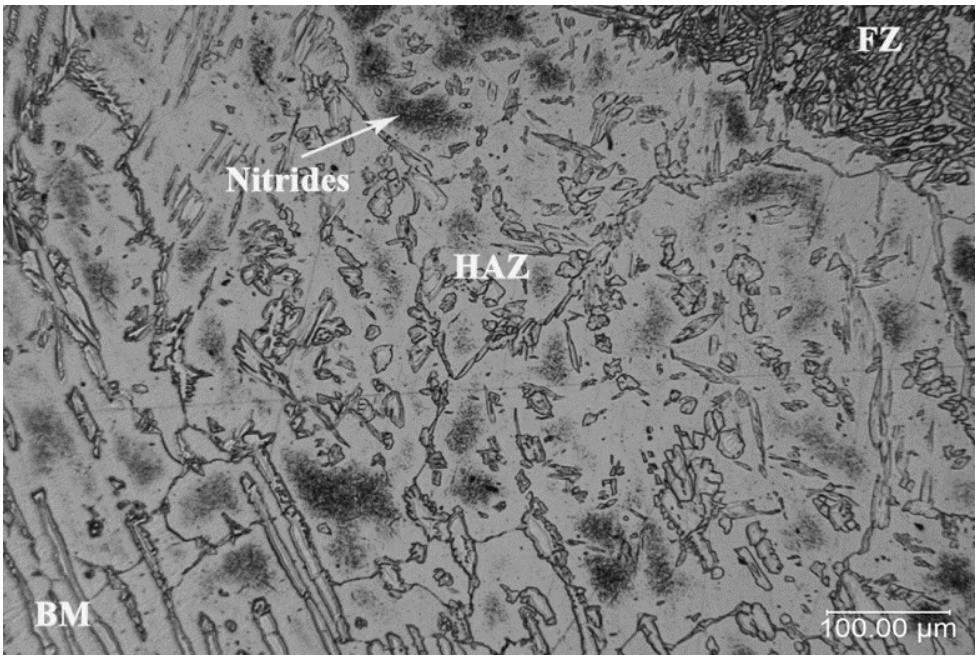

Figure 6.1: OM micrographs of nitride colonies in the interior of a ferrite grain in HAZ of UNS S32304 (FCAW top region and 2209 as filler metal).

Transmission electron microscopy indicated the presence of precipitates in the welded specimens as shown in Figure 6.2. Electron diffraction studies were incomplete, but comparison with the results of other studies indicates that the precipitates are Cr_2N [23].

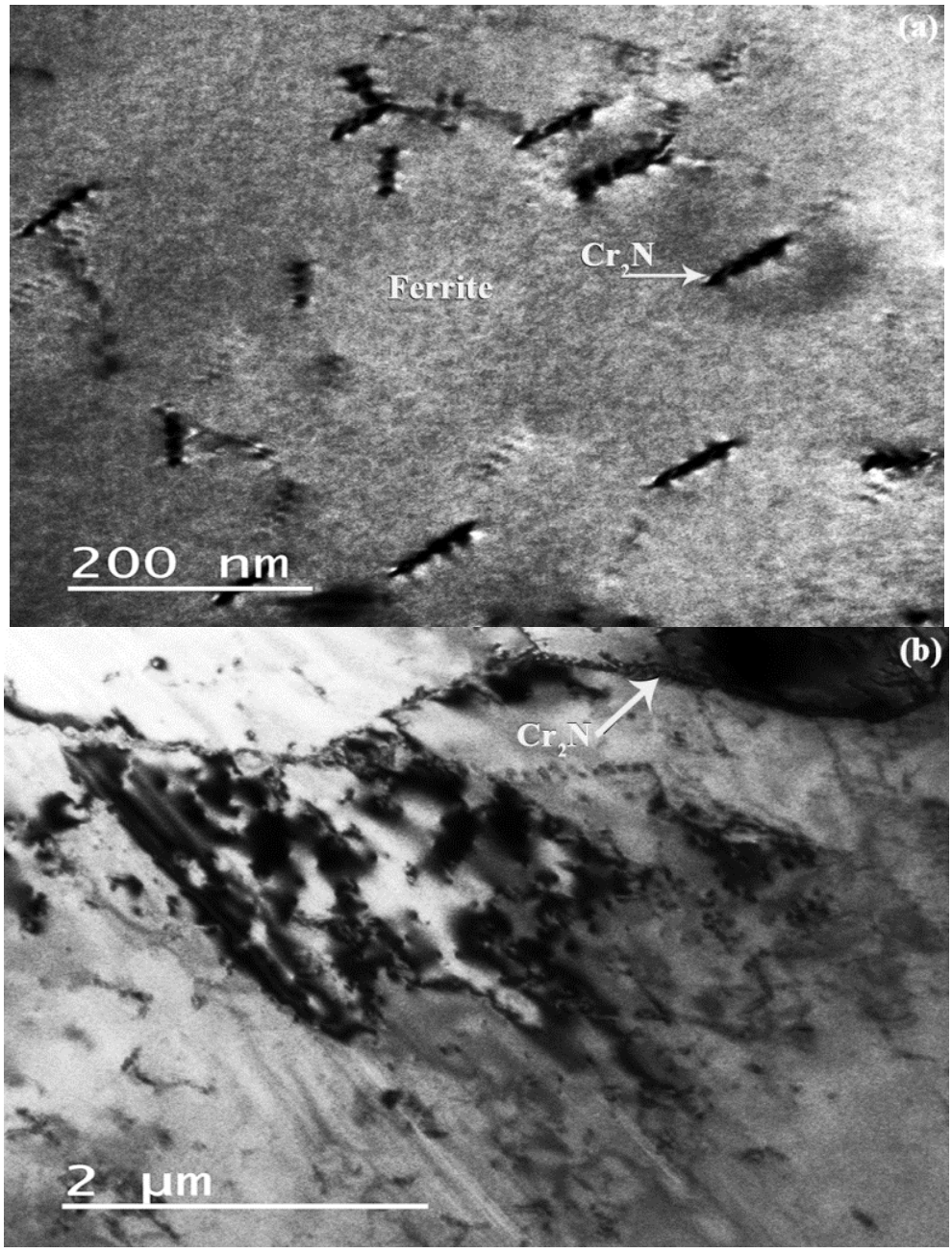

Figure 6.2: Transmission electron micrograph of Cr_2N of the HAZ of welded joints. (a)Transmission electron micrograph of the intragranular nitrides and (b) transmission electron micrograph of the nitrides precipitated at the ferrite/austenite interfaces (FCAW top region and 2307 as filler metal).

Figure 6.2a and 6.2b shows the results of the TEM analysis of the Cr_2N formed in the HAZ of as-welded sample. Figure 6.2a indicates that all precipitates observed in the HAZ are rod-like Cr_2N precipitated intragranularly. In addition to the intragranular rod-

like nitrides, some Cr_2N particles are also observed along the ferrite/austenite interfaces (Figure 6.2b).

6.3.2. Electrochemical behavior

Figure 6.3(a-c) shows typical cyclic potentiodynamic polarization curves obtained for samples welded using SMAW, GMAW and FCAW processes, respectively. The OCP values and breakdown potentials (E_b) from polarization tests are summarized in Figure 6.4.

The welded joints exhibited higher values of corrosion potential than the lean duplex steel in the as received condition, except for the root region of joint welded using SMAW process and 2307 consumable, which showed the lowest corrosion and breakdown potentials among the studied samples, which can be related with the lowest heat input used in the welding process in the case of SMAW 2307 root region, as showed in a previous work [22]. The highest breakdown potential was identified for the top region of the lean duplex joint welded using SMAW process and 2209 consumable, which can be related with the highest heat input used for this sample. This difference in the heat input was described by Cardoso Junior *et al.* [21] as being an experimental deviation occurred during the manual welding process SMAW. In general, top samples showed higher values of E_b than root samples, due to higher filler metal dilution for root regions. Considering the standard deviation, no remarkable difference between the welding processes was observed (Fig. 6.4).

As the potential increased, a sharp rise in current density was seen, suggesting the occurrence of pitting corrosion. Wide passive regions were observed for all the samples tested and the pitting potentials were all 200-400 mV higher than the corresponding open circuit potentials. These observations indicate that the samples have excellent resistance to the initiation of pitting corrosion in this chloride environment. In general, no remarkable decrease in pitting potential was found after the welding. The repassivation potentials during the reverse scans were also similar. The backward polarization (Fig. 6.3) showed a large hysteresis loop and low repassivation potential, similar in value to the OCPs, which indicate that pitting corrosion might occur over long periods of open circuit exposure to the acidified glycerin solution, which contained 3% NaCl. According to Marcus *et al.* [32], after depassivation, the repassivation can be hindered by chloride adsorbed on the metal surface resulting in formation of nanopits.

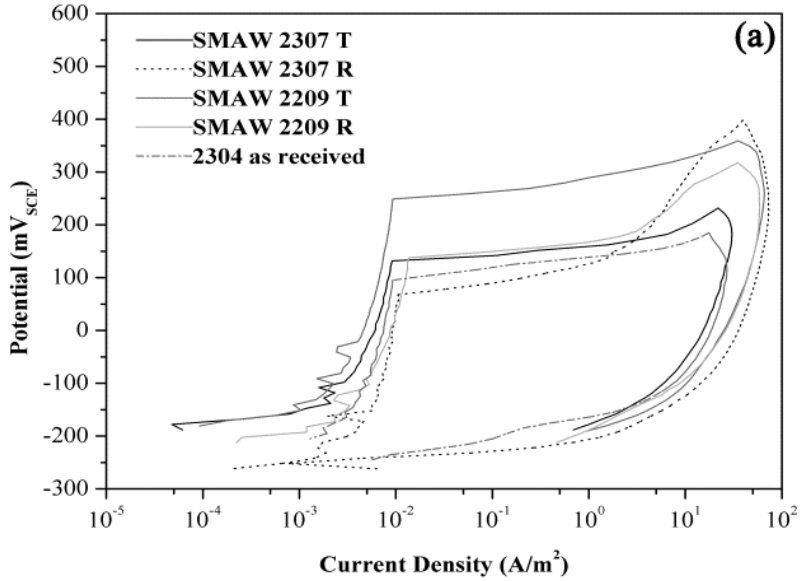
(a)
SMAW 2307 T
SMAW 2307 R
SMAW 2209 T
SMAW 2209 R
2304 as received
Potential (mV$_{SCE}$)
Current Density (A/m^2)

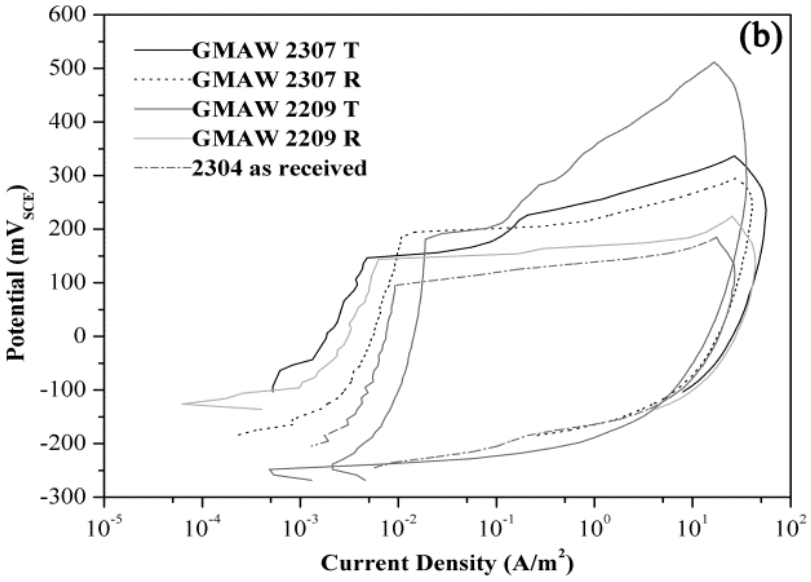
(b)
GMAW 2307 T
GMAW 2307 R
GMAW 2209 T
GMAW 2209 R
2304 as received
Potential (mV$_{SCE}$)
Current Density (A/m^2)

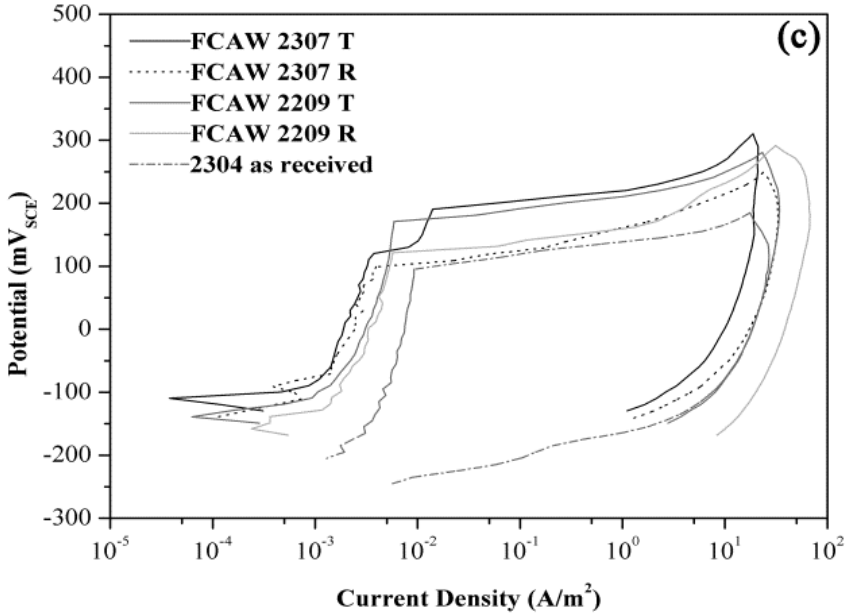

Figure 6.3: Cyclic potentiodynamic polarization curves for (a) SMAW (b) GMAW and (c) FCAW process. T – top of weld, R – root of weld.

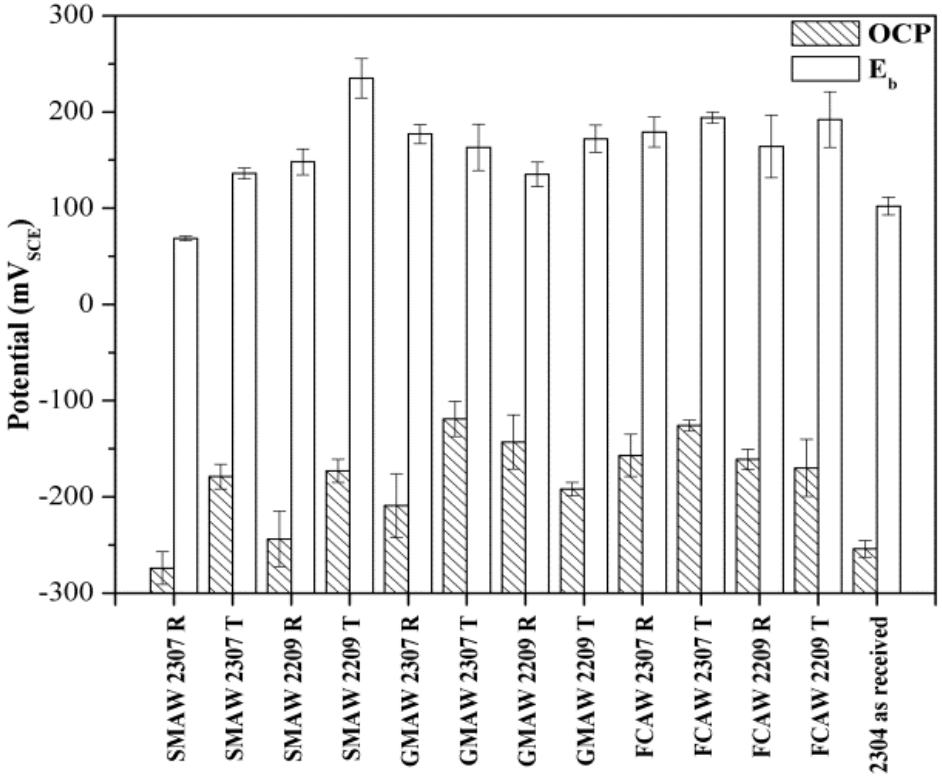

Figure 6.4: Experimental data for cyclic polarization tests. T – top of weld, R – root of weld.

For a more detailed understanding of the pitting corrosion of the joints, the samples were observed using SEM analysis after the cyclic potentiodynamic testing. An example is shown in Figure 6.5.

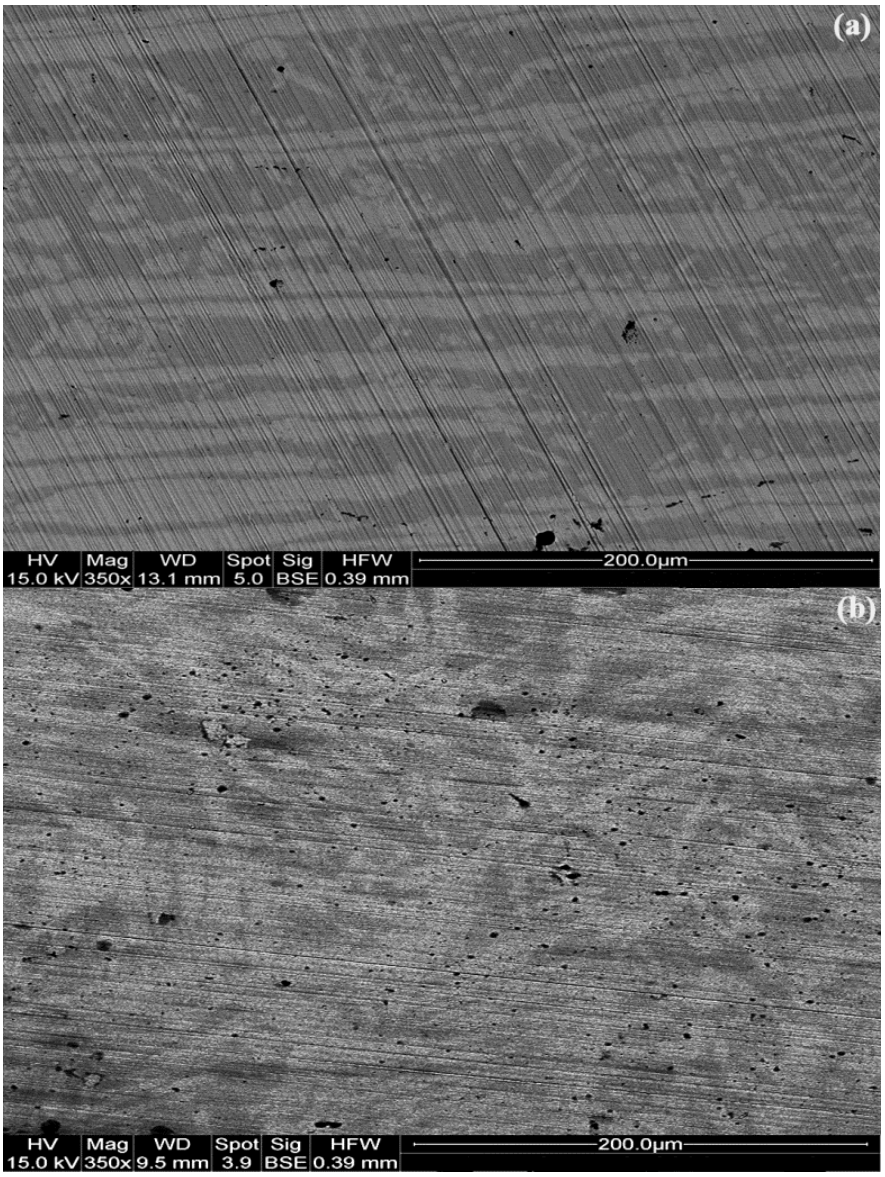

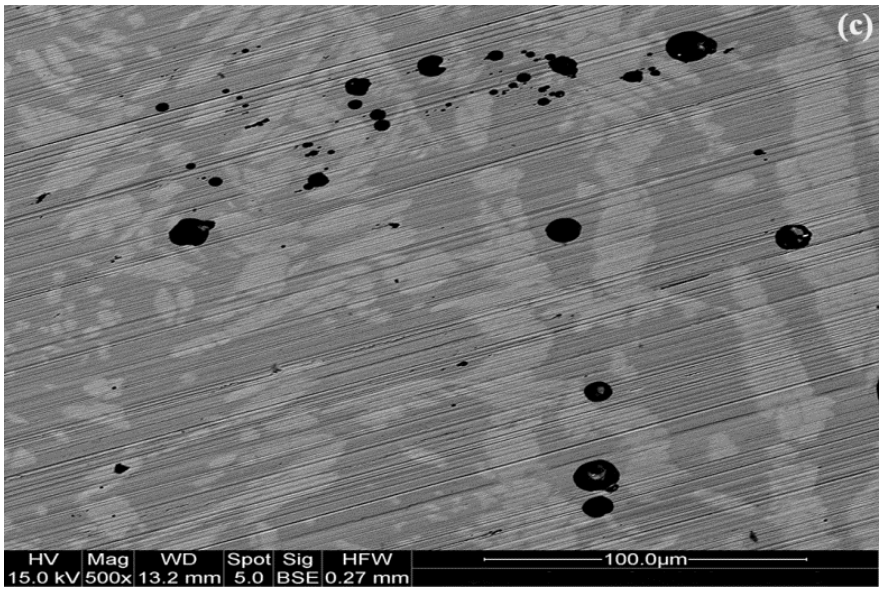

Figure 6.5: Pit morphologies after polarization measurements (SMAW 2307 top region): (a) BM (b) FZ and (c) HAZ.

As shown by the authors in a previous work [22], the FZ was more resistant than the HAZ and the pits, in all of the welded joints, occurred mostly in the HAZ (Fig. 6.5). The sites for nucleation of pits were probably chromium nitride particles, as suggested by Tan *et al.* [20]. All of the HAZ regions exhibited more pits than the other regions and the HAZ was always the most susceptible zone. Some pits were found to initiate in the vicinity of inclusions in either the δ or γ phase. Others were formed at the δ/γ interface or within the δ phase.

The higher susceptibility of the HAZ to pitting corrosion was found for all welded joints, and it resulted from two aspects of the microstructure evolution during welding. The Cr and Mo contents are diluted by an increase in the δ volume fraction, so Cr and Mo content of ferrite phase in the HAZ is lower than in the parent metal and, also, Cr_2N precipitation in the ferrite phase due to the lower solubility of nitrogen in ferrite [6,8,9,14,20,25-30]. According to Hsieh *et al.* [18] the reformation of austenite in HAZ is limited with nitrogen and nickel contents lower than 0.15 and 5.5% (as the studied

UNS S32304), respectively, even in the cases of increased cooling time [18]. The austenite content in the HAZ cannot fall below 25% in order to avoid precipitation of Cr_2N and guarantee superior pitting corrosion resistance at the HAZ [18]. The pits showed in Fig. 6.5 were believed to be related to the Cr_2N precipitates. These precipitates resulted in depletion in Cr in the adjacent matrix region. The chromium-depleted zones provide a favorable site for pitting corrosion nucleation, as reported by several authors [6,8,9,14,20,25-30].

Theories for passive film breakdown and pit initiation have been summarized in three main mechanisms that focus on passive film penetration, film breaking, or adsorption [31]. These three mechanisms of pit initiation are not necessarily mutually exclusive. In this study, a combination of these mechanisms is possible. According to Marcus *et al.* [32], the presence of microstructural defects on the samples such as metal grain boundaries or interfaces between the matrix and inclusions or second phase particles can promote local breakdown. In this work the breakdown has, preferentially, occurred at surface defect sites such as non-metallic inclusions or precipitates. According to Tan [33] the electrode inhomogeneity such as material impurities, metallurgical defects, inclusions, different phases, grain boundaries appears to determine the pitting nucleation stage while the electrochemical heterogeneity, that is believed to initiate from pre-existing active electrode inhomogeneity sites, appears to control the propagation stage.

It has been proposed by some authors [32,34-36] that adsorption of aggressive anions (Cl^-) reduces the surface tension of the passive film leading to cracks, allowing anions to reach the metal surface. Marcus *et al.* [32] have shown evidence for both chloride

adsorption and penetration for the pitting corrosion in chloride solutions. If Cl^- ions are present in the electrolyte, they will compete with OH^- for adsorption on the oxide surface [33,36,37]. Cl^- can penetrates through intergranular boundaries and migrate to the metal/oxide interface, resulting in the formation of Cl^--containing particles that will cause stress-induced fracture of the passive film due to the growth of these particles [32].

6.4. Conclusions

The corrosion behavior of joints of lean duplex stainless steel, UNS S32304, welded by three different processes, was studied. The following was observed:

- All the welded samples exhibited similar or higher corrosion resistance, compared with the corresponding base metal.
- The pitting corrosion resistance of the whole joint has improved compared to as received samples, as a consequence of alloying elements enhanced in ferrite and austenite.
- Considerable precipitation of chromium nitrides was observed at grain boundaries or ferrite grains on the as-welded specimens.
- Some pits were found to initiate in the vicinity of inclusions and others were formed at the interface δ/γ or within δ phase.
- The pits in HAZ are believed to be related to the Cr_2N precipitates.

6.5. References

[1] Asif MM, Shrikrishna KA, Sathiya P, Goel S (2015) The impact of heat input on the strength, toughness, microhardness, microstructure and corrosion aspects of friction welded duplex stainless steel joints, J Manuf Proces 18: 92-106.

[2] Garzón CM, Ramirez AJ (2006) Growth kinetics of secondary austenite in the welding microstructure of a UNS S32304 duplex stainless steel, Acta Mater 54: 3321-3331.

[3] Alvarez SM, Bautista A, Velasco F (2011) Corrosion behaviour of corrugated lean duplex stainless steels in simulated concrete pore solutions, Corros Sci 53: 1748-1755.

[4] Westin EM, Olsson C-OA, Hertzman S (2008) Weld oxide formation on lean duplex stainless steel, Corros Sci 50: 2620-2634.

[5] Westin EM (2010) Microstructure and properties of welds in the lean duplex stainless steel LDX 2101. PhD dissertation, Royal Institute of Technology.

[6] Tan H, Wang Z, Jiang Y, Yang Y, Deng B, Song H, Li J (2012) Influence of welding thermal cycles on microstructure and pitting corrosion resistance of 2304 duplex stainless steels, Corros Sci 55: 368-377.

[7] Pilhagen J, Sandström R (2014) Influence of nickel on the toughness of lean duplex stainless steel welds, Mater Sci Eng A 602: 49-57.

[8] Chen L, Tan H, Wang Z, Li J, Jiang Y (2012) Influence of cooling rate on microstructure evolution and pitting corrosion resistance in the simulated heat-affected zone of 2304 duplex stainless steels, Corros Sci 58: 168-174.

[9] Jiang Y, Tan H, Wang Z, Hong J, Jiang L, Li J (2013) Influence of Creq/Nieq on pitting corrosion resistance and mechanical properties of UNS S32304 duplex stainless steel welded joints, Corros Sci 570: 252-259.

[10] Nowacki J, Łukoj´c A (2005) Structure and properties of the heat-affected zone of duplex steels welded joints, J Mater Process Technol 164–165: 1074-1081.

[11] Kang DH, Lee HW (2013) Study of the correlation between pitting corrosion and the component ratio of the dual phase in duplex stainless steel welds, Corros Sci 74: 396-407.

[12] Souza CS, Lins VFC, Silveira DM, Costa CGF, Cardoso Junior R, Campos FR, Bracarense AQ (2012) Avaliação da Soldagem Multipasse de Chapas Espessas de Aços Inoxidáveis Lean Duplex UNS S32304 Soldadas pelos Processos SMAW, GMAW e FCAW – Parte II: Resistência à Corrosão, Soldagem e Inspeção 18: 257-267.

[13] Weber L, Uggowitzer PJ (1998) Partitioning of chromium and molybdenum in super duplex stainless steels with respect to nitrogen and nickel content, Mater Sci Eng A 242: 222-229.

[14] Ha H-Y, Jang M-H, Lee T-H, Moon J (2014) Interpretation of the relation between ferrite fraction and pitting corrosion resistance of commercial 2205 duplex stainless steel, Corros Sci 89: 154-162.

[15] Mesquita TJ, Chauveau E, Mantel M, Kinsman N, Roche V, Nogueira RP (2012) Lean duplex stainless steels—The role of molybdenum in pitting corrosion of concrete reinforcement studied with industrial and laboratory castings, Mater Chem Phys 132: 967-972.

[16] Ramirez AJ, Brandi SD, Lippold JC (2004) Secondary austenite and chromium nitride precipitation in simulated heat affected zones of duplex stainless steels, Sci Technol Weld Join 9: 301-313.

[17] Garzon CM, Serna CA, Brandi SD, Ramirez AJ (2007) The relationship between atomic partitioning and corrosion resistance in the weld-heat affected zone microstructures of UNS S32304 duplex stainless steel, J Mater Sci 42: 9021-9029.

[18] Hsieh R-I, Liou H-Y, Pan Y-T (2001) Effects of Cooling Time and Alloying Elements on the Microstructure of the Gleeble-Simulated Heat-Affected Zone of 22% Cr Duplex Stainless Steels, J Mater Eng Perform 10: 526-536.

[19] Bhatt RB, Kamat HS, Ghosal SK, De PK (1999) Influence of Nitrogen in the Shielding Gas on Corrosion Resistance of Duplex Stainless Steel Welds, J Mater Eng Perform 8: 591-597.

[20] Tan H, Wang Z, Jiang Y, Han D, Hong J, Chen L, Jiang L, Li J (2011) Annealing temperature effect on the pitting corrosion resistance of plasma arc welded joints of duplex stainless steel UNS S32304 in 1.0M NaCl, Corros Sci 53: 2191-2200.

[21] Cardoso Junior R, Bracarense AQ, Campos FR, Souza CS, Silveira DM, Lins VFC (2012) Avaliação da Soldagem Multipasse de Chapas Espessas de Aços Inoxidáveis Lean Duplex UNS S32304 soldadas pelos processos SMAW, GMAW e FCAW – Parte 1: Propriedades Mecânicas, Soldagem e Inspeção 17: 306-316.

[22] Sicupira DC, Frankel GS, Lins VFC (2015) Pitting corrosion of welds in UNS S32304 lean duplex stainless steel, Mater Corros. doi: 10.1002/maco.201508502.

[23] Yang Y, Yan B, Li J, Wang J (2011) The effect of large heat input on the microstructure and corrosion behaviour of simulated heat affected zone in 2205 duplex stainless steel , Corros Sci 53: 3756-3763.

[24] Kim H-J, Jeon S-H, Kim S-T, Park Y-S (2015) Influence of the shielding gas composition on the passive film and erosion corrosion of tube-to-tube sheet welds of hyper duplex stainless steel, Corros Sci 91: 140-150.

[25] Ramirez AJ, Lippold JC, Brandi SD (2003) The Relationship between Chromium Nitride and Secondary Austenite Precipitation in Duplex Stainless Steels, Metallurg Mater Trans A 34: 1575-1597.

[26] Liou H-Y, Hsieh R-I, Tsai W-T (2002) Microstructure and pitting corrosion in simulated heat-affected zones of duplex stainless steels, Mater Chem Phys 74: 33-42.

[27] Chehuan T, Dreilich V, Assis KS, Sousa FVV, Mattos OR (2014) Influence of multipass pulsed gas metal arc welding on corrosion behaviour of a duplex stainless steel, Corros Sci 86: 268-274.

[28] Bettini E, Kivisäkk U, Leygraf C, Pan J (2013) Study of corrosion behavior of a 22% Cr duplex stainless steel: Influence of nano-sized chromium nitrides and exposure temperature, Electrochim Acta 113: 280-289.

[29] Zhang Z, Wang Z, Jiang Y, Tan H, Han D, Guo Y, Li J (2012) Effect of post-weld heat treatment on microstructure evolution and pitting corrosion behavior of UNS S31803 duplex stainless steel welds, Corros Sci 62: 42-50.

[30] Zhang Z, Zhao H, Zhang H, Yu Z, Hu J, He L, Li J (2015) Effect of isothermal aging on the pitting corrosion resistance of UNS S82441 duplex stainless steel based on electrochemical detection, Corros Sci 93: 120-125.

[31] Frankel GS (1998) Pitting Corrosion of Metals, J Electrochem Soc 6: 2186-2198.

[32] Marcus P, Maurice V, Strehblow HH (2008) Localized corrosion (pitting): A model of passivity breakdown including the role of the oxide layer nanostructure, Corros Sci 50: 2698-2704.

[33] Tan Y (2011) Understanding the effects of electrode inhomogeneity and electrochemical heterogeneity on pitting corrosion initiation on bare electrode surfaces, Corros Sci 53: 1845-1864.

[34] Baker MA, Castle JE (1992) The initiation of pitting corrosion of stainless steels at oxide inclusions, Corros Sci 33: 1295-1312.

[35] Hoar TP (1967) The production and breakdown of the passivity of metals, Corros Sci 7: 341-355.

[36] Sato N (1990) An overview on the passivity of metals, Corros Sci 3: 1-19.

[37] Soltis J (2015) Passivity breakdown, pit initiation and propagation of pits in metallic materials – Review, Corros Sci 90: 5-22.

7. FINAL CONSIDERATIONS

Welded joints of lean duplex stainless steel fabricated under different conditions were tested in acidified glycerin. Based on the results, is possible to conclude:

- Welds produced with 2209 filler metal showed a higher pitting corrosion resistance than the welds produced with 2307 filler metal, indicating that a higher-alloyed specimen exhibited a higher corrosion performance, for both whole samples and the weldment zones tested by using the microcell technique. The pitting susceptibility is comparable in the HAZ and the BM. The pitting corrosion resistance of the FZ was improved after welding as a consequence of the enrichment of alloying elements in these regions from the filler metals.
- The results of the impedance measurements confirm the semiconducting nature of the passive films investigated. The capacitance study shows that the passive films formed on welded DSS behave as n-type and p-type semiconductors above and below the flat band potential, respectively. The highest values of R_{ct} and the lowest values of donor/acceptor densities in acidified glycerin were obtained for the lean duplex joints welded using GMAW process and 2307 consumable.
- The pitting corrosion resistance of the whole joint has improved compared to as received samples, as a consequence of alloying elements enhanced in ferrite and austenite phases. Considering corrosion resistance and microstructure phase balance, GMAW welding process is the most adequate welding process for 2304 duplex stainless steel.